ALL-RUSSIAN RESEARCH INSTITUTE FOR AGRICULTURAL MICROBIOLOGY

As a manuscript

Tsyganova Anna Viktorovna

Symbiotic interface in the development of legume nodules

Scientific Specialty 1.5.21. Plant physiology and biochemistry

Thesis for the Degree of Doctor of Biological Sciences

Translation from Russian

Scientific Advisor:

Doctor of Biological Sciences
Tsyganov Viktor Evgen’evich

Saint Petersburg
2024

TABLE OF CONTENTS

INTRODUCTION. Symbiotic interface in legume nodules — modifications during colonization and differentiation

In the course of evolution, plants have utilized certain functional capabilities of microorganisms to expand their adaptive potential. Thus, legumes and actinorhizal plants belonging to the nitrogen-fixing clade FaFaCuRo and including four orders — *Fabales*, *Fagales*, *Curcubitales*, and *Rosales* [Forest, Chase, 2009], have acquired the ability to develop endosymbiotic relationships with proteobacteria called rhizobia and actinobacteria from the genus *Frankia* that reduce atmospheric nitrogen to ammonia [van Rhijn, Vanderleyden, 1995; Pawlowski, Sirrenberg, 2003]. The order *Fabales* includes the most important legume crops such as soybean, peanut, pea, chickpea, alfalfa and many others. Legumes are considered key for the development of ecologically oriented agriculture because of their high protein content and low dependence on mineral nitrogen fertilizers, due to their ability to fix atmospheric nitrogen [Considine et al., 2017; Adams et al., 2018]. Symbiotic bacteria fix nitrogen in a reaction catalyzed by the enzyme nitrogenase and provide it to plants in exchange for carbon sources. One of the features associated with symbiotic interaction is the formation of specialized organs called nodules, which provide a favorable microenvironment for bacterial nitrogenase activity [Oldroyd et al., 2011]. The placement of bacteria within plant cells is key to the success of the symbiosis and is one of the most unique features of this mutualistic association.

Two parallel but interrelated processes ensure the nodule development: nodule organogenesis and its infection (colonization) by rhizobia [Guinel, 2009]. In all the diversity of symbiotic nodules, two main types are usually distinguished: determinate and indeterminate [Guinel, 2009]. The first type of nodules is characteristic of tropical legumes and the second type of nodules is characteristic of temperate legumes. During organogenesis of indeterminate nodules, Nod-factors (signaling lipochito-oligosaccharides secreted by rhizobia) induce cell division in the pericycle and inner root cortex [Timmers et al., 1999], while during the formation of determinate nodules, cell division resumes in the outer root cortex [van Spronsen et al., 2001].

During the development of legume-rhizobial symbiosis, bacteria colonizing plant roots follow different routes using a variety of penetration mechanisms determined by the host plant [Ibáñez et al., 2016]. The best characterized is the infection process through root hairs, which is a common mechanism for about 75% of all legume plant species [Sprent et al., 2017]. Rhizobial infection proceeds in at least three steps: penetration through the epidermis, spread between cortical cells and intracellular penetration of rhizobia [Brewin, 1991]. In this case, the infection process is governed by a highly regulated genetic program that ensures controlled colonization of plant cells [Guinel and Geil, 2002; Tsyganov et al., 2002; Madsen et al., 2010] and consistent modification of plant-rhizobia interactions. Thus, nodule development requires the synthesis and recognition of signaling and other molecules that are produced by both bacterial and plant partners [Zipfel and Oldroyd, 2017]. Symbiotic interactions, in which plant-microorganism metabolism occurs, achieve full functionality through the development of an extensive contact surface between host and microsymbiont — the symbiotic interface [Rich et al., 2014].

The spread of infection from the epidermis to the cortex and further to the primordium of the developing nodule is mediated by tubular structures, so-called infection threads [Brewin, 2004; Gage, 2004]. Infection threads are unique invasive structures of plant origin that are capable of crossing cellular boundaries [*Tsyganova et al., 2021*]. This process continues in many cell layers as a tree-like network [Monahan-Giovanelli et al., 2006]. The infection thread consists of various components of both plant (cell wall polysaccharides, intercellular matrix glycoproteins, various enzymes, receptors and structural proteins of the plasma membrane) and bacterial origin (bacterial surface polysaccharides and secreted proteins). The direct interaction between plant and bacterial cell surfaces plays a crucial role in the formation of the infection thread. At each stage, the plant-microbial interaction surface (symbiotic interface) must adapt to allow the bacteria to exist in the new environment and to prevent the development of host plant defense responses [*Tsyganova et al., 2021*].

The molecular mechanisms of infection thread growth in the root cortex and in infected nodule tissue are hardly described, and our understanding is based on imaging.

The distribution of polysaccharides, cell wall proteins and matrix glycoproteins of infection threads was mainly investigated using antibodies, cytochemical reagents, and enzymes [*Tsyganova et al., 2021*]. Using mutants of model legumes with defects in the growth and development of infection threads in combination with monoclonal antibodies that react with components of the symbiotic interface in infection threads, it became possible to analyze surface interactions between symbiotic partners [*Tsyganova et al., 2021*].

The growth of the infection thread requires the construction of a new cell wall, as well as rearrangement with local degradation and subsequent new synthesis of the cell wall when the infection thread passes the cell walls of host cells. Numerous bacterial [Robledo et al., 2008; Lionetti et al., 2012; Pogorelko et al., 2013] and plant cell wall-modifying enzymes, such as pectin methylesterases [Lievens et al, 2002; Rodríguez-Llorente et al., 2004], pectate lyases [Xie et al., 2012], polygalacturonase [Muñoz et al., 1998; Rodríguez-Llorente et al., 2003] and endo-β-1,4-glucanase [Sujkowska et al., 2011] are involved in this process.

Bacterial components of plant-microbial interaction surface are also actively involved in the growth and development of infection thread [*Tsyganova, Tsyganov, 2012*]. There is a large amount of experimental data proving that the production of exopolysaccharides (EPS) by rhizobia forming nodules of indeterminate type is necessary for root hair curling, proper infection thread formation, bacterial release, bacteroid differentiation and efficient nodule formation [Fraysse et al., 2003; Skorupska et al., 2006; Cho et al., 2014; Zgadzaj et al., 2015]. Capsular polysaccharides (KPS) may play a role in indeterminate [Kiss et al., 2001; Le Quéré et al., 2006] and determinate nodulation [Parada et al., 2006]. Lipopolysaccharide (LPS) deficiency in bacteria during indeterminate nodule formation can lead to both a lack of effect (Nod^+Fix^+) and an inability of bacteria to release from infection threads (Nod^+Fix^-) [Campbell et al., 2002; Ferguson et al., 2002; Keating et al., 2002].

Infection is completed by the placement of rhizobia in the cells of the developing nodule in a process morphologically resembling endocytosis, but similar in molecular components to cell exocytosis [Ivanov et al., 2012]. The exact mechanism for triggering

the transition of rhizobia from the extracellular space (apoplast) to intracellular existence is not yet known, but it is associated with further remodeling of the cell wall. This is done by forming outgrowths devoid of cell wall at the tip of an infection thread that has entered the cell, so-called infection droplets, from which rhizobia are locally released to form symbiosomes surrounded by a membrane derived from the plasma membrane of the host cell [Coba de la Peña et al., 2018]. Glycoproteins associated with symbiosome and plasma membranes, such as the lectin-like glycoprotein in *P. sativum* NLEC1 [Kardailsky et al., 1996; Davies et al., 1997; Bolaños et al., 2001; Redondo-Nieto et al, 2008], an arabinogalactan-like glycolipid protein recognized by the MAC206 antibody [Bolaños et al., 2001; Bolaños et al., 2004; Redondo-Nieto et al, 2008], the synaptotagmins MtSyt1, MtSyt2, and MtSyt3 of *M. truncatula* [Gavrin et al., 2017], and glycosylated forms of an inositol-containing phospholipid recognized by the JIM18 antibody [Perotto et al., 1995] may play a direct role in surface interactions with rhizobia. On the rhizobia side, the *BacA* gene, which controls modification of the bacterial cell wall, including the development of lipid A derivatives with long-chain fatty acids, is involved in the process of bacterial release from infection droplets [Ferguson et al., 2002].

After rhizobia release into the plant cell, the bacteria differentiate into bacteroids inside the host cytoplasm [Oldroyd et al., 2011]. In this process, the bacteroids are surrounded by a plant membrane enriched with bacterial proteins [Parniske, 2008]. Bacteroids are surrounded by a peribacteroid space, which is filled with proteins of both macro- and microsymbionts, suggesting that this space is the basis for symbiotic nitrogen fixation [Emerich and Krishnan, 2014].

Unlike cell walls, for which glycoproteins are thought to be involved in binding their components to the underlying plasma membrane via non-covalent binding [Seifert and Roberts, 2007; Su and Higashiyama, 2018], the symbiosome membrane does not bind to plant cell wall components such as pectins, xyloglucan and cellulose. Symbiosome membrane glycoproteins can interact with surface polysaccharides of the bacterial outer membrane, particularly LPS, which are major contributors to the symbiotic interface of symbiosomes by rhizobia [Haag et al., 2013; Bourassa et al., 2017].

Nodule senescence is the final stage of nodule function, during which symbiosomes and infected cells are destroyed and the plant reuses nutrients accumulated in nodules. During senescence, the cells of both symbiotic partners are degraded [Brewin, 1991]: there is an increase in the electron transparency of the cytoplasm as a result of plasmolysis, there is an increase in cellular detritus, and the symbiosomes are the last to be destructed [Timmers et al., 2000; Van de Velde et al., 2006]. Programmed senescence of nitrogen-fixing bacteroids is an integral part of the developmental sequence of indeterminate nodules [Vasse et al., 1990], but free-living rhizobia are always present within the nodule and they can grow saprophytically in senescent tissues [Brewin, 1991].

Despite the identification of components of the signaling cascade, that initiates infection and the transcriptional network responsible for host cell reprogramming [Mbengue et al., 2020], the analysis of complex cell wall components such as polysaccharides and structural proteins is difficult due to the structural complexity of these macromolecules. Therefore, along with molecular biological research methods, the use of monoclonal antibodies that react with components of the symbiotic interface, including plant and bacterial cell wall polysaccharides, glycoproteins and glycolipids, is an adequate method to study it [Perotto et al., 1991; Brewin, 2004; Verhertbruggen et al., 2017; Rydahl et al., 2018].

In the case of legume-rhizobial symbiosis, the interactions of molecules in the symbiotic interface are complex, multifaceted and mostly poorly understood. Some evidence suggests that infection of tissues and cells by rhizobia activates legume plant genes that are also expressed in plant responses to other forms of biotic and abiotic stress. As a result, the colonization process appears to depend on the suppression of host defence responses that would otherwise halt infection progression, causing interruption of infection thread growth, lack of rhizobia release into the cytoplasm of the plant cell or early senescence of symbiosomes.

Thus, the **purpose** of this work was to study the component composition of the symbiotic interface and its changes during the development of nitrogen-fixing nodules of legumes.

The study was aimed at solving the following **tasks**:

1. To analyze the composition and distribution of individual components of plant cell wall and infection thread wall in legume nodules.
2. To identify changes in the component composition of the intercellular matrix and infection thread matrix in legume nodules.
3. To determine markers of symbiotic symbiosome interface development in nitrogen-fixing nodules of legumes.
4. To study the modification of the component composition of the symbiotic interface in symbiotically inefficient mutants of *Pisum sativum* and *Medicago truncatula*.
5. To identify characteristic features of the plant defense response under ineffective symbiotic interaction in *P. sativum* nodules.
6. To identify the role of reactive oxygen species, antioxidant system, phytohormones and vesicular transport in the development of nitrogen-fixing nodule of *P. sativum* at late stages.

The novelty of the work.

For the first time, a comprehensive study of the components of the symbiotic interface in nitrogen-fixing nodules of several species of legumes forming nodules of different types was carried out using immunocytochemical analysis. The presence of both general and species-specific features of formation and modification of plant apoplast in legume nodules was shown. Thus, the presence of highly methyl esterified homogalacturonan and rhamnogalacturonan I (its polysaccharide backbone and arabinan side chain) in all cell walls and infection thread walls in all studied legume species was shown. The most striking features of the symbiotic interface in indeterminate nodules include the presence of the linear galactan side chain of rhamnogalacturonan I in the walls of infection threads in *P. sativum*, *Galega orientalis*, and *Vavilovia formosa*. Species-specific features include the absence of fucosylated xyloglucan in cell walls in *P. sativum* nodules, its presence in cell walls of uninfected cells in *M. truncatula* nodules and in all cell walls in *V. formosa* nodules. Variations were observed in the localisation of low methyl esterified homogalacturonan in the walls of infection threads in *Vicia villosa* nodules, in the cell walls of uninfected cells in *G. orientalis* nodules (as well as Ca^{2+}-bound homogalacturonan) and in all cell walls and infection thread walls in *V. formosa*.

The unbranched rhamnogalacturonan I backbone was predominantly detected in meristematic cells in *P. sativum* nodules and in cell walls of uninfected cells in *G. orientalis* nodules. The presence of the galactan side chain of rhamnogalacturonan I in the cell walls of uninfected cells and the predominant accumulation of fucosylated xyloglucan in the infection thread walls should be considered as striking species-specific features of the symbiotic interface of determinate nodules (using *Glycine max* as an example).

Immunocytochemical analysis of symbiosome membranes revealed the dependence of the presence and localization of arabinan epitopes on the degree of symbiosome membrane maturity. Species-specific markers of symbiosome membrane maturation in *P. sativum* nodules — arabinoagalactan proteins with a glycosylphosphatidylinositol anchor — were identified for the first time.

New manifestations of defense reactions at late stages of ineffective nodule formation were revealed. Increased stiffness of the infection thread wall with increased accumulation of low methyl esterified homogalacturonan in the mutants of *P. sativum* (SGEFix$^-$-2 (*Pssym33-3*)) and *M. truncatula* (TR3 (*Mtipd3*)) with orthologous genes of the key transcription factor of nodule formation CYCLOPS/IPD3, characterized by ‘locked’ infection threads and absence of bacterial release into the cytoplasm of plant cells. A pathogen-like defense response was demonstrated in the *P. sativum* mutant RisFixV (*Pssym42*), expressed as the accumulation of callose in cell walls and infection thread walls and encapsulation of degenerating bacteroids by de-esterified homogalacturonan. The accumulation of cell wall material, namely rhamnogalacturonan I (especially the galactan side chain), highly methyl esterified homogalacturonan and suberin around the vacuole in a *P. sativum* mutant SGEFix$^-$-2 (*Pssym33-3*) characterized by sporadic bacterial release from infection droplets was shown.

The participation of reactive oxygen species (H_2O_2), antioxidant system (glutathione), phytohormones (trans-zeatin riboside and gibberellic acid GA_3) and vesicular transport in the development and modification of symbiotic interface in *P. sativum* nodules in effective and ineffective interaction was shown for the first time.

Theoretical and practical significance

The significance of the modification of the symbiotic interface during the development of nitrogen-fixing nodule, which plays a role both in the natural ontogeny of infected cells and in the activation of defense reactions in case of ineffective symbiotic interaction, has been shown. A methodology for using immunocytochemical analysis to identify and localize symbiotic interface components and positional information during the infection process has been developed. Using approaches of comparative cell biology of legumes, common and species-specific features of the modification of the symbiotic interface were identified both during the growth of the infection thread and during the formation of temporary cell organelles of microbial origin — symbiosomes.

Mechanisms of defense response development in case of ineffective symbiotic interaction have been studied, which can become theoretical bases for the creation of highly effective plant-microbe interactions. A model of infection thread functioning in a mature nodule has been proposed, which can be used for further study of legume-rhizobial symbiosis and creation of symbiotic associations in non-legume plants. The results obtained in the course of the thesis can be used in lecture courses at the Faculty of Biology, Saint Petersburg State University.

Degree of reliability and approbation of the results

High reliability of the obtained results is provided by the use of adequate genetic models, repeated repetitions of experiments, the use of modern high-precision precision equipment, statistical processing of the obtained results. Materials of the thesis were presented at domestic and international conferences, including: VI congress of OFR (2007 Syktyvkar), 8th European Conference on nitrogen fixation (2008, Ghent, Belgium), 11th European Conference on Nitrogen Fixation (2014, Tenerife, Spain), 3rd International Symposium on Signalling and Plant Behaviour (2015, Paris, France), VIII Congress of OFR (2015, Petrozavodsk), 4th International Symposium on Signalling and Plant Behaviour (2016. St. Petersburg), 20th International Congress on Nitrogen Fixation (2017 Granada, Spain), I International Conference 'Plants and Microorganisms: Biotechnology of the Future' (PLAMIC2018) (2018 Ufa), 13th European Conference on Nitrogen Fixation (2018. Stockholm, Sweden), International Congress ‘VII Congress of

the Vavilov Society of Geneticists and Breeders dedicated to the 100th anniversary of the Department of Genetics, SPbSU, and associated symposia' (2019 St. Petersburg), IX Congress of OFR (2019 Kazan), II International Conference 'Plants and Microorganisms: Biotechnology of the Future' (PLAMIC2020) (2020. Saratov), III International Scientific and Practical Conference 'Cell Biology and Plant Biotechnology' (2022, Minsk, Republic of Belarus), III International Conference 'Plants and Microorganisms: Biotechnology of the Future' (PLAMIC2022) (2022, St. Petersburg), X Congress of OFR (2023, Ufa).

The author's personal contribution consists in planning the research, setting the goal and objectives, analyzing and summarizing the available literature data, determining the research methods, direct participation in data collection and processing during the experiments, in statistical processing, analysis, synthesis and interpretation of the obtained data, formulation and interpretation of conclusions, as well as in writing articles published on the topic of the thesis work and presenting the results at scientific conferences. In addition, the author supervised the experimental work on the study of morphology and component composition of the symbiotic interface used in the thesis research, conducted in the laboratory of molecular and cell biology of ARRIAM. The supervision consisted of the study design, participation in most of the experiments, data processing and interpretation, manuscript editing and preparation of responses in correspondence with reviewers. Experiments on pectin methylesterase gene expression were performed jointly with K. A. Ivanova and P. G. Kusakin; immunogold studies were performed jointly with E. V. Seliverstova. A detailed description of the methods and approaches used is given in the articles published on the results of the work. The studies were carried out at the John Innes Centre (Norwich, UK), the Genomic Technologies, Proteomics and Cell Biology Collective Use Centre of ARRIAM, and the Centre for Development of Molecular and Cellular Technologies of the SPbSU Science Park.

The results presented in this thesis were supported by RSF grants (16-16-10035, 14-24-00135, 17-76-30016, 23-16-00090); RFBR (14-04-00383-a, 13-04-40344-N, 11-04-01675-a, 08-04-01656-a, 08-04-90051-Bel_a, 05-04-49105-a); Russian Presidential Grants Council (NSh-6759. 2016.4, NSh-4603.2014.4, NSh-337.2012.4, NSh-3440.2010.04, NSh-5399.2008.04, NSh-9744.2006. 04); INTAS (YSF 04-83-3196);

Ministry of Education and Science (02.442.11.7130, 16.552.11.7085, 16.551.11.7047, 02.740.11.0276, P290, P1301, №8056, №8109).

Main scientific results

1. The component composition and modification of the symbiotic interface (cell walls) in nodules of *P. sativum* [*Ivanova et al., 2015* (section ‘Immunocytological localisation of unesterified pectin in IT wall in the symbiotic nodules of ineffective pea mutants’, Figure 1, Table 3); *Tsyganova et al, 2019c; Tsyganova et al., 2023b; Tsyganov, Tsyganova, 2020*], *M. truncatula* [*Tsyganova et al., 2019c; Tsyganova et al., 2023b*], *G. orientalis* [*Tsyganova et al., 2023a*], *G. max* [*Tsyganova et al., 2023a*] were studied using an immunocytochemical method. The personal contribution is at least 75%. General and species-specific changes of cell walls and infection thread walls in nodules of the studied legume species under effective and ineffective interaction were revealed.

2. The composition of the infection thread matrix and its modifications during development and ineffective interactions have been studied in *P. sativum* [*Brewin et al, 2008; Tsyganova et al., 2009; Tsyganova et al., 2019c; Tsyganov, Tsyganova, 2020; Tsyganova et al., 2023b*], *M. truncatula* [*Tsyganova et al., 2023b*], *G. orientalis* [*Tsyganova et al., 2023a*] and *G. max* [*Tsyganova et al., 2023a*]. The personal contribution is at least 90%.

3. Markers of symbiosome differentiation have been identified [*Tsyganova et al., 2018* (section ‘Differentiation of symbiosomes’)] — arabinans in juvenile and poorly differentiated symbiosomes in nodules of *P. sativum* [*Tsyganova et al., 2023b*], *M. truncatula* [*Tsyganova et al., 2023b*], *G. orientalis* [*Tsyganova et al, 2023a*] and *G. max* [*Tsyganova et al., 2023a*], and arabinogalactan proteins with a glycosylphosphatidylinositol anchor in mature symbiosomes in *P. sativum* nodules [*Tsyganova et al., 2019c*]. The personal contribution is at least 80%.

4. Using our own research and literature data, a model of infection thread functioning in indeterminate nodules of legumes was created [*Tsyganova et al., 2011; Tsyganova, Tsyganov, 2012; Tsyganova, Tsyganov, 2019; Tsyganova, Tsyganov, 2019b; Tsyganova et al., 2021*]. The personal contribution is at least 80%.

5. A variety of plant defence reactions in nodules of symbiotically ineffective *P. sativum* mutants were shown: stiffening of the infection thread wall [*Ivanova et al., 2015* (section ‘Immunocytological localisation of unesterified pectin in IT wall in the symbiotic nodules of ineffective pea mutants’, Figure 1, Table 3)], deposits of callose and suberin in cell walls and walls of infection threads [*Ivanova et al, 2015* (section ‘Histochemical localisation of suberin and callose depositions in the symbiotic nodules of ineffective pea mutants’, Figures 2,3,4); *Tsyganov et al., 2012*], deposition of cell wall material around the vacuole [*Tsyganova et al, 2019b*], encapsulation of degenerating bacteroidetes by pectins [*Ivanova et al., 2015* (section ‘Immunocytological localisation of unesterified pectin in IT wall in the symbiotic nodules of ineffective pea mutants’, Figure 1i)], degeneration of bacteria inside ‘locked’ infection threads [*Tsyganov et al, 2011; Tsyganov et al., 2014; Tsyganova et al., 2019*], development of oxidative stress [*Tsyganova et al., 2009; Provorov et al., 2012*] and premature senescence of symbiotic structures [*Serova et al., 2018* (section ‘Nodule histological and ultrastructural organisation in mutants SGEFix$^-$-3 (*sym26*) and SGEFix$^-$-7 (*sym27*)’, Figures 1,2)]. Personal contribution is at least 80%.

6. We studied the participation in the development and modification of the symbiotic interface (infection thread walls and symbiosomes) in *P. sativum* nodules in the effective and ineffective interaction of H_2O_2 [*Brewin et al., 2008; Tsiganova et al., 2009; Provorov et al., 2012* (section ‘Host control over the population dynamics of endosymbiotic bacteria’, second paragraph, Figure 2)], glutathione [*Ivanova et al, 2022* (section ‘Immunogold localisation of the reduced form of glutathione in the infection structures of wild-type and mutant nodules’, Figure 4, Table 2)], cytokinins (trans-zeatin riboside) [*Dolgikh et al, 2020* (section ‘Immunolocalisation of trans-zeatin riboside and N6-isopentenyladenosine in the wild type and mutants blocked at different stages of nodule development’, Figure 6)], gibberellins (GA_3) [*Serova et al, 2019* (section ‘Immunogold localisation of GA_3 in nodules of wild-type SGE and mutant SGEFix$^-$-3 (*sym26*)’, Figure 5, Table 2)] and endoplasmic reticulum [*Tsyganova, Tsyganov, 2019a*]. The personal contribution is at least 75%.

The following statements are presented for the consideration

1. The symbiotic interface (apoplast and membranes) is a complex and mobile formation in nitrogen-fixing nodules of legumes that has both common and species-specific features.

2. The development of symbiotic legume nodule is accompanied by ontogenetic modifications of the symbiotic interface: the degree of methylation of homogalacturonan molecules changes in cell walls, the side chains and block character of the rhamnogalacturonan I backbone are modified, and the composition of hemicelluloses changes.

3. Arabinans and arabinogalactan proteins can serve as markers of symbiosome differentiation in indeterminate nodules.

4. The inefficient nature of symbiosis caused by mutations in the genes *PsSym33*, encoding the key transcription factor CYCLOPS/IPD3, and *Pssym42* activate a wide range of defense responses aimed at isolating the microsymbiont in infection threads and infected cells with the development of premature senescence of the symbiotic nodule of *P. sativum*.

5. Hydrogen peroxide is involved in increasing the stiffness of the infection thread wall during its growth in *P. sativum* nodules and the development of oxidative stress during ineffective interaction.

The thesis includes an Introduction, four Chapters, a Conclusion and an Appendix, consists of 122 pages, and contains 4 figures in the text and 29 figures in Appendix A, 10 tables and 198 references.

For better orientation in the system of literary references, references to the used literary data are given in regular font, and references to the works with the participation of the author, in which the data, which are the subject of the thesis research, are published, are given in italics.

CHAPTER 1. Modification of cell walls and infection thread walls in legume nodules of different types

Plant cell walls are a specialized extracellular matrix composed mainly of carbohydrate polymers and serve as the dynamic support structure of plants [Cosgrove, 2005]. The primary cell wall surrounding actively growing plant cells is composed of cellulose, hemicelluloses, pectins and structural glycoproteins, and contains a wide range of enzymes and other proteins that can modify cell wall structure or respond to internal and external stimuli [Keegstra, 2010; Anderson, 2015]. Cellulose-hemicellulose networks act as major load-bearing components of plant cell walls [Wang et al., 2013], and pectins have important functions in wall architecture, cell growth, and tissue morphogenesis [Palin and Geitmann, 2012; Wolf and Greiner, 2012; Anderson, 2015].

The data accumulated in recent years indicate the variability of cell wall composition in symbiotic nodules of legumes and the fine regulation of its structure [*Tsyganova et al., 2019c; Tsyganova et al., 2021; Tsyganova et al., 2023a; Tsyganova et al., 2023b*]. The study of cell walls using molecular genetic approaches, including immunochemical methods, has formed an idea of the dynamism of the cell wall structure in symbiotic nodules, allowed characterization of its components and their modification depending on the developmental stage and spatial arrangement of cells and infection structures [*Tsyganova et al., 2021; Tsyganova et al., 2023a; Tsyganova et al., 2023b*].

Homogalacturonan (HG) has been most studied in the formation and functioning of the symbiotic interface in nodules of legumes [*Tsyganova, Tsyganov, 2019b*], which is explained by the presence of highly specific monoclonal antibodies to this polysaccharide. The functions of HG in nodules, as in other plant organs, are determined by the degree of its methylation [Wolf et al., 2009; Su, 2023; Su et al., 2023]. The distribution of HG has been studied in detail in various legumes inoculated with rhizobial symbionts. Thus, in the symbiotic nodules of *P. sativum* [VandenBosch et al., 1989; Rae et al., 1992; *Ivanova et al., 2015; Tsyganova et al., 2019c; Tsyganova et al., 2023b*], *M. truncatula* [*Tsyganova et al, 2019c; Tsyganova et al., 2023b*], *Vicia hirsuta* [Rae et al.,

1992] and *V. villosa*, *G. orientalis* [*Tsyganova et al., 2023a*], *G. max* [Gavrin et al., 2016; *Tsyganova et al., 2023a*], *Phaseolus vulgaris* [Rae et al., 1992], *Lupinus luteus* [Wilmowicz et al., 2022], *Chidlowia sanguinea*, *Entada polystachya*, *Erythrophleum* spp, *Moldenhawera* spp. and *Pentaclethra macroloba* [de Faria et al., 2022] and *V. formosa*, the presence of HGs with different degrees of methyl esterification has been shown both in cell walls and in the walls of infection and fixation threads.

The degree of HG methylation is regulated by the plant, and there is a tissue-specific and spatiotemporal pattern of their localization [Vincken et al., 2003; Anderson, 2015; Levesque-Tremblay et al., 2015]. Studies using antibodies against highly methylated (JIM7 and LM20) or low methylated HG (JIM5 and LM19) have shown that the distribution of HG with different methylation levels can vary greatly between neighbouring sites in symbiotic nodule tissues, indicating its important role in cell development [Gavrin et al, 2016; *Tsyganova et al., 2019c;* Su et al., 2023; *Tsyganova et al., 2023a; Tsyganova et al., 2023b*].

During cell differentiation, HG is synthesized by the plant cell in the Golgi apparatus, from where it is transported to the cell wall via secretory vesicles. During synthesis, the carboxyl groups of galacturonic acid are methyl esterified, and it is in this form (methyl esterified HG) that pectins are integrated into the cell wall, which enables plant cell growth [Mohnen, 2008; Anderson, 2015]. In legume nodules forming different nodule types, highly methyl-esterified HG is the predominant pectin in all cell walls and infection thread walls (Figure A.1) and is present at all stages of nodule development (Figure A.2A-D) [*Tsyganova et al., 2019c; Tsyganova and Tsyganov, 2019b; Tsyganova et al., 2023a; Tsyganova et al., 2023b*], consistent with isodiametrically growing cells. At the same time, some deviations in the degree of HG methylation were observed in mutants blocked at different stages of development of infection structures, in particular infection threads. Thus, in mutants for the orthologous genes *MtEfd* and *PsSym40*, highly methylated HG was either completely absent in the meristem or was detected at the junctions of the three cells (Figure A.2G,H), although it was present in the infection zone (Figure A.2I,J). In mutants for the orthologous *MtIpd3* and *PsSym33* genes, highly methyl esterified HG was not detected in cell walls and infection thread walls (Figure A.2E,F).

The latter observation can be explained by the abnormal thickening of infection threads and cell walls characteristic of these mutants [Tsyganov et al., 1998; *Ivanova et al., 2015; Tsyganova et al., 2019c; Tsyganova et al., 2023b*]. In addition, using the mutant SGEFix$^-$-3 (*Pssym26*), which is characterized by early senescence, it was shown that in the senescence zone, highly methyl esterified HG disappears from the cell walls of degrading infected cells, remaining in the cell walls of uninfected cells (Figure A.2K,L).

Once in the cell wall, methylated HGs can undergo demethylesterification under the action of pectin methylesterases (PMEs) and transform into de-esterified pectins [Palin and Geitmann, 2012; Levesque-Tremblay et al., 2015]. PME activity can be inhibited by proteins called PME inhibitors [Giovane et al., 2004]. Unesterified HGs can either bind Ca^{2+} to form dimeric 'egg box'-like structures that contribute to cell wall stiffness [Wormit, Usadel, 2018; Cao et al., 2020], or they can be cleaved by pectate lyases and polygalacturonases, causing cell wall loosening [Wormit, Usadel, 2018].

The study of low methyl esterified HG revealed differences in the localisation and distribution of this pectin among legume species (Figure A.3). Thus, low methyl esterified HG in nodules of *V. formosa* and *G. max* was localized ubiquitously in cell walls and infection thread walls (Figure A.3D,F), while in nodules of *M. truncatula* and *V. villosa* it was observed mainly at the junctions of three cells and in infection thread walls (Figure A.3B,E) [*Tsyganova et al., 2019c*]. In *G. orientalis* nodules, quantitative analysis revealed that this HG accumulated to a greater extent in the cell walls of uninfected cells (82.08±7.97 compared to cell walls of infected cells, 63.64±13.09, $p < 0.05$) (Figure A.3C) [*Tsyganova et al., 2023a*]. When another antibody was used to detect low methylated HG in nodules of *P. sativum* and *M. truncatula*, it was shown that fully demethylated HG in the meristem was present at the junctions of the three cells (Figure A.4A,B), in the infection zone mainly in the walls of the infection threads (Figure A.4A,B), and in the nitrogen-fixing zone in the cell walls (Figure A.4C,D) [*Tsyganova et al., 2023b*].

HG demethylation is carried out by PME enzymes, which are widely represented in plants [Levesque-Tremblay et al., 2015]. Analysis of the expression patterns of different PME genes revealed several genes showing significant expression levels in *G.*

max nodules (*GmPME11*, *GmPME58*, *GmPME70*, *GmPME105*; Figure 1). The *GmPME58* and *GmPME105* genes showed an increase in their activity in both roots and nodules, but their expression in nodules was many times higher than in root samples (Figure 1). It is worth noting that in a recent study of PME genes in soybean cultivar Williams 82, the expression values of some genes in nodules and roots differed [Wang et al., 2021]. Thus, *GmPME11* was activated predominantly in nodules. The differences obtained are probably related to the use of different genotypes of *G. max*.

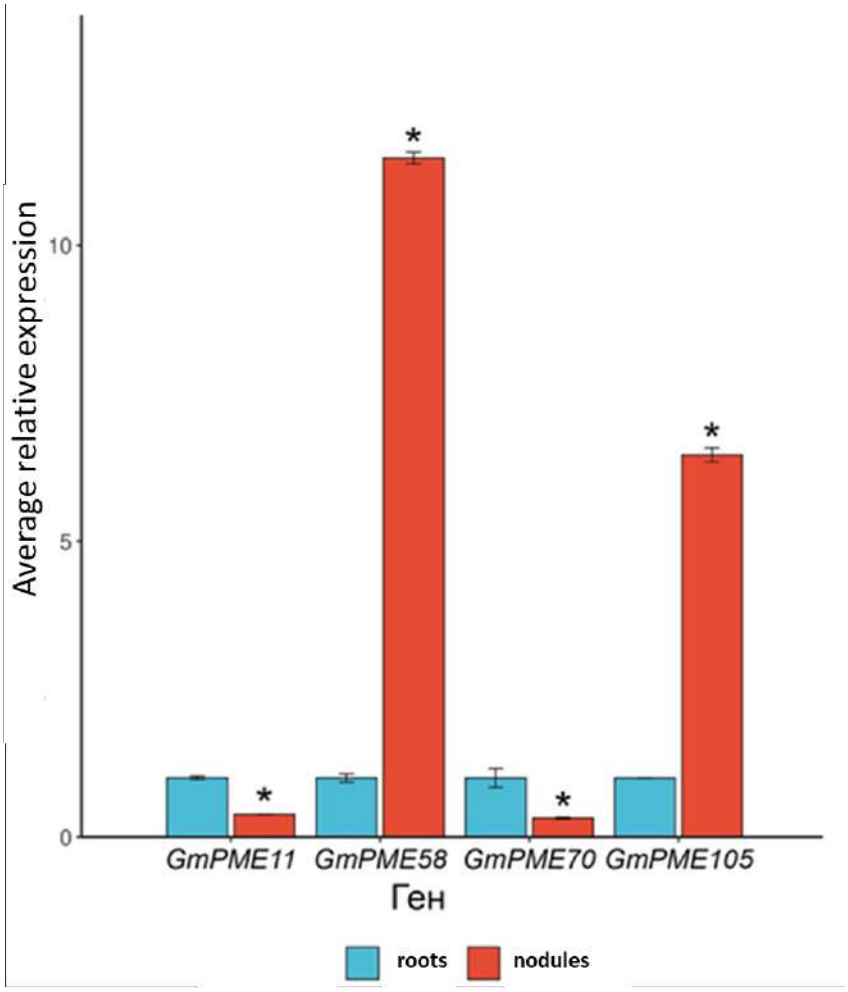

Relative expression level of pectin methylesterase genes *GmPME11*, *GmPME58*, *GmPME70*, *GmPME105* in nodules and roots of *Glycine max* line Merrill K-5892 Fiskeby V. * - statistically significant differences (t-test with adjustments for multiple comparisons, $p < 0.05$).

Figure 1 — Expression of pectin methylesterase genes in roots and nodules of *Glycine max*

In mutants of both *P. sativum* and *M. truncatula* showing abnormalities in the development of infection structures, particularly infection threads, some abnormalities in

the localization and distribution of low methylated HG were observed (Figure A.4E-L). For example, in the *P. sativum* mutant SGEFix⁻-1 (*Pssym40-1*) (characterized by hypertrophy of infection droplets), low methylated HG was more abundant in cell walls than in the wild type (Figure A.4I), and in the *M. truncatula* mutant TR3 (*Mtipd3*) (with thickened infection thread walls and no bacterial release), this HG was more represented in infection thread walls than in cell walls (Figure A.4E). In the *P. sativum* mutant SGEFix⁻-3 (*Pssym26*) characterized by early senescence, HG with a low degree of methyl esterification was more abundant in the walls of degenerating cells (Figure A.4J) [*Tsyganova et al., 2019c; Tsyganova et al., 2023b*].

Electron microscopic analysis of the localization of low-methylated HG showed significant differences in its distribution in the infection thread walls between different genotypes of *P. sativum* (Figure A.5) [*Ivanova et al., 2015; Tsyganova et al., 2019c*] and *M. truncatula* [*Tsyganova et al., 2019c*]. Thus, in *P. sativum* nodules of wild-type SGE, low-methylated HG was uniformly distributed in the infection thread wall (Figure A.5A,B) [*Ivanova et al., 2015*]. A similar distribution was characteristic of *P. sativum* nodules of wild-types Finale, Sprint-2, and the mutant SGEFix⁻-1 (*Pssym40-1*), and its level was slightly reduced in the mutants SGEFix⁻-3 (*Pssym26*) and Sprint-2Fix⁻ (*Pssym31*) compared with the corresponding wild types (Table 1) [*Tsyganova et al., 2019c*]. Single and double mutants of *P. sativum* for the *PsSym33* gene showed increased deposition of low-methylated HG in the infection thread walls (Figure A.5C-F, Table 1) [*Ivanova et al., 2015*]. In the mutant RisFixV (*Pssym42*), the JIM5 label was localized in excessively thickened infection thread walls, but it formed clusters that were unevenly distributed (Figure A.5G,H; Table 1) [*Ivanova et al., 2015*]. It is possible that this pattern of distribution of HG with a low degree of methylesterification may be due to the activation of the cellular defense response in these mutants. It was previously reported that pectin methyl esterification plays a role in the interaction of plants with pathogens and affects plant resistance to diseases [Lionetti et al., 2012].

To elucidate the role of PMEs in regulating HG methylation in different *P. sativum* genotypes, we analyzed the expression of members of the multigene PME family acting

at different stages of the infection process in symbiotic nodules of wild types and mutants for the *PsSym33* and *PsSym40* genes (Figure 2).

Table 1 — Distribution of low methyl esterified homogalacturonan labeled with JIM5 antibody in the infection thread walls in 2-week-old nodules of wild-types and mutants of *Pisum sativum*

Genotypes	Mean value	SE
SGE (wild-type)	139	20,6
SGEFix⁻-1 (*Pssym40-1*)	112	18,8
SGEFix⁻-2 (*Pssym33-3*)	506[a]	25,0
RBT3 (*Pssym33-3*, *Pssym40-1*)	569[a]	39,4
RBT4 (*Pssym33-3*, *Pssym42*)	575[a]	35,7
Finale (wild-type)	157	22,4
RisFixV (*Pssym42*)	231[b]	23,7
SGE (wild-type)	123	6,5
SGEFix⁻-3 (*Pssym26*)	93[c]	8,1
Sprint-2 (wild-type)	112	8,6
Sprint-2Fix⁻ (*Pssym31*)	103[d]	8,3

Results are presented as the number of gold particles/μm^2. Mean value (n = 20–25) are shown. Letters indicate statistically significant differences (t test, P value ≤ 0.001).
[a] From the wild-type SGE and the corresponding mutant.
[b] From the wild-type Finale and the corresponding mutant.
[c] From the wild-type SGE and the corresponding mutant (second experiment).
[d] From the wild-type Sprint-2 and the corresponding mutant.

Thus, in nodules of the mutant SGEFix⁻-1 (*Pssym40-1*) of *P. sativum* the expression level of the *PsPME53* gene two weeks after inoculation, and the expression levels of *PsPME53*, *PsPME61*, and *PsPME1* genes three weeks after inoculation were lower than in the wild type. On the contrary, the expression levels of *PsPME1* gene after two weeks and *PsPME2* after three weeks were higher in mutant nodules compared with the wild type (Figure 2). In nodules of the mutant SGEFix⁻-2 (*Pssym33-3*) of *P. sativum*, the expression levels of *PsPME51*, *PsPME53*, and *PsPME61* genes two weeks after inoculation and *PsPME51*, *PsPME53*, *PsPME61*, and *PsPME1* genes three weeks after

inoculation were lower than in wild-type nodules. Conversely, the expression levels of *PsPME41*, *PsPME1* and *PsPME2* after two weeks and *PsPME2* after three weeks were higher in mutant nodules (Figure 2).

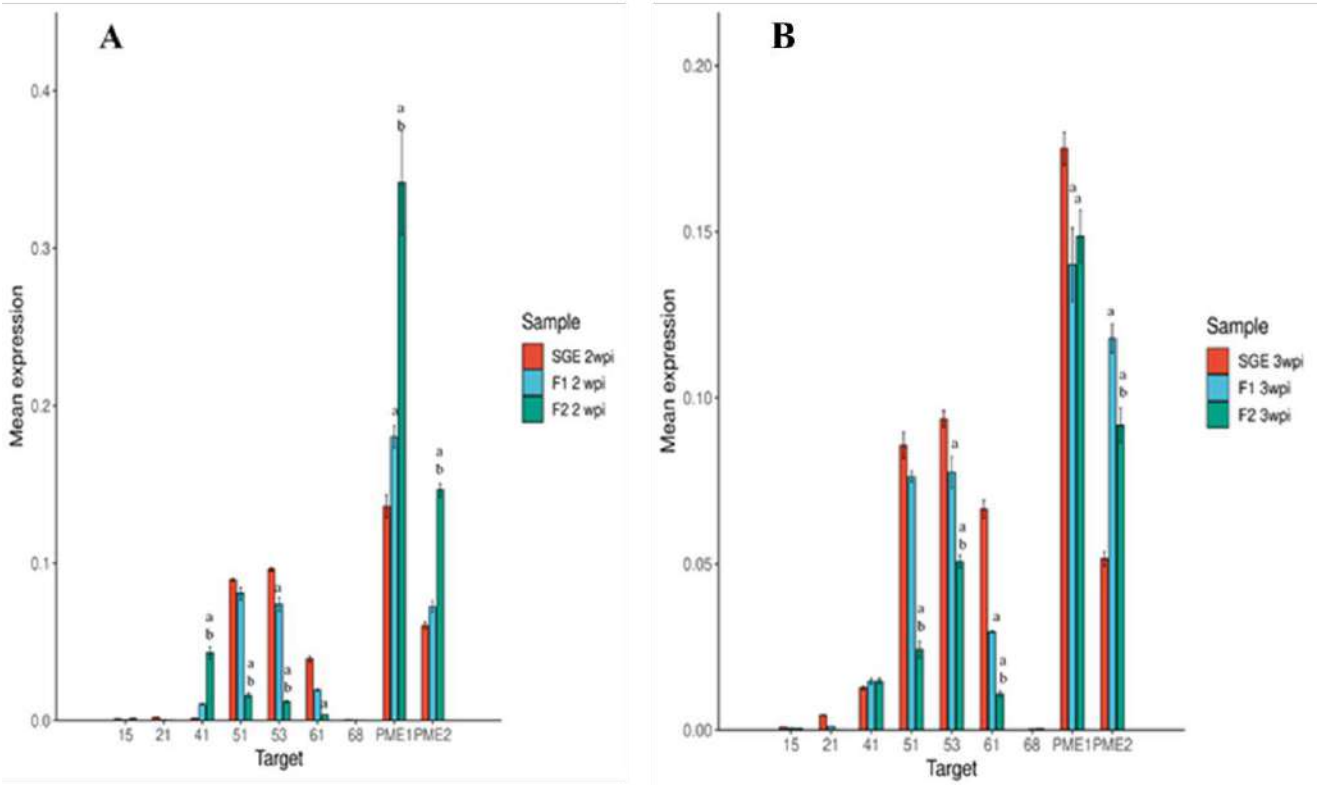

A — nodules two weeks after inoculation (2wpi). B — nodules three weeks after inoculation (3wpi). Graphs show the results of three independent experiments. Letters indicate significant differences ($p \leq 0.05$): a, between wild-type (SGE) and the mutant nodules; b, between SGEFix$^-$-1 (*Pssym40-1*) (F1) and SGEFix$^-$-2 (*Pssym33-3*) (F2) mutant nodules.

Figure 2 — Relative expression level of pectin methylesterase genes in *Pisum sativum* nodules of the wild-type (SGE) and mutants SGEFix$^-$-1 (*Pssym40-1*) (F1) and SGEFix$^-$-2 (*Pssym33-3*) (F2)

According to transcriptome analysis combined with laser microdissection, the expression level of the gene encoding the PME / PME inhibitor *PsPME41* was dramatically decreased, while the expression level of the genes encoding the PMEs / PME inhibitors *PsPME51* and *PsPME61*, as well as *PsPME53*, was increased in the late zone of infection and the nitrogen-fixation zone compared with the early infection zone in wild-type pea nodules (SGE) [Kusakin et al., 2021]. In a study of early responses to Nod factors of *Mesorhizobium loti* R7A strain in root hairs and roots of *Lotus japonicus*, PME genes, including a gene annotated as PME / PME inhibitor *LjPME41*, were identified among the

most strongly specifically induced 93 genes at 1 and 3 days after inoculation [Kelly et al., 2018]. Thus, this gene is likely involved in infection thread formation and development from the earliest stages of infection, in root hairs, and up to the formation of the mature nitrogen-fixing nodule, in the early infection zone. This correlates with the findings that the maximum level of *PsPME41* gene expression was observed at 2 weeks after inoculation in nodules of the mutant SGEFix$^-$-2 (*Pssym33-3*), characterized by the development of numerous branched infection threads, compared with wild-type and mutant SGEFix$^-$-1 (*Pssym40-1*) nodules (Figure 2A). In addition, the expression of *PsPME51*, *PsPME53*, and *PsPME61* genes was also dramatically reduced in mutant nodules compared with wild-type nodules, especially in nodules of the mutant SGEFix$^-$-2 (*Pssym33-3*), which lacks the late infection zone and nitrogen-fixing zone.

In the roots of *G. max* grown under nitrogen and phosphorus deficiency conditions, a decrease in the expression level of several PME family genes [Wang et al., 2020], annotated as PME / PME inhibitor *GmPME41*, *GmPME51*, and *GmPME53* [Nezamivand-Chegini et al., 2022], was shown. It is likely that the decreased expression of these genes in *P. sativum* mutant nodules can be at least partially explained by the development of ineffective symbiosis and deficiency of a macronutrient such as nitrogen. In addition, it is possible that the decrease in the level of *PsPME61* gene expression in nodules of the mutant SGEFix$^-$-2 (*Pssym33-3*) is associated with the activation of defense reactions associated with ineffective symbiosis [*Ivanova et al., 2015; Tsyganova et al., 2019b*].

The pH gradient created by PME1 affects the cell surface charge, and thus the changes in cell morphology and function, which may play an important role in the process of symbiotic nodule development and differentiation of its cells [Collmer and Keen, 1986; Gorshkova et al., 1997]. Since the nodules of wild-type and mutants of *P. sativum* differ in their morphology, this may explain the difference in the expression level of the *PsPME1* gene. The role of PME1 in nodule formation of *Sesbania rostrata* was revealed in interaction with its microsymbiont *Azorhizobium caulinodans* ORS571 [Lievens et al., 2002]. *In situ* localization of *SrPME1* transcripts in symbiotic nodules revealed several expression patterns indicating a role for SrPME1 in the development of vascular bundles,

cell division and growth, and in the differentiation of uninfected nodule cells [Lievens et al., 2002]. Thus, the role of PMEs in the functioning of symbiotic nodules is complex, probably due to functional redundancy within the large PME family.

The nodules of *M. truncatula* mutants showed a slightly different pattern of HG distribution with a low degree of methyl esterification in the walls of infection threads (Table 2) [*Tsyganova et al., 2019c*]. In 2-week-old nodules of all mutant genotypes analyzed, the number of HG was reduced compared with the wild type. However, in 4-week-old nodules of the *MtIpd3* gene mutant orthologous to *PsSym33* [Ovchinnikova et al., 2011], the amount of low-methyl esterified HG was higher than that of the wild type (Table 2). However, in SGEFix$^-$-2 (*Pssym33-3*) nodules, the increase in the amount of low-methylated HG was more pronounced and markedly increased in the walls of infection threads in 2-week-old nodules [*Ivanova et al., 2015*]. It should be noted that the doubling of the amount of de-esterified HG was also observed in the *M. truncatula* mutant of the *Mtdnf1-1* gene (Table 2), which is characterized by undifferentiated bacteroids [Van de Velde et al., 2010].

Table 2 — Distribution of de-esterified homogalacturonan labeled with JIM5 antibody in infection thread walls in wild-type and mutants of *Medicago truncatula*

Genotypes	Days after inoculation (DAI)	Mean value	SE
cv Jemalong A17 (wt)	13	68.4[c]	4.3
	28	84.4	2.7
Mtefd–1	11	57.1[a]	3.1
	28	59.3[b]	2.3
TR3 (*Mtipd3*)	16	47.2[ac]	3.5
	28	94.8[b]	4.0
Mtdnf1–1	13	34.5[ac]	2.7
	28	64.6[b]	4.2

Results are presented as the number of gold particles/μm^2. Mean value±SE (n=20-25) are shown. *Letters* indicate statistically significant differences (*t*-test, *P* value ≤ 0.001).
[a] From the wild-type A17 of corresponding mutant lines at 11-16 DAI.
[b] From the wild-type A17 of corresponding mutant lines at 28 DAI.
[c] Within genotype compared with 28 DAI.

In nodules of all analyzed genotypes of *P. sativum* and *M. truncatula* in all histological zones, Ca^{2+}-bound HG was detected in the infection thread walls, especially

at their penetration points with cell walls (Figure A.6) [*Tsyganova et al., 2023b*]. However, in the *P. sativum* mutant SGEFix^{-}-2 (*Pssym33-3*), unlike the *M. truncatula* mutant TR3 (*Mtipd3*), no Ca^{2+}-bound HG was detected in the walls of some infection threads (Figure A.6H).

Analysis of Ca^{2+}-bound HG localization in nodules of other legume species forming nodules of different types revealed some species specificity (Figure A.7). Thus, in determinate nodules of *G. max*, this polymer was detected in the cell walls of the endoderm (Figure A.7F), while in indeterminate nodules of *G. orientalis*, it accumulated in the junctions of three cells in the nodule parenchyma and was absent in the cell walls of meristematic and colonized cells (Figure A.7E).

Importantly, all three types of HGs were found in the infection thread walls in both nodule types, which is not surprising since demethylated and Ca^{2+}-bound HGs determine cell wall stiffness [*Ivanova et al., 2015; Tsyganova et al., 2019c*; de Faria et al., 2022; Wilmowicz et al., 2022]

Recently, the coordinated action of one of the symbiosis-specific PMEs (SyPME1) and nodule pectate lyase (NPL) has been described at sites of infection thread penetration and their transcellular passages. Their coordinated operation promotes space-limited HG changes at the intercellular interface, resulting in the creation of a specific apoplastic compartment from which bacteria penetrate into host cells. This process ensures successful intracellular promotion of infection threads in nodules [Su et al., 2023].

Another common cell wall pectin is rhamnogalacturonan I (RG-I) [*Tsyganova, Tsyganov, 2019b*]. The RG-I backbone plays an important role in the integrity and functioning of the cell wall, since degradation of RG-I under the action of hydrolases leads to its morphological changes [Pogorelko et al., 2013]. Among other pectins, the presence of RG-I has also been shown in nodules of *P. sativum*, *M. truncatula*, *G. orientalis*, *G. max*, *L. luteus*, *Erythrophleum* spp. and *P. macroloba* [*Tsyganova et al., 2019c*; de Faria et al., 2022; Wilmowicz et al., 2022; *Tsyganova et al., 2023a; Tsyganova et al., 2023b*]. The nodules showed localization of the RG-I backbone (using the CCRC-M36 antibody) (Figure A.8) [*Tsyganova et al., 2023a; Tsyganova et al., 2023b*], the linear galactan side chain (using the LM5 antibody) (Figure A.9) [*Tsyganova et al., 2019c*; de

Faria et al., 2022; Wilmowicz et al., 2022; *Tsyganova et al., 2023a*] and linear arabinan side chain (using the LM6-M antibody) [*Tsyganova et al., 2023a; Tsyganova et al., 2023b*].

Localization of RG-I using the CCRC-M36 antibody, which binds to at least three unbranched disaccharide repeats in the nodules of *P. sativum* and *M. truncatula*, clearly shows that long-chain repeats of the unbranched backbone of RG-I are widely distributed in nodules (Figure A.8) [*Tsyganova et al., 2023b*]. This polymer is localized in the cell walls of colonized and recently infected cells in the infection zone in nodules of *M. truncatula* and *P. sativum* (Figure A.8B,E). In addition, in *P. sativum* nodules, RG-I was also detected in the cell walls of meristematic cells (Figure A.8D), but the RG-I label was significantly reduced in the nitrogen fixation zone, remaining in the infection thread walls (Figure A.8F). In *G. max* nodules, the RG-I backbone was localized in small amounts in the cell walls of infected cells (Figure A.8H), while in indeterminate nodules of *G. orientalis* it was observed mainly in the cell walls of uninfected cells (Figure A.8G) [*Tsyganova et al., 2023a*]. In nodules of *V. formosa* and *V. villosa*, the RG-I backbone was detected in small amounts both in the cell walls and in the walls of infection threads (Figure A.8I-L).

RG-I is the most structurally heterogeneous of the pectins, and the number and composition of RG-I side chains vary considerably between different cell types, developmental stages, and species [Komalavilas and Mort, 1989; Silva et al., 2016]. Arabinan and galactan side chains of RG-I often have different localization patterns; in general, arabinan is predominant in juvenile cells, while growing cells contain more galactan [Willats et al., 1999; McCartney et al., 2000; McCartney et al., 2003].

Species specificity of localization and distribution of the linear galactan side chain of RG-I in nodules of M. *truncatula* and *P. sativum* has been shown [*Tsyganova et al., 2019c*]. Thus, fluorescence microscopy of the epitope of the linear (1→4)-β-D-galactan side chain of RG-I showed that this polysaccharide was detected only in the cell walls of the meristem (Figure A.9G), endoderm (Figure A.9H), and phloem in symbiotic nodules of *M. truncatula* and *P. sativum* wild-type and mutants. However, in nodules of all genotypes of *P. sativum* (Figure A.9A-F), *G. orientalis* (Figure A.9J), and *V. formosa*

(Figure A.9I), the galactan side chain label of RG-I was actively detected in the infection thread walls [*Tsyganova et al, 2019c; Tsyganova et al., 2023a*], while in *G. max* nodules (Figure A.9L), a similar label was detected in the cell walls of uninfected cells [*Tsyganova et al., 2023a*]. In contrast, the arabinan side chain of RG-I was detected in cell walls and walls of infection threads in nodules of all studied species [*Tsyganova et al., 2023a; Tsyganova et al., 2023b*].

In addition to pectins, xyloglucans (XG, hemicelluloses) are widespread and play a major role in cell wall composition. XGs are thought to cross-link cellulose microfibrils, while pectins such as HG and RG-I form a structurally diverse glue that provides flexibility or stiffness to cell walls depending on chemical modifications [Keegstra, 2010]. Fucosylation of XGs is important in plant morphogenesis. For example, the *Arabidopsis thaliana* mutant *Atmur1* of with an altered cell wall, which is characterized by dwarfism and reduced stem strength, was found to have up to 98% reduction in fucose content in cell walls [Reiter et al., 1993; Freshour et al., 2003].

In indeterminate nodules of *P. sativum* and *M. truncatula*, a certain species specificity in the localization of fucosylated XG was shown (Figure A.10) [*Tsyganova et al., 2023b*]. Thus, in nodules of *M. truncatula* in the nitrogen fixing zone, this polymer was detected in the cell wall of uninfected cells and in the walls of colonized cells and infection threads in the infection zone (Figure A.10B), whereas in nodules of *P. sativum* in the nitrogen fixed zone, the fucosylated XG label was present only in the infection thread walls (Figure A.10G). At the same time, in *M. truncatula* mutants blocked at early developmental stages, the content of fucosylated XG was increased in cell walls and infection thread walls. And in the *P. sativum* mutant SGEFix^{-}-2 (*Pssym33-3*), which is characterized by suberization of cell walls and infection thread walls [*Ivanova et al., 2015*], fucosylated XG was not observed in the walls of some infection threads [*Tsyganova et al., 2023b*].

In indeterminate nodules of *G. orientalis*, localization of fucosylated XG was similar to that in indeterminate nodules of *M. truncatula* (Figure A.10C,D) [*Tsyganova et al., 2023a; Tsyganova et al., 2023b*]. In determinate nodules of *G. max*, fucosylated XG was the predominant polysaccharide in infection thread walls (154.26 ± 38.10

compared to cell walls of infected cells 73.49 ± 12.92, $P < 0.05$) (Figure A.10H) [*Tsyganova et al., 2023a*]. In addition, *G. max* demonstrated the absence of fucosylated XG in the cell walls of uninfected cells (Figure A.10M). In *V. villosa* nodules, a preferential localization of fucosylated XG in the cell walls of infected cells was observed (Figure A.10O), and in *V. formosa* nodules, in addition, in the walls of infection threads (Figure A.10L,P).

In addition to carbohydrate polymers, plant cell walls contain structural proteins such as proteins rich in hydroxyproline, proline, and glycine, as well as arabinogalactan proteins (AGP), which can modify cell wall properties [Showalter and Basu, 2016].

One of the cell wall AGP recognized by the JIM13 antibody was previously shown to be associated with the organization of cortical microtubules [Nguema-Ona et al., 2007] and cell wall formation of labyrinthine invaginations of transfer cells in symbiotic nodules of *P. sativum* [Dahiya and Brewin, 2000]. In nodules of wild-type and mutants of *P. sativum* and *M. truncatula*, this AGP localized in endodermal cells in the form of two arcs without affecting the meristem at the top of the nodule (Figure A.11) [*Tsyganova et al., 2023b*]. In young endodermal cells at the border with the nodule meristem, in which the JIM13 antigen has not yet been detected at the light microscopy level, the appearance and accumulation of the label in vesicles near the plasma membrane has been shown by electron microscopy [Rae et al., 1991]. The observed localization pattern of the JIM13 epitope coincides with the localization of suberin in wild-type pea nodules [*Ivanova et al., 2015*]. It is known that the walls of mature endodermal cells are suberized during development, forming a physiological barrier to the penetration of water and soluble compounds. In addition, the endoderm serves as a defense against the penetration of pathogenic microbes. Therefore, both suberization [*Ivanova et al., 2015*] and accumulation of JIM13 antigen in endodermal cells completely surrounding nodules in *M. truncatula* mutants *Mtefd-1* (Figure A.11H) and TR3 (*Mtipd3*) (Figure A.11I) and *P. sativum* mutant SGEFix$^-$-2 (*Pssym33-3*) (Figure A.11D), as well as the formation of a "barrier layer" in this mutant, separating cells with overgrown and curved infection threads from the rest of the nodule parenchyma (Figure A.11E), can be attributed to defense reactions.

The participation of reactive oxygen species (ROS) in the modification of the symbiotic interface has been shown previously [*Tsyganova et al., 2021*]. Class III peroxidases (Prx-III) as well as rhizobial catalases [Jamet et al., 2007] contribute to the stiffening of the infection thread wall and matrix [Wisniewski et al., 2000]. During infection, superoxide anion (O_2^-) and H_2O_2 production has been observed in infection threads and infected cells [Santos et al., 2001; Ramu et al., 2002; Rubio et al., 2004]. The accumulation of H_2O_2 can be traced first on the inner surface of the infection thread wall (Figure A.12A,B), then throughout its thickness (Figure A.12C,D) and then within the matrix of the infection thread and infection droplet (Figure A.12E,F) [*Tsyganova et al., 2009a*], possibly contributing to its hardening as a result of cross-linking of tyrosine residues of arabinogalactanprotein-extensin (AGPE) molecules [Brewin, 2004; Brewin et al., 2008]. Thus, the traced dynamics of hydrogen peroxide accumulation in growing infection threads gave grounds to suggest that the role of H_2O_2 during infection thread elongation is associated with modification of the structure of the cell wall and matrix glycoproteins, namely, with the stiffness of the infection thread [Rathbun et al., 2002; Rathbun, Brewin, 2009; *Tsyganova et al., 2009a*; Puppo et al., 2013].

CHAPTER 2. Development of defense reactions when rhizobia are perceived as pathogens

The plant cell wall is not only a molecular monitoring system [Engelsdorf and Hamann, 2014] that responds to numerous biotic and abiotic stresses, but also an interface for some of the earliest interactions between plants and a wide range of other organisms, including insects, pathogens, and symbionts [Brewin, 2004; Cantu et al., 2008].

Plant cell wall alterations through disruption or overexpression of cell wall-related genes have a significant impact on disease resistance and/or abiotic stresses [Bellincampi et al., 2014; Miedes et al., 2014]. Initially, disease resistance phenotypes associated with changes in cell wall integrity [Fagard et al., 2000] were thought to manifest due to the inability of incompetent pathogens to overcome modified cell wall composition or structure in plant mutants. However, defense signaling pathways have been found to be activated in plant mutants with cell wall modifications [Miedes et al., 2014; Houston et al., 2016].

Rhizobial infection shares many similarities with pathogen infection, and induction of defense responses accompanies both interactions, but defense responses are successfully suppressed when the legume plant interacts with the microsymbiont. The development of an effective symbiotic nodule requires rhizobia to overcome a wide range of plant defense responses [*Tsyganova, Tsyganov, 2012*]. During the development of nitrogen-fixing nodules, synthesis of defense components is relatively low compared to pathogenesis. As a result, invading microorganisms are not completely inactivated, and host defense reactions limit their multiplication and localization in certain compartments provided by the host plant.

A typical response of a plant attacked by a pathogen is the build-up of papillae, which are dome-shaped formations between the epidermal cell wall and the plasma membrane, synthesized as a reinforcement of the plant cell wall near the site of pathogen invasion [Hückelhoven, 2007]. The main component of papillae is callose, β-1,3-glucan,

but other substances such as polysaccharides, phenolic compounds, ROS and proteins have also been found [Bestwick et al., 1997; Thordal-Christensen et al., 1997].

Callose deposition was observed in cell walls and infection thread walls in the *P. sativum* mutant RisFixV (*Pssym42*) inoculated with an effective rhizobium strain (Figure A.13) [*Ivanova et al., 2015*]. Previously, callose deposition was described in the formation of pseudonodules in *M. truncatula* inoculated with *Sinorhizobium meliloti* mutants with impaired exopolysaccharide synthesis [Niehaus et al., 1993]. In such pseudonodules, callose deposition in cortical cell walls was observed. Callose deposition was also observed in infection threads in *P. sativum* nodules formed by *Rhizobium* lipopolysaccharide mutants [Perotto et al., 1991]. Symbiotically inefficient mutants of legumes showing enhanced callose deposition have not been described previously. Exopolysaccharides and lipopolysaccharides are involved in the suppression of defense responses triggered by rhizobia [Fraysse et al., 2003]; in this context, the callose deposition observed in the mutant RisFixV (*Pssym42*) may indicate that the *PsSym42* gene is involved in the perception of polysaccharides or the signaling pathway of their perception by plants. Alternatively, the *PsSym42* gene may be involved in symbiosome membrane maturation, which is usually accompanied by changes in the composition of its epitopes **[**Brewin, 2004]; in nodules of the mutant RisFixV (*Pssym42*), it is possible that incorrect epitope composition could lead to callose deposition. The second assumption seems preferable due to the fact that callose deposition in cell walls and infection thread walls occurs during their maturation, and deesterified pectin was detected around bacteroids in degenerating infected cells (Figure A.5I) [*Ivanova et al., 2015*]. This phenotype has not been previously observed in either wild-type [Rae et al., 1992] or mutant nodules of *P. sativum*; however, the reason for this encapsulation of degenerating bacteroids is still unknown.

In wild-type *P. sativum* nodules, suberin deposits in the nodule endoderm are physiologically important to protect nodules from excessive dehydration, salt stress, and pathogen invasion [Schreiber et al., 1999]. The intense level of suberization observed in nodules of the *P. sativum* mutant SGEFix^{-}-2 (*Pssym33-3*) is an example of a plant defense

response that prevents the release of bacteria into the plant cytoplasm and their subsequent differentiation into bacteroids (Figure A.14) [*Ivanova et al., 2015*].

It was previously shown that the accumulation of polyphenolic substances in the walls of thickened infection threads is characteristic of the *M. truncatula* mutant TE7 in the *MtSym1* gene [Benaben et al., 1995]. The *MtSym1* gene is an ortholog of the *PsSym33* gene [Ovchinnikova et al., 2011]; they encode a key transcription factor CYCLOPS/IPD3, which interacts with the calcium-dependent and calmodulin-dependent kinase CCaMK, activating a further signaling cascade through another transcription factor NIN, leading to the induction of nodule organogenesis [Singh et al., 2014]. Thus, mutation in the key gene *PsSym33* leads to the perception of rhizobia as pathogens, causing strong defense responses manifested in suberization of inefficient nodule cells [*Ivanova et al., 2015*].

In addition, in white nodules of the *P. sativum* mutant SGEFix$^-$-2 (*Pssym33-3*), in which bacterial release into the plant cell cytoplasm occurred, cell wall material was deposited around the vacuole in uninfected, colonized, and infected cells (Figure A.15, Table 3) [*Tsyganova et al., 2019b*]. Moreover, this cell wall material was associated with the tonoplast (Figure A.15C-G), and further accumulations of cell wall material were observed in the vacuole lumen (Figure A.15H-J). Analysis of the composition of cell wall material components around vacuoles in SGEFix$^-$-2 (*Pssym33-3*) nodules showed deposition of suberin and highly methyl esterified HG, as well as the linear (1→4)-β-D-galactan side chain of RG-I, but not low methyl esterified HG. These abnormalities characteristic of the mutant have never been observed in wild-type nodules.

Table 3 — Quantification of different cell types in white nodules with bacterial release in *Pisum sativum* mutant SGEFix$^-$-2 (*Pssym33-3*)

Type of nodule cell	Percentage of different cell types in nodule	Percentage of the cell wall depositions in each cell type
Uninfected cells	35	43
Colonized cells (containing infection thread / infection droplet)	52	75
Infected cells	13	86

Results are based on a count of 2104 cells from 67 optical sections obtained from 13 nodules

To our knowledge, this is the first time that deposition of cell wall material around the vacuole has been described in ineffective nodules. This phenomenon was observed only in the *P. sativum* mutant SGEFix⁻-2 (*Pssym33-3*), as it carries a weak allele of the *PsSym33* gene, forming pinkish nodules along with white ones. In some white nodules, bacterial release into the cytoplasm of plant cells occurs in individual cells and in pinkish nodules [Tsyganov et al., 1998; Ovchinnikova et al., 2011]. Two other alleles, *Pssym33-1* (in the mutant RisFixU) and *Pssym33-2* (in the mutant SGEFix⁻-5), have been described as strong alleles showing only white nodules with blocked infection threads and no bacterial release [Voroshilova et al., 2001; Ovchinnikova et al., 2011; *Tsyganova et al., 2019d; Tsyganov, Tsyganova, 2020*]. Thus, it seems unlikely that these mutants would exhibit ectopic accumulation of cell wall material due to bacterial infection. In contrast, the mutant SGEFix⁻-5 (*Pssym33-2*) was characterized by the presence of some infection threads in which bacteria do not diverge after division, forming clusters and subsequently undergoing complete degradation (Figure A.16). This phenotype can be explained by the activation of strong plant defense reactions that affect the bacteria within the infection threads [*Tsyganova et al., 2019d*].

Also in the *P. sativum* mutant SGEFix⁻-2 (*Pssym33-3*), a striking feature of white nodules with bacterial release is the presence of hypertrophied infection droplets labeled with the JIM7 antibody (highly methyl esterified HG) (Figure A.15K,L) [*Tsyganova et al., 2019b*]. Infection droplet formation was previously observed in pinkish nodules of this mutant [Tsyganov et al., 1998], as well as in some white nodules [*Tsyganov et al., 2011*]. However, hypertrophy of infection droplets was previously described only for another *P. sativum* mutant SGEFix⁻-1 (*Pssym40-1*) [Tsyganov et al., 1998].

Thus, deposition of suberized cell wall material around vacuoles and formation of a pectin gel (identified by the LM5 antibody to the linear (1→4)-β-D-galactan side chain of RG-I) in the matrix of infection threads (Figure A.15M,N) are signs of a pathogen-like defense response in the *P. sativum* mutant SGEFix⁻-2 (*Pssym33-3*) [*Tsyganova et al., 2019b*]. Overall, this suggests that an important function of the CYCLOPS/IPD3

transcription factor is to suppress the defense response during the establishment of legume-rhizobium symbiosis.

The arrest of symbiotic nodule development during bacteroids differentiation in the *P. sativum* mutant SGEFix⁻-1 (*Pssym40-1*) also indicates the misperception of the microsymbiont as a potential plant pathogen. The entire nodule becomes topologically isolated from the rest of the plant through a “circular” zone of suberization of the nodule endoderm [*Ivanova et al., 2015*]. Previously, a similar phenotype was observed in two *M. truncatula* mutants, *Mtsym6* [Tirichine et al., 2000] and the RNAi mutant *MtHAP2-1* [Combier et al., 2006]. Both mutants are also characterized by early arrest of the nodule meristem, which is associated with circular closure of the nodule endoderm, but the reason for this correlation is still unknown [Guinel, 2009]. The *PsSym40* gene is an ortholog of the *MtEFD* gene of *M. truncatula*, which encodes a transcription factor that is a negative regulator of the cytokinin signaling cascade [Vernié et al., 2008; *Tsyganov, Tsyganova, 2020*]. Disruption of the *PsSym40* gene results in numerous abnormalities in nodule development, including early meristem arrest [Voroshilova et al., 2009], hypertrophied infection droplets, massive bacterial release into the host cell cytoplasm, and premature degradation of symbiotic structures [Tsyganov et al., 1998]. The wide range of nodule abnormalities observed in this mutant suggests that *PsSym40* is important for nodule formation, as disruption of the gene apparently induces a strong defense response.

Also in nodules of the *P. sativum* mutant SGEFix⁻-1 (*Pssym40-1*), excessive accumulation of hydrogen peroxide in infection threads (Figure A.17A), infection droplets (Figure A.17B), and juvenile bacteroids (Figure A.17C,D) was observed [*Tsyganova et al., 2009b; Provorov et al., 2012*]. As a result, the SGEFix⁻-1 (*Pssym40-1*) mutant exhibits enhanced oxidative stress compared to the wild type, as manifested by excessive H_2O_2 accumulation. The strong increase in the expression level of the *Ps7RA84* gene encoding peroxidase in nodules of the mutant SGEFix⁻-1 (*Pssym40-1*) [*Ivanova et al., 2015*] can also be explained by the development of oxidative stress similar to that in incompatible pathogen interactions [Hancock et al., 2002]. Increased oxidative processes lead to the fact that bacteroids of *R. leguminosarum* bv. *viceae* become unable to

overcome this stress, and the differentiation process goes wrong, as indicated by the presence of abnormal bacteroids (Figure A.17C,D) in the cytoplasm of infected nodule cells and their early senescence.

CHAPTER 3. The infection thread matrix is the main extracellular habitat of rhizobia

The production and secretion of various compounds that make up the intercellular matrix are stimulated in response to rhizobial infection. Most of these compounds accumulate in the lumen of the infection thread. It has been estimated that for pea and other legumes that form indeterminate nodules, the amount of matrix material in the infection thread lumen is about five times the amount of rhizobia inside [Brewin, 1991]; in contrast, in determinate nodules, the infection thread wall is tightly pressed against the bacteria that fill it and matrix material is reduced or almost completely absent [Rae et al., 1992]. The main component of the intercellular matrix and matrix within the infection thread lumen are plant glycoproteins, which are extremely dynamic components of the plant surface [Cassab, 1998; Brewin, 2004]. Moreover, a tissue-specific set of AGP are synthesized in symbiotic nodules of legumes [*Tsyganova et al, 2021*], which are complex co-polymers of arabinogalactanprotein-extensin (AGPE) that contains alternating arabinogalactanprotein and extensin motifs [Goodrum et al., 2000; Rathbun et al., 2002; Brewin, 2004; Nguema-Ona et al., 2013; Showalter, Basu, 2016].

AGPE are more soluble than conventional extensins as a result of their high carbohydrate content. These 95-kDa glycoproteins, or rather proteoglycans, are recognized by the monoclonal antibodies MAC265, MAC204, and MAC236 [Bradley et al., 1988; VandenBosch et al., 1989]. AGPE molecules combine the biophysical properties of soluble gum (characteristic of AGP) with the structural and protective properties of extensins (which normally serve to reinforce plant cell walls in response to pathogen attack or mechanical stress). Because of the very high content of tyrosine residues, it has been suggested that AGPE macromolecules may cross-link and convert to an insoluble form under oxidizing and hydrogen peroxide-rich conditions. This cross-linking may play a role in regulating the growth of infection threads as a result of the gradual transition of the liquid state of AGPE to a solid state in the matrix of the infection thread, thereby controlling the infection process [Wisniewski et al., 2000; Rathbun et al.,

2002; Brewin, 2004; Gucciardo et al., 2005; Rathbun, Brewin, 2009; Reguera et al., 2010].

In nodules of wild-type and mutant plants of *P. sativum*, the MAC265, MAC204, and MAC236 antibodies recognized both infection structures in the infection zone and mature infection threads in the nitrogen fixing zone (Figure A.18; Figure A.19; Figure A.20) [*Tsyganova et al., 2009; Tsyganova et al., 2019a*]. Morphometric analysis of the localization and distribution of AGPE carrying the MAC204 and MAC236 label showed that in the *P. sativum* mutant SGEFix$^-$-1 (*Pssym40-1*) with hypertrophied infection droplets showed an increased amount of labeling of both epitopes in the infection droplets compared to the original line, while the mutant SGEFix$^-$-2 (*Pssym33-3*) with “locked” infection threads and absence of rhizobia release into the cytoplasm of the plant cell showed a maximum increase in the amount of labeling of both epitopes in the infection threads (Table 4) [*Tsyganova et al, 2019a*]. When quantifying the distribution of different epitopes of AGPE in infection threads and infection droplets in single and double mutants of *P. sativum* carrying *Pssym33-3* and *Pssym40-1* alleles, it was shown that in the double mutant RBT3 (*Pssym33-3*, *Pssym40-1*) the amount of labeling of both epitopes was intermediate between the parental mutant genotypes SGEFix$^-$-1 (*Pssym40-1*) and SGEFix$^-$-2 (*Pssym33-3*). These results may indicate complementation of *Pssym33-3* and *Pssym40-1* mutations with respect to the feature of AGPE number detected by the MAC204 and MAC236 antibodies in the matrix of infection threads. Thus, although the *Pssym33-3* mutation is epistatic over the *Pssym40-1* mutation with respect to nodule structural organization [*Tsyganov et al., 2011*], the *PsSym33* and *PsSym40* genes may participate in independent pathways involved in the formation of the matrix of infection threads and infection droplets.

In addition, *P. sativum* single and double mutants in the *PsSym33* gene showed heterogeneous accumulation of AGPE carrying the MAC265 label: in some infection threads the label was absent (Figure A.18E,F; Figure A.19C). Such infection threads showed signs of bacterial degradation in the lumen with lysis of bacterial cells. The absence of AGPE labeling may be due to peroxidative cross-linking of AGPE molecules via hydrogen peroxide [Wisniewski et al., 2000; Brewin, 2004]. In addition, in the *P.*

sativum mutant RisFixV (*Pssym42*), the absence of the MAC265 label was observed in part of the matrix of some infection threads (Figure A.19F). This is probably a consequence of the germination of a new infection thread along the course of the old one, which may indicate that the growth and development of infection structures in symbiotically inefficient mutants is a complex and uneven process [*Tsyganova et al., 2009b*].

Table 4 — Distribution of arabinogalactan-protein extensin epitopes labelled with monoclonal antibodies MAC204 and MAC236 in infection structures in the nodules of *Pisum sativum* wild type and mutants at 14 days after inoculation

Genotype	Infection threads		Infection droplets	
	MAC204	MAC236	MAC204	MAC236
SGE (*wild type*)	5.10 ± 0.34^{b}	5.57 ± 0.25^{ab}	8.52 ± 1.16^{c}	7.20 ± 0.55^{c}
SGEFix−-1 (*Pssym40*)	14.38 ± 0.45^{d}	4.78 ± 0.13^{a}	24.42 ± 1.08	13.03 ± 0.91^{d}
SGEFix−-2 (*Pssym33-3*)	28.05 ± 0.92	22.09 ± 0.95	nd	nd
RBT3 (*Pssym33-3, Pssym40*)	20.65 ± 0.73	9.18 ± 0.52	nd	nd

Results are presented as the number of gold particles/μm^2. Mean value ± SEM (n = 20-25) are shown. Means denoted by the same letters within a column (a) and within a row (b-d) are not significantly different at $P < 0.05$ based on Dunn's test.
nd, not detectable

In the *P. sativum* mutant SGEFix^{-}-1 (*Pssym40-1*), an impaired targeted secretion of AGPE recognized by the MAC265 antibody was detected, resulting in the accumulation of large amounts of the label in the intercellular space (Figure A.18D; Figure A.19B) and accompanied by a change in the direction of movement of vesicles carrying the label from the infection thread wall to the cell wall in the lumen of the infection thread [*Tsyganova et al., 2009b*]. In the *P. sativum* mutant for the *PsSym40* gene, abnormal secretion into the intercellular space was detected with respect to the AGPE epitope recognized by the MAC236 antibody, whereas the AGPE epitope recognized by MAC204 impregnated both the matrix of the intercellular space and the cell wall [*Tsyganova et al., 2019a*]. In the *PsSym33* gene mutant, the epitope recognized by the MAC204 antibody was detected in the walls of infection threads. In the double mutant RBT3 (*Pssym33-1*, *Pssym40-1*), small transport vesicles carrying MAC265 (Figure A.19D), MAC204 (Figure A.21B), and MAC236 (Figure A.21E) labels were

clearly distinguishable near the plasma membrane and infection thread membrane [*Tsyganova et al., 2009b; Tsyganova et al., 2019a*]. In addition, the double mutant RBT3 (*Pssym33-3, Pssym40-1*) showed the MAC204 label as part of cell walls and infection thread walls (Figure A.21A,C), as well as in infection thread walls in the mutant SGEFix^{-}-2 (*Pssym33-3*) and in cell walls in the mutant SGEFix^{-}-1 (*Pssym40-1*) [*Tsyganova et al., 2019a*]. The results indicate complementation of *Pssym33-3* and *Pssym40-1* mutations with respect to the AGPE localization signature detected by MAC204 and MAC236 antibodies. The appearance of excessive amounts of AGPE in the intercellular space may be due to an alteration in the directed secretion of AGPE as a result of disruption of normal infection thread development [*Tsyganova et al., 2009b; Tsyganova et al., 2019a*].

The observed abnormalities in the targeted secretion of AGPE may be related to improper delivery of transport vesicles, which is presumably carried out by proteins of the PUMILIO family. It was previously shown that the 3' untranslated region (3' UTR) of the mRNA of the gene encoding AGPE is highly conserved in *P. sativum* compared to that of the orthologous *M. truncatula MtN12* gene [Rathbun et al., 2002]. In this case, the 3' UTR of *MtN12* mRNA contains multiple UGUA sites, which is a canonical sequence called PUMILIO response element (PRE) [Prasad et al., 2016; Huang et al., 2021]. These proteins are involved in the maintenance of cell polarity, for example in budding yeast [García-Rodríguez et al., 2007]. It can be hypothesized that PUMILIO proteins are involved in the polar apical growth of infection threads. Thus, in mutants with abnormal infection thread development, the directional vesicular transport performed by these proteins may be impaired.

The exact way in which AGPE functions in the growth and development of infection structures, especially infection threads, is unknown because these glycoproteins have a complex structure. It is also unknown whether the entire AGPE molecule or specific sequences in this molecule are responsible for its biological activity [Brewin, 2004; Nguema-Ona et al., 2013]. The monoclonal antibodies MAC204, MAC236 and MAC265 recognize different epitopes on AGPE macromolecules with a molecular mass of 95 kDa in infection threads [VandenBosch et al., 1989]. The epitopes recognized by MAC236 and MAC265 are mutually exclusive, and MAC204 recognizes a periodate-

sensitive epitope common to both the acidic and neutral forms of the 95-kDa macromolecule [VandenBosch et al., 1989]. Both epitopes were present in equal amounts in infection threads and infection droplets in *P. sativum* wild-type SGE nodules. At the same time, in the mutant SGEFix^{-}-1 (*Pssym40-1*) and the double mutant RBT3 (*Pssym33-3*, *Pssym40-1*), the epitope recognized by the MAC204 antibody accumulated in greater amounts than the epitope recognized by the MAC236 antibody (Table 4), which may indicate that mutation in the *Pssym40-1* gene may result in differences in the accumulation of AGPE epitopes [*Tsyganova et al, 2019a*]. The existing variation in the number of three different AGPE-related epitopes in the matrix of infection threads and infection droplets suggests that specific sequences of the AGPE macromolecule may play different roles in symbiotic nodule development.

Extensins are cell wall proteins belonging to the superfamily of hydroxyproline-rich glycoproteins, and they are known to be involved in many processes during plant growth and development. In addition, these proteins are involved in plant interactions with both pathogens [Bellincampi et al., 2014] and mutalistic microorganisms [Brewin, 2004; Rich et al., 2014]. Potential involvement of extensins in legume-rhizobial symbiosis has been reported, among others [Dahiya, Brewin, 2000; Sujkowska-Rybkowska, Borucki, 2014]. When studying the symbiotic interaction of *P. sativum* with *R. leguminosarum*, LM1 and LM3 antibodies [Smallwood et al., 1995], which recognize extensin epitopes, were shown to label the matrix of infection threads as strongly as MAC265 [Dahiya, Brewin, 2000; Sujkowska-Rybkowska, Borucki, 2014]. The involvement of the JIM11 epitope was previously identified in the mycorrhizal symbiosis of the orchid plant *Dendrobium officinale* [Li et al., 2018].

Extensin recognized by the JIM11 antibody in wild-type nodules of *P. sativum* SGE and *M. truncatula* A17 was deposited in the intercellular spaces of nodule parenchyma near the endodermis (Figure A.22B,H), in the matrix of infection threads and infection droplets (Figure A.22A,C-E,G,I,J,L) [*Tsyganova et al., 2023b*], in contrast to extensin LM1, which was also deposited in the cell walls of the nodule cortex and in the cell walls of the parenchyma [Sujkowska-Rybkowska, Borucki, 2014]. LM1 labeling was continuous throughout the nodule, from the mature base to the infection zone bordering

the meristem. However, the label was absent in meristematic and infected cells [Sujkowska-Rybkowska, Borucki, 2014]. Upon exposure to aluminum, the amount of extensins recognized by the LM1 antibody also increased dramatically, especially in the matrix of infection threads and in the intercellular space [Sujkowska-Rybkowska, Borucki, 2014]. However, when ineffective symbiosis develops, extensins (labeled JIM11) appear in the cell walls of nodule cortex cells in the *M. truncatula* mutant TR3 (*Mtipd3*) with no bacterial release into plant cells (Figure A.22K) and accumulate in the intercellular space in the mutants *P. sativum* Sprint-2Fix$^-$ (*Pssym31*) and *M. truncatula Mtdnf1-1* with poorly differentiated symbiosomes (Figure A.22F,L, respectively) [*Tsyganova et al., 2023b*]. In other legumes, AGPE (labeled with the MAC265 antibody) and extensins (labeled with the JIM11 antibody) were shown to be the predominant glycoproteins of the infection thread matrix in indeterminate nodules of *G. orientalis* (Figure A.23A,B), whereas in determinate nodules of *G. max* these polymers are found mainly in the intercellular spaces of nodule parenchyma (Figure A.23D,E) [*Tsyganova et al., 2023a*]. The absence of AGPE in determinate nodules was confirmed by immunolocalization with the MAC265 antibody in *P. vulgaris*, which showed a complete absence of labeling associated with infection threads, although labeling was observed in some intercellular spaces in the central infected region of the nodule [Rae et al., 1992]. These legumes have also been shown to have small amounts of extensin binding to the JIM19 antibody (Figure A.23C,F), which may indicate the diversity of these proteins within the symbiotic interface [*Tsyganova et al., 2023a*].

CHAPTER 4. The symbiosome is a temporary organelle with an advanced symbiotic interface

The exact mechanism triggering the transition of rhizobia from the extracellular space (apoplast) to intracellular existence is not yet known, but it is associated with further remodeling of the cell wall. Glycoproteins associated with symbiosomal and plasma membranes, such as the *P. sativum* lectin-like glycoprotein PsNLEC1 [Kardailsky et al., 1996; Redondo-Nieto et al., 2008], an arabinogalactan-like glycolipid protein recognized by the MAC206 antibody [Bolaños et al., 2001; Bolaños et al, 2004; Redondo-Nieto et al., 2008], the synaptotagmins MtSyt1, MtSyt2, and MtSyt3 of M. truncatula [Gavrin et al., 2017], and glycosylated forms of an inositol-containing phospholipid recognized by the JIM18 antibody [Perotto et al., 1995] may play a direct role in surface interactions with rhizobia.

Rhizobia released from the wall-free infection droplet into the cytoplasm of the host cell are surrounded by a plant membrane whose source is initially the plasma membrane of the host cell [Roth and Stacey, 1989; Coba de la Peña et al., 2018; Fedorova, 2023]. In indeterminate nodules, symbiosome differentiation is a gradual process [Tsyganov et al., 2003] that depends both on the differentiation of bacteria into bacteroids and on symbiosome membrane maturation and remodeling of the symbiotic interface.

Analysis of membrane markers revealed an intermediate identity of symbiosome membranes [Bapaume and Reinhardt, 2012]. The specific localization of MtSYP132 syntaxin on the symbiosome membranes of *M. truncatula* is identical to that on the plasma membrane, i.e. bacteroidetes are essentially located in the “intracellular domain of the apoplast” [Catalano et al., 2004; Limpens et al., 2009]. Recently, arabinan epitopes with polymerization degree 2-7, detected using the LM6-M antibody [Pedersen et al., 2012], were shown to label not only the cell wall but also the symbiosome membrane of juvenile symbiosomes in the infection zone of indeterminate nodules of *P. sativum* (Figure A.24A; Figure A.25A), *M. truncatula* (Figure A.24C) [*Tsyganova et al., 2023b*], and *G. orientalis*

(Figure A.24D) [*Tsyganova et al., 2023a*], as well as the symbiosome membrane in determinate nodules of *G. max* (Figure A.24F) [*Tsyganova et al., 2023a*].

With the onset of nitrogenase activity in mature differentiated bacteroids, the symbiosome membrane acquires the Rab7 GTPase [Clarke et al., 2015], a marker of late endosomal or early vacuolar membranes. Consequently, the symbiosome membrane undergoes a transition phase between plasma and vacuolar membranes [Limpens et al., 2009]. Thus, in mature symbiosomes, the arabinan label disappears in the cells of the nitrogen-fixation zone in all studied species with indeterminate nodules (Figure A.24B,E; Figure A.25C; Table 5) [*Tsyganova et al., 2023a; Tsyganova et al., 2023b*].

Table 5 — Distribution of arabinans in rhamnogalacturonan I and arabinogalactan protein in symbiosomes of infected cells in *Galega orientalis* and *Glycine max* nodules

	Galega orientalis, juvenile symbiosome	*Galega orientalis*, mature symbiosome	*Glycine max*, symbiosome
LM6-M	7.03±1.08	0.67±0.21[a]	2.59±0.41[ab]
LM2	9.87±0.95	1.01±0.11[a]	2.42±0.25[ab]

Results are presented as the number of gold particles/μm^2 .Mean value ± SE **(**n = 100–150) are shown. Letters indicate statistically significant differences (t test, $p < 0.05$):
[a] From juvenile symbiosomes of *Galega orientalis*
[b] From mature symbiosomes of *Galega orientalis*

When symbiotically inefficient mutants of *P. sativum* and *M. truncatula* were studied, the same pattern was observed: arabinan label was associated mainly with symbiosomes containing juvenile (Figure A.25B) and poorly differentiated (Figure A.25D) bacteroids. In multibacteroid symbiosomes that formed in infected cells in the nodules of some mutants, the amount of label depended on the degree of differentiation of the bacteroids (Figure A.25E). On symbiosomes with abnormal or degenerating bacteroids, the amount of arabinan label was sharply reduced (Figure A.25F) [*Tsyganova et al., 2023b*].

A similar distribution pattern of AGP identified with the LM2 antibody was observed in nodules of both types (Figure A.24G-I; Table 5). Recently, similar AGP (labeled with the LM2 antibody) was detected in the fixation threads of *Erythrophleum* sp. and on the symbiosome membrane in *P. macroloba* nodules [de Faria et al., 2022]. The amount of both arabinans RG-I and AGP label in symbiosomes of determinate

nodules of *G. max* was almost the same, but higher than in mature symbiosomes of *G. orientalis* (Table 5) [*Tsyganova et al., 2023a*].

The possibility that AGP is anchored to the plasma membrane via the GPI-anchor indicates their possible role in cell wall remodeling during the development and modification of the symbiotic interface [Sherrier et al., 1999]. GPI-anchored AGP recognized by the JIM1 antibody were previously shown to be present on the symbiosome membrane in *P. sativum* nodules (Figure A.26B) in contrast to *M. truncatula* (Figure A.26A) [*Tsyganova et al., 2019c*]. The increased amount of JIM1 label in symbiosomes of 4-week-old nodules compared with 2-week-old nodules suggests that this AGP is involved in symbiosome maturation in wild-type nodules of *P. sativum* (Figure A.26C; Table 6) [*Tsyganova et al., 2019c*].

Table 6 — Distribution of arabinogalactan protein with a glycosylphosphatidylinositol anchor in symbiosomes of infected cells in wild-type and mutant nodules of *Pisum sativum*

Genotypes	Weeks after inoculation (WAI)	Mean value	SE
SGE (wt)	2	4.10[e]	0.40
	4	6.13	0.71
SGEFix$^-$-1 (*Pssym40*)	2	3.28[ae]	0.35
	4	1.09[b]	0.25
SGEFix$^-$-2 (*Pssym33*)	2	7.38[ae]	0.79
	4	4.65[b]	0.49
SGEFix$^-$-3 (*Pssym26*)	2	11.46[ae]	0.66
	4	2.04[b]	0.33
Sprint-2 (wt)	2	4.50[e]	0.46
	4	6.54	0.52
Sprint-2Fix$^-$ *(Pssym31*)	2	1.07[c]	0.35
	4	1.11[d]	0.26

Results are presented as the number of gold particles/μm^2. Mean value ± SE (n=100-150) are shown. Letters indicate statistically significant differences (*t*-test, *P* value ≤ 0.001).
[a] From the wild-type SGE of corresponding mutant lines at 2 WAI.
[b] From the wild-type SGE of corresponding mutant lines at 4 WAI.
[c] From the wild-type Sprint-2 of corresponding mutant line at 2 WAI.
[d] From the wild-type Sprint-2 of corresponding mutant line at 4 WAI.
[e] Within genotype compared with 4 WAI.

The *P. sativum* mutant Sprint-2Fix$^-$ (*Pssym31*), characterized by undifferentiated bacteroidetes [Borisov et al., 1997], showed preferential localization of anchored AGP at the plasma membrane (Figure A.26D) and constant low levels in symbiosomes, confirming the reduced level of symbiosome membrane differentiation in this mutant (Table 6) [*Tsyganova et al., 2019c*]. Symbiosome development of the mutant Sprint-2Fix$^-$ (*Pssym31*) was previously studied using the JIM18 antibody that recognized the glycolipid component of the plasma membrane in juvenile symbiosomes [Perotto et al., 1995]. In this mutant, the JIM18 label was evenly distributed throughout the infected nodule cells, confirming the presence of only the juvenile form of the symbiosome membrane in the nodules of this mutant [Sherrier et al., 1997; Dahiya et al., 1998].

The *P. sativum* mutant SGEFix$^-$-3 (*Pssym26*), which has an early senescence phenotype, exhibited significantly higher numbers of GPI-anchored AGP in 2-week nodules than in wild-type nodules, with a dramatic decrease in the number of AGP in 4-week nodules in this mutant (Figure A.26F; Table 6) [*Tsyganova et al., 2019c*]. A similar pattern was observed in another *P. sativum* mutant SGEFix$^-$-2 (*Pssym33-3*), which was characterized by periodic rhizobia release in some cells of individual nodules [Voroshilova et al., 2001]. In the *P. sativum* mutant SGEFix$^-$-1 (*Pssym40-1*), which forms nodules with abnormally shaped bacteroids [Tsyganov et al., 1998], the amount of anchored AGP was also reduced in 4-week-old nodules compared with 2-week-old ones, but at the same time, 2 weeks after inoculation, the amount of GPI-anchored AGP in nodules of this mutant and in wild-type nodules did not differ (Table 6) [*Tsyganova et al., 2019c*]. The observed differences in the distribution of GPI-anchored AGP in nodules of the *P. sativum* mutants *Pssym33-3*, *Pssym26*, and *Pssym40-1* and the overall sharp decrease in their amounts in 4-week-old nodules may indicate the activation of early senescence in the nodules of these mutants [*Serova et al., 2018*]. Thus, it is hypothesized that mebrane-associated AGP may be a marker of symbiosome maturation and/or play a role in symbiosome differentiation [*Tsyganova et al., 2019c*].

It has been shown previously that symbiosome membrane glycoproteins carry ontogenetically regulated antigens depending on the stage of nodule development. In particular, a number of epitopes associated with glycoprotein and glycolipid components

of the symbiosomal membrane (antibody classes I-III) have been identified [Perotto et al., 1991]. AGP recognized by class I antibodies (MAC207) appear to be stably associated with symbiosomal membranes in the infection zone and early nitrogen fixation zone, but their amounts are reduced in the late nitrogen fixation zone. Glycoproteins and glycolipids recognized by class II antibodies (MAC255) were detected in the nitrogen fixation zone. Membrane antigens and soluble components of the peribacteroid fluid recognized by class III antibodies (MAC266, PsNLEC-1) were associated with mature nitrogen-fixing and senescent cells [Kardailsky et al., 1996]. In addition, significant amounts of AGPs (Figure 3; Figure A.27), whose function is currently unknown, were found on the symbiosome membrane in nodules of *G. orientalis* and *G. max* [*Tsyganova et al., 2023a*].

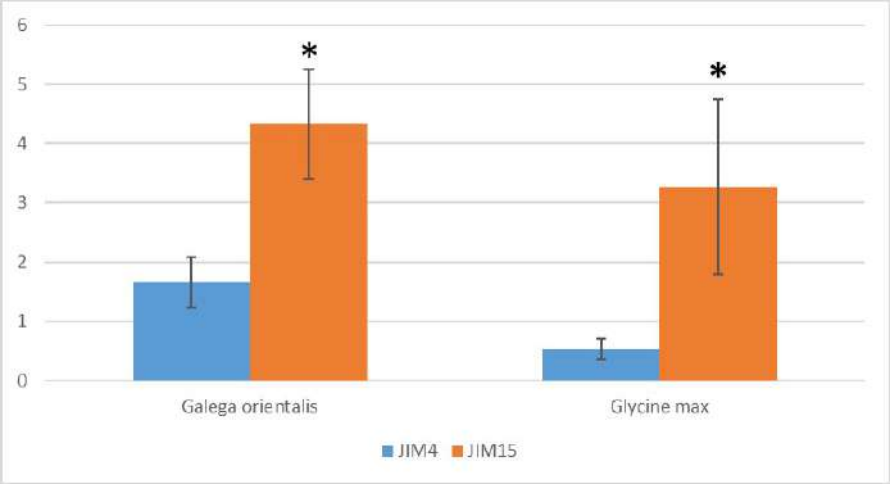

Data are presented as the number of gold particles/μm^2. Asterisks indicate statistically significant differences from JIM4 labeling (two-sample t-test, $p < 0.05$; $n = 28$-46), vertical bars represent standard deviation.

Figure 3 — Distribution of arabinogalactan proteins recognized by the JIM4 and JIM15 antibodies in symbiosomes of infected cells in *Galega orientalis* and *Glycine max* nodules

At the onset of senescence, the appearance of the SNARE markers SYP22 and VTI11 on the symbiosome membrane indicates a transition to a lytic vacuole in which bacteroids are utilized [Limpens et al., 2009]. Thus, the symbiosome membrane is unique, combining features of the plasma membrane, tonoplast, and a specific, inherently symbiotic compartment identical to the periarbuscular membrane [Pumplin and Harrison,

2009], and arabinans (as part of RG-I and AGP) appear to play an important role in the development of infection structures, particularly symbiosomes.

During symbiosome formation, the induction *nif* and *fix* genes in rhizobia required for nitrogen fixation is controlled by oxygen rather than nitrogen status [Dixon and Kahn, 2004]; therefore, a very low partial pressure of oxygen is maintained in nodules using leghemoglobin, which prevents nitrogenase inactivation. The precise regulation of the redox state and the presence of an antioxidant system at the same time is crucial for the stability of bacteroides [Ivanova, Tsyganov, 2017; Matamoros and Becana, 2020]. Various defense mechanisms against ROS have been described in nodules, which include enzymes such as superoxide dismutases, catalases and peroxidases and the non-enzymatic molecules ascorbate and glutathione [Santos et al., 2000; Santos et al., 2001; Matamoros et al., 2003; Rubio et al., 2004; Frendo et al., 2013; *Ivanova et al., 2022*].

In wild-type and mutant nodules of *P. sativum*, a high amount of glutathione label was shown in symbiosomes with mature bacteroids in cells in the nitrogen fixation zone and its decrease in senescent bacteroids (Table 7) [*Ivanova et al., 2022*]. These data support the observation that the highest amounts of both reduced and oxidized forms of glutathione were observed in bacteroids of mature nodules of *P. sativum*, but were markedly reduced in senescent nodules [Matamoros et al., 2013]. Recently, it was demonstrated that glutathione deficiency in *S. meliloti* 2011 (*gshB*) does not affect bacteroid differentiation but causes early nodule senescence [Yang et al., 2020], indicating that glutathione content in bacteroids is essential for their proper function.

In bacteria in infection threads in wild-type nodules of *P. sativum*, the amount of glutathione was quite low (Table 7). However, the most intense labeling was observed in bacteria in some “locked” infection threads of the *P. sativum* mutant SGEFix$^-$-2 (*Pssym33-3*) and juvenile bacteroids in mutants SGEFix$^-$-2 (*Pssym33-3*) and SGEFix$^-$-1 (*Pssym40-1*) [*Ivanova et al., 2022*]. These effects can be explained by the activation of strong defense responses in these mutants, including suberization of infection thread walls in SGEFix$^-$-2 (*Pssym33-3*) nodules [*Ivanova et al., 2015*] and accumulation of hydrogen peroxide around juvenile bacteroids in SGEFix$^-$-1 (*Pssym40-1*) nodules [*Tsyganova et*

al., 2009a]. This suggests that rhizobia utilize glutathione to mitigate the stress caused by the activation of plant defense responses in these mutants.

Table 7 — Distribution of glutathione in infection structures in wild-type and mutant nodules of *Pisum sativum*

Genotype	Type	Bacteroids	Peribacteroid space	Infection thread /droplet	Cytoplasm
SGE (*wild type*)	juvenile	4,71 ± 0,41	6,3 ± 0,63[&]	3,93 ± 0,23	8,94 ± 0,43
	mature	78,59 ± 5,74[a]	3,42 ± 0,28[a,&]		8,74 ± 0,73
	senescent	7,52 ± 0,83[b]	4,6 ± 0,58[&]		7,9 ± 0,51
SGEFix⁻-1 (*Pssym40-1*)	juvenile	24,71 ± 0,8[a,b,c]	8,07 ± 0,4[b,c,&]	7,37 ± 0,31[a]	14,03 ± 0,91[a,b,c]
	abnormal	6,25 ± 0,33[b,d]	7,89 ± 0,41[b,c,&]		
SGEFix⁻-2 (*Pssym33-3*)	abnormal	10,59 ± 0,48[b,d]	7,59 ± 0,33[b,c,&]	4,08 ± 0,22[d]	24,12 ± 1,01[a,b,c,d]

Values are means ± SE. The results are presented as the number of gold particles/μm^2. Letters indicate statistically significant differences (t-test corrected for multiple comparisons, padj < 0.05).

[a] From the juvenile wild-type (WT) cell region (or WT value of the same cell region).

[b] From the mature WT cell region.

[c] From the senescent WT cell region.

[d] From the juvenile cell region *Pssym40-1* (or *Pssym40-1* value of the same cell region).

[&] From the bacteroid value of the same genotype.

Phytohormonal regulation has a great influence on the development of symbiotic nodules [Tsyganova, Tsyganov, 2015; Dolgikh et al., 2016a; Dolgikh et al., 2016b; Tsyganova, Tsyganov, 2018; Mathesius, 2020]. Phytohormones also play an important role in the formation and modification of the symbiotic interface in nodules, especially in the differentiation of the symbiosome membrane and the formation of the peribacteroid space.

In wild-type *P. sativum* nodules, we demonstrated the presence of trans-zeatin riboside in the matrix of infection droplets and in the exopolysaccharide capsule of bacteria (Figure A.28A), in symbiosomes, both in the peribacteroid space and within bacteroids (Figure A.28B), and in vesicles that were associated with symbiosomes, and a significant decrease in its amount in senescent symbiosomes [Dolgikh et al., 2020]. In addition, in the mutant SGEFix⁻-2 (*Pssym33-3*), the amount of labeled trans-zeatin

riboside was increased in infection threads (Figure A.28C), and cytokinin was not detected in hypertrophied infection droplets in the nodules of the mutant SGEFix$^-$-1 (*Pssym40-1*), but was observed in high amounts in the multibacteroid symbiosomes formed by this mutant (Figure A.28D). In infection threads of the *P. sativum* mutant RisFixV (*Pssym42*) with callose-impregnated walls, trans-zeatin riboside was absent from the matrix but was found in small amounts in thickened walls (Figure A.28E). The observed distribution of trans-zeatin riboside may indicate that in mature nodules some forms of cytokinins are involved in the negative regulation of infection by limiting the growth of infection threads and, in particular, the development of infection droplets. It should be noted that in nodules of mutants SGEFix$^-$-5 (*Pssym33-2*) and SGEFix$^-$-2 (*Pssym33-3*), infection threads are highly branched [Voroshilova et al., 2009; *Tsyganova et al., 2019d*], probably due to the reduced levels of cytokinins and the absence of their negative effect on infection thread growth [*Dolgikh et al., 2020*].

High amounts of gibberellin (GA_3) were found in infected cells in the nitrogen-fixing zone, where it was bound mainly to the cytoplasm and symbiosomes, both in nodules of *P. sativum* wild-type SGE and in the early senescent mutant SGEFix$^-$-3 (*Pssym26*) [*Serova et al., 2019*]. At the same time, the amount of label was higher in juvenile symbiosomes than in mature and senescent symbiosomes (Table 8). It should be noted that the amount of gibberellin was lower in symbiosomes of the mutant SGEFix$^-$-3 (*Pssym26*) compared with wild-type nodules (Table 8), which is probably due to the early senescence of symbiotic structures in this mutant, i.e. the amount of gibberellin in symbiosomes decreased with increasing age of wild-type and early senescent mutant nodules. It is worth noting that gibberellin has recently been found to promote the function of nitrogen-fixing nodules [McAdam et al., 2018]. However, the exact function of gibberellin in the development of infected cells and symbiosomes needs to be elucidated. A negative effect of gibberellin on infection thread development was previously identified [McAdam et al., 2018]. Indeed, the amount of gibberellin was lower in infection threads than in symbiosomes (Table 8). However, gibberellin was detected in the walls of infection threads [*Serova et al., 2019*]. The function of gibberellin in infection thread development is currently unknown. Interestingly, gibberellin has recently been suggested

to be involved in facilitating bacterial release from infection threads [Tatsukami and Ueda, 2016], as well as its role in delaying nodule senescence. Down-regulation of senescence-related genes, reduction of senescence zone and increase of nitrogen-fixation zone in wild-type nodules of *P. sativum* treated with exogenous GA_3 confirms the negative regulation of nodule senescence by gibberellin and the involvement of GA_3 in mature nodule function [*Serova et al., 2019*].

Table 8 — Distribution of gibberellin (GA_3) in 2-week-old nodules of pea wild-type SGE and mutant SGEFix$^-$-3 (*Pssym26*)

Genotype	Localization	Mean value	SE
SGE	Juvenile symbiosomes	61.25[ad]	2.73
	Mature symbiosomes	43.03[bd]	2.46
	Senescent symbiosomes	19.90[cd]	2.94
	Infection threads and infection droplets	11.15[f]	2.78
SGEFix$^-$-3 (*Pssym26*)	Juvenile symbiosomes	40.95[ae]	6.29
	Mature symbiosomes	32.28[be]	3.38
	Senescent symbiosomes	24.85[ce]	2.98
	Infection threads and infection droplets	15.36[f]	2.23

Results are presented as the number of gold particles/μm^2. Mean value ± SE (n = 30–60) are shown. Letters indicate statistically significant differences by the Tukey multiple range test (P value ≤ 0.001).

[a] Between juvenile symbiosomes of wild type and the mutant.
[b] Between mature symbiosomes of wild type and the mutant.
[c] Between senescent symbiosomes of wild type and the mutant.
[d] Between juvenile, mature, and senescent symbiosomes in wild type.
[e] Between juvenile, mature, and senescent symbiosomes in the mutant.
[f] Between infection threads and infection droplets in wild type and the mutant.

During the formation of compartments infested by both symbiotic bacteria and fungi and pathogenic ones, membranes are rearranged and restructured [Wang and Dong, 2011]. This requires significant reorganization not only of membrane systems, but also of the plant cell cytoskeleton [Kitaeva et al., 2016]. The endoplasmic reticulum (EPR) plays an important role in this rearrangement [*Tsyganova, Tsyganov, 2019b*]. It is closely related to infection structures. Thus, the tubules of granular EPR are in close contact with

the infection thread wall (Figure A.29A), and vesicles of smooth or agranular EPR are located near infection droplets and contain material similar in electron density to the matrix of infection droplets (Figure A.29B). Such vesicles are actively involved in the release of bacteria from infection droplets by delivering membrane material to the plasma membrane (Figure A.29C,G). In addition, vesicular transport is involved in the delivery to symbiosomes of phytohormones: gibberellin (Figure A.29E,H) **[**Serova et al., 2019] and trans-zeatin riboside (Figure A.29D) [*Dolgikh et al., 2020*], as well as glutathione, which may indirectly confirm the presence of plant glutathione transport to bacteroids (Figure A.29F) [*Ivanova et al., 2022*].

Symbiotically inefficient mutants of *P. sativum* show changes in the pattern and direction of vesicular transport correlated with their phenotypes [*Tsyganova et al., 2009b; Serova et al., 2019; Tsyganova et al., 2019a; Dolgikh et al., 2020; Ivanova et al., 2022*]. Thus, the mutant SGEFix$^-$-6 (*Pssym40-2*) exhibited an increased number of vesicles delivering membrane material to the hypertrophied infection droplets characteristic of this mutant (Figure A.29G). In the mutant SGEFix$^-$-2 (*Pssym33-3*), vesicular transport is involved in the abnormal secretion of trans-zeatin riboside into the vacuole, which correlates well with previous findings of reduced levels of this phytohormone in mutant nodules [*Dolgikh et al., 2020*]. In the mutant SGEFix$^-$-3 (*Pssym26*), characterized by morphologically differentiated bacteroids undergoing rapid degradation, vesicles delivering GA_3 to symbiosomes were observed (Figure A.29H), similar to the wild type [*Serova et al., 2019*]. The mutant SGEFix$^-$-1 (*Pssym40-1*) showed impaired transport of infection thread matrix glycoproteins into the intercellular space (Figure A.18D; Figure A.19B) [*Tsyganova et al., 2009b*]. In addition, the double mutant RBT3 (*Pssym33-3*, *Pssym40-1*) exhibited AGPE transport vesicles labeled with the MAC265 (Figure A.19D), MAC204 (Figure A.21B) and MAC236 (Figure A.21E) antibodies, not only to the infection thread but also to the intercellular space, demonstrating impaired transport in this mutant [*Tsyganova et al., 2009b; Tsyganova et al., 2019a*].

SUMMARY

During the development of legume-rhizobial symbiosis, the process of rhizobia internalization depends on the modification of plant-microbial surfaces (symbiotic interface) and, first of all, on changes in the composition and ratio of its components in the cell walls of both plant cells and infection threads. The various components of the symbiotic interface play an important role in providing positional information during rhizobial infection and nodule development. Differentiation of infected cells and successive changes in their morphology correspond to successive changes in the molecular composition of the apoplast and surface membrane structures (plasma membrane and symbiosome membrane). The studies of the symbiotic interface allowed us to identify its common and species-specific features in plants forming different nodule types (Table 9) [*Tsyganova et al., 2019c; Tsyganova et al., 2023a; Tsyganova et al., 2023b*].

Table 9 — Species-specific features of symbiotic interface in nodules of legumes

Species	Cell wall				Infection thread wall
	Meristematic cell	Colonized cell	Infected cell	Uninfected cell	
Pisum sativum	RG-I backbone	Ca^{2+}-bound HG	*	*	Galactan RG-I
Medicago truncatula	Galactan RG-I	XG	*	XG Ca^{2+}-bound HG	Ca^{2+}-bound HG
Galega orientalis	Galactan RG-I	XG	XG	LM HG RG-I backbone	Galactan RG-I
Vavilovia formosa	XG, LM HG	XG, LM HG	XG, LM HG	КГ	Galactan RG-I
Vicia villosa	*	LM HG	Galactan RG-I	*	LM HG
Glycine max	–	–	LM HG, Ca^{2+}-bound HG	Galactan RG-I	XG

Only major compounds according to fluorescence and immunogold microscopy data are given. * — cell walls include common components for all studied species and cell types: high methyl esterified HG and RG-I (backbone or arabinan side chain). LM HG — low methyl esterified HG, Galactan — the linear (1→4)-α-L-galactan side chain. A dash indicates the absence of this cell type in determinate nodules of *G. max*. Other abbreviations are given according to the main text.

All studied legume species were characterized by the presence of highly methyl esterified HG and RG-I (its polysaccharide backbone and arabinan side chain) in all cell walls and infection thread walls, which corresponds to isodiametrically growing cells [*Tsyganova et al., 2019c; Tsyganova et al., 2023a; Tsyganova et al., 2023b*]. The most striking species-specific features of the symbiotic interface in indeterminate nodules include the presence of a linear galactan side chain of RG-I in the walls of infection threads in *P. sativum*, *G. orientalis*, and *V. formosa*, in contrast to nodules of *M. truncatula* and *V. villosa* belonging to the same inverted repeats lacking clade (IRLCs) [*Tsyganova et al, 2019c; Tsyganova et al., 2023a; Tsyganova et al., 2023b*]. Also, the absence of fucosylated XG in cell walls in *P. sativum* nodules, its presence in cell walls of colonized and uninfected cells in *M. truncatula* nodules, and in cell walls of all cell types in *V. formosa* nodules can be attributed to species-specific features. Variations in the localization of HG, especially low-methylated HG, are also observed; it is present in the walls of infection threads in *V. villosa* nodules, in the cell walls of uninfected cells in *G. orientalis* nodules, and in the cell walls of all cell types in *V. formosa* nodules. Ca^{2+}-bound HG was characteristic of the cell walls of colonized cells of *P. sativum*, uninfected cells and the infection threads walls of *M. truncatula*. The unbranched RG-I backbone was predominantly detected in meristematic cells in *P. sativum* nodules and in the cell walls of uninfected cells in *G. orientalis* nodules [*Tsyganova et al., 2019c; Tsyganova et al., 2023a; Tsyganova et al., 2023b*]. In contrast to indeterminate nodules originating from pericycle cells and the inner layer of the root cortex, the composition and ratio of apoplast components in determinate nodules originating from cells of the outer layer of root cortex cells may differ from those in indeterminate ones. The presence of the galactan side chain of RG-I in the cell walls of non-infected cells and the preferential accumulation of fucosylated XG in the walls of infection threads can be considered as striking species-

specific features of the symbiotic interface of determinate nodules (using *G. max* as an example) [*Tsyganova et al., 2023a*].

The identified species-specific differences in the components of the symbiotic interface seem intriguing, considering that the studied species belong to the same clade with no inverted repeats (IRLC). The basis of these differences may be related to the formation of symbioses in *P. sativum*, *G. orientalis*, *V. villosa* and *M. truncatula* with rhizobia belonging to different genera, *Rhizobium* and *Sinorhizobium* (*Ensifer*). At the same time, rhizobia in the nodules of these legumes differ significantly in the morphology of nitrogen-fixing bacteroids. Previously, differences between *P. sativum* and *M. truncatula* in the organization of tubulin cytoskeleton were revealed [*Kitaeva et al., 2016*]. The observed differences in the composition of the symbiotic interface once again indicate the need to study each individual legume species. The results obtained in numerous studies of the model species *M. truncatula* may not always be applicable to other legume species.

The study of the symbiotic interface of symbiosomes also revealed some species specificity (Table 10). Thus, in nodules of *P. sativum*, an AGP with a GPI anchor was found to label not only the plasma membrane, as was demonstrated in nodules of *M. truncatula*, but also the symbiosome membrane, especially in symbiosomes with mature nitrogen-fixing bacteroids [*Tsyganova et al., 2019c*]. In studies of plant-microbial surface interactions in symbiosomes in indeterminate nodules of *P. sativum*, *G. orientalis*, and *M. truncatula*, the presence of arabinan, containing 2 to 7 arabinan residues and cross-linked to the arabinan side chain of RG-I, and membrane-bound AGP in symbiosomes with juvenile bacteroids and their absence in symbiosomes with mature bacteroids were shown [*Tsyganova et al, 2023a; Tsyganova et al., 2023b*]. At the same time, in nodules of the determinate type of *G. max*, arabinans were found in constant amounts in all symbiosomes in infected cells (Figure A.24F,I; Table 5) [*Tsyganova et al., 2023a*].

The ontogenetic changes of the symbiotic interface in indeterminate nodules of *P. sativum* have been described most completely [*Tsyganova et al., 2009b; Tsyganova et al., 2019a; Tsyganova et al., 2019c; Tsyganova et al., 2023b*]. Indeterminate nodules are characterized by the presence of a permanently active meristem and pronounced zonality

[Newcomb, 1976; Guinel, 2009]; therefore, in such nodules, a gradient of cell differentiation can be traced when they are infected with rhizobia. Cell walls undergo changes during infection of plant cells. Thus, at the initial stages of infection, fucosylated XG, cross-linked by Ca^{2+} ions HG molecules and RG-I molecules with block branching character appear in cell walls, which may be related to the strengthening of defense reactions and increase of cell wall stiffness. With further development of infection, fucosylated XG disappears from cell walls, but the content of low methyl esterified HG increases, which reaches a maximum in senescent infected cells with degenerating symbiosomes. Both wall and matrix composition of infection threads practically do not change in the mature nodule regardless of the histological zone: AGPE and extensins are determined in the matrix, HGs with different degrees of methylation are determined in the walls, and arabinan side chains are replaced by galactan side chains in RG-I molecules. During bacterial release from infection threads (juvenile symbiosomes), arabinans similar to arabinan side chains of RG-I are common in symbiosomes; during symbiosome maturation and differentiation of bacteroidetes, arabinans disappear in symbiosomes, but the number of GPI-anchored AGP increases, which can be considered a marker of symbiosome membrane maturity.

Table 10 — Species specificity of symbiosome symbiotic interface in legume nodules

Species	Symbiosomes with		
	juvenile bacteroids	mature bacteroids	poorly differentiated bacteroids
Pisum sativum	Arabinan RG-I	AGP with GPI-anchor	–
Medicago truncatula	Arabinan RG-I	–	–
Galega orientalis	Arabinan RG-I, AGP	–	–
Glycine max	–	–	Arabinan RG-I, AGP

Only major compounds according to fluorescence and immunogold microscopy data are given. Arabinan — linear (1→5)-α-L-arabinan side chain (LM6-M antibody). Other abbreviations are given according to the main text.

Some differences in the distribution of polysaccharides and cell wall proteins between wild-type and mutant nodules can be explained by activation of defense reactions or premature senescence in mutants. For example, the *P. sativum* mutant SGEFix^{-}-2 (*Pssym33-3*) exhibits intense defense reactions such as suberization of cell walls and infection thread walls, deposition of de-esterified pectin in infection thread walls, and increased expression level of the gene encoding peroxidase [*Ivanova et al., 2015*]. The formation of suberized cell wall material around the vacuole and the formation of pectin gel (identified using the LM5 antibody) in the matrix of infection threads are additional features of a pathogen-like defense response to bacterial infection in this mutant [*Tsyganova et al., 2019b*]. In the SGEFix^{-}-5 (*Pssym33-2*) mutant carrying a strong allele of the *PsSym33* gene, defense responses result in the degradation of rhizobia within infection threads [*Tsyganova et al., 2019*]. Overall, this suggests that an important function of the transcription factor CYCLOPS/IPD3 is to suppress defense responses during the establishment of legume-rhizobial symbiosis. Another *P. sativum* mutant SGEFix^{-}-1 (*Pssym40-1*) develops oxidative stress that leads to abnormal differentiation of bacteroides [*Tsyganova et al., 2009a; Provorov et al., 2012*]. The *P. sativum* mutant RisFixV (*Pssym42*), characterized by premature senescence of infection structures, demonstrates a different response to rhizobial infection: synthesis and accumulation of callose in the cell walls of infected cells and infection threads, in addition, bacteroid encapsulation by low-methylated pectin occurs in degenerating cells [*Ivanova et al., 2015*].

An attempt was made to create a model of infection thread functioning in legume nodules, a universal apoplastic compartment serving to deliver rhizobia inside the root and symbiotic nodule [*Tsyganova, Tsyganov, 2012; Tsyganova, Tsyganov, 2019a; Tsyganova, Tsyganov, 2019c; Tsyganova et al., 2021*].

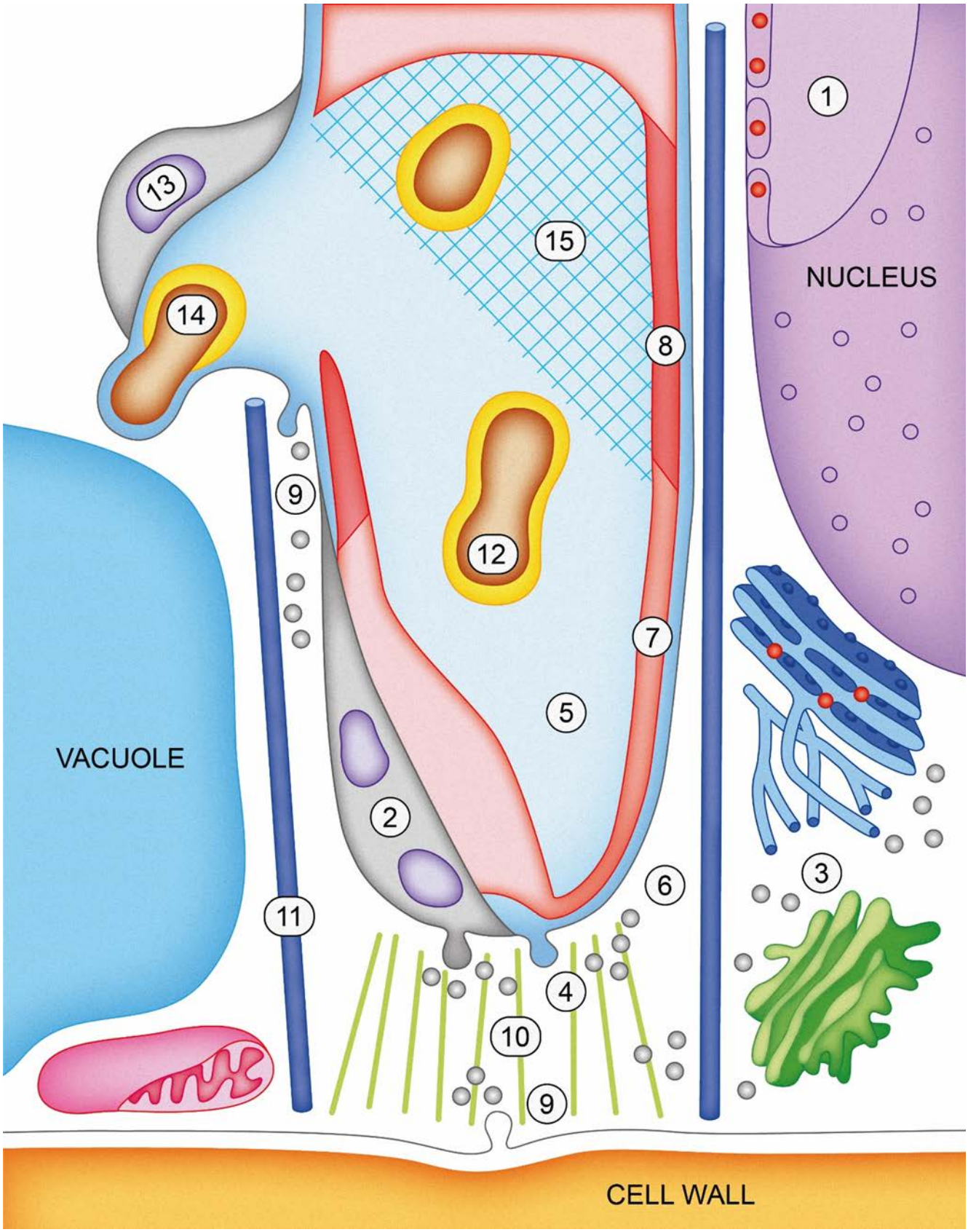
1
NUCLEUS
13
15
14
8
9
12
7
5
VACUOLE
2
3
6
11
4
10
9
CELL WALL

(**1**) Transcription factors modify the course of host cell development. (**2**) Plant proteins and glycoproteins are localized in the microdomains of the plasma membrane of the infection thread. (**3** and **4**) Vesicles derived from the endoplasmic reticulum and Golgi apparatus are directed to the plasma membrane at the tip of the infection thread, releasing their contents into the wall and extracellular matrix. This secretory mechanism is the driving force for the growth of the infection thread, coupled with the growth of bacterial cells within the luminal matrix. (**5**) Glycoproteins, proteins and polysaccharides influence the biophysical properties of the infection thread wall and luminal matrix. (**6**) Cell wall proteins and polysaccharides are transferred in vesicles from the Golgi apparatus. (**7**) In the nascent wall of the infection thread, there is a layer of α-cellulose and HG is predominantly in the highly methyl-esterified form. (**8**) The mature wall of the infection thread contains cellulose, xyloglucan, and HG with decreasing degrees of methyl-esterification. This creates a more rigid structure reinforced by bridging with Ca^{2+} ions. Also present is RG-I and RG-II (in the form of dimers with the borate ion), extensins, AGPs and expansins. (**9**) During the development of the infection droplet, enzymes are involved in the modification and degradation of the cell wall. (**10**) The actin cytoskeleton is involved in the organization of polar growth. (**11**) The microtubular cytoskeleton forms a tunnel for orientation. (**12**) Polysaccharides and proteins of the bacterial cell wall and capsule play an important role in the progression of the infection thread. (**13**) The symbiosome membrane contains a new range of proteins associated with nitrogen fixing endosymbiosis. (**14**) Within the symbiosomes, rhizobial cells lose their exopolysaccharide capsule and the structure of LPS is modified. (**15**) H_2O_2 plays a role in cross-linking of AGPEs and hardening of the infection thread matrix. HG, homogalacturonan; RG-I, rhamnogalacturonan I; RG-II, rhamnogalacturonan II. Green lines are actin microfilaments; blue lines are microtubules; ● - Ca^{2+}; light blue extracellular matrix is fluid; shaded blue matrix is solid; pink cell wall is newly synthesized; red cell wall is mature or modified. Objects are not scaled [*Tsyganova et al., 2021*].

Figure 4 — A model of growth and development of the legume-rhizobial symbiotic interface in infection threads of legumes (using *Pisum sativum* as an example)

The initiation and growth of the infection thread is a consequence of the exchange of signals with infecting Rhizobium bacteria and changes in transcriptional activity in the host cell nucleus. Among others, this leads to the synthesis and deposition of new proteins in the microdomains of the plasma membrane of the infection thread. Vesicles originating from EPR and AG fuse with the plasma membrane at the tip of the infection thread, releasing their contents into the wall and extracellular matrix. Targeted secretion from the vesicles (along with bacterial growth and division in the matrix of the infection thread lumen) is the driving force behind the growth of the infection thread. The glycoproteins, proteins and polysaccharide components of the infection thread matrix are represented by

AGPE, hydroxyproline-rich proteins, ENOD2/11, lipooxygenases, diamine oxidases and RG-II. In addition, H_2O_2 likely plays a role in cross-linking AGPE molecules and altering the biophysical properties of the infection thread matrix. Vesicles originating from AG also contain cellulose synthases, XGs, and pectins (HG, RG-I, and RG-II). HG is synthesized in a highly methyl esterified form and can be transported together with PME / PMEI complexes. All these components and other cell wall remodeling enzymes are released into the apoplast.

In the nascent infection thread wall, cellulose synthases are incorporated into the membrane and synthesize crystalline cellulose. At this stage, the major component of the infection thread wall is highly methyl esterified HG. At the mature stage, the main polysaccharide components are: cellulose, XG and HG with varying degrees of methyl esterification. HG with a low level of methyl esterification binds Ca^{2+} ions to each other, thereby increasing its stiffness. In the infection thread wall, RG-I is present as well as RG-II in the form of dimers with boron ion. The infection thread wall also contains extensins, AGPs and expansins. In addition, callose and phenolic compounds such as suberin may accumulate as part of defense reactions in response to ineffective symbiosis.

Many enzymes are involved in cell wall modification and degradation during infection thread growth and infection droplet formation. Polar growth of the infection thread is mediated by the actin cytoskeleton, and the arrangement of microtubules creates a restrictive tunnel for infection thread growth. Within the lumen, bacterial polysaccharides play an important role: EPS, KPS, LPS, cyclic β-glucan, RosR and peroxidases induced by rhizobia (Rip1-10).

After bacterial cells release from the infection droplet, several plant proteins associate with the symbiosome membrane. These include: lectin-like glycoprotein (PsNLEC1), synaptotagmin (MtSyt1/2/3), syntaxin (MtSYP132), inositol-containing phospholipid (JIM18 antigen), GPI-anchored AGP (JIM1 antigen), and arabinans (either as part of RG-I (LM6 antigen) or AGP (LM2 antigen)). Within the symbiosome, rhizobia differentiate into nitrogen-fixing bacteroids: they lose their exopolysaccharide capsule, and the structure of the lipid-A and O-antigenic groups of LPS is modified, partly by the action of the BacA protein.

The cell wall surrounding the infection thread is a dynamic and constantly changing system that performs both structural and protective functions [Tsyganova et al., 2021]. Its structure at an early stage in a root hair or root cortex cell may be very different from that of a host cell deep in the maturing nodule tissue. The dynamism of the infection thread complicates its study.

From an evolutionary perspective, the nature of the symbiotic interaction between legumes and rhizobia has become increasingly intimate and complex. On the one hand, it involves new aspects of cellular morphogenesis, notably the infection thread and symbiosomal compartments. On the other hand, there is a precise system for suppressing host defense responses. The challenge for future research will be to use genetics, genomics and cytological studies to integrate the many parameters involved in infection thread development, from signal transduction and protein transport to plant cell wall deposition and remodeling.

CONCLUSION

1. It has been shown that both indeterminate and determinate nodules are characterized by a universal distribution pattern of highly methyl esterified homogalacturonan and unbranched rhamnogalacturonan I backbone in cell walls and infection thread walls, which is associated with isotropic growth of infected cells.

2. Species-specific features of formation and modification of cell walls and infection thread walls were revealed: the presence of a linear galactan side chain of rhamnogalacturonan I in the walls of infection threads in *P. sativum*, *G. orientalis* and *V. formosa*, the presence of fucosylated xyloglucan in the cell walls of uninfected cells in *M. truncatula* and low methyl esterified homogalacturonan in *G. orientalis*, as well as variations in the localization of fucosylated xyloglucan and de-esterified homogalacturonan in cell walls and infection thread walls of the studied legume species forming indeterminate nodules. The presence of galactan side chain rhamnogalacturonan I in the walls of uninfected cells and fucosylated xyloglucan in the infection thread walls was detected in determinate nodules (*G. max* as an example).

3. Variation in the distribution and number of different arabinogalactan-protein extensin epitopes in the matrix of infection threads and infection droplets in nodules of wild-type and ineffective mutants of *P. sativum* was shown, suggesting a different role of specific sequences of the arabinogalactan-protein extensin macromolecule in the development of symbiotic nodules.

4. New markers of symbiosome differentiation in nodules of P. sativum, *M. truncatula*, *G. orientalis* and *G. max* were identified. Thus, arabinogalactan protein anchored in the membrane with a glycosylphosphatidylinositol anchor can be a marker of symbiosome maturation in *P. sativum* nodules, and arabinans with a chain length of 2-7 residues (both in the arabinan side chain of rhamnogalacturonan I and arabinogalactan proteins) are involved in symbiosome differentiation at early stages.

5. It was revealed that mutants of *P. sativum* and *M. truncatula* by orthologous genes *PsSym33* and *PsIPD3* are characterized by different manifestations of defense

reactions leading to an increase in cell wall stiffness. The mutant allele *Pssym33-3* leads to the formation of suberized cell wall material around the vacuole and pectin gel formation in the infection thread matrix in *P. sativum* nodules. This indicates that an important function of the key transcription factor CYCLOPS/IPD3 is to suppress defense responses during the development of legume-rhizobial symbiosis.

6. Deposition of pectin (deesterified homogalacturonan) around senescent bacteroids and callose around infection threads, infected cells and degenerating bacteroids in nodules of the *P. sativum* mutant RisFixV (*Pssym42*) was detected. Thus, the pea gene *PsSym42* (whose sequence has not yet been identified at this time) is also involved in the suppression of defense responses activated by rhizobial infection.

7. We traced the dynamics of hydrogen peroxide accumulation and determined the patterns of its localization in *P. sativum* nodules in effective and ineffective interaction, based on which we identified the role of H_2O_2 in infection thread growth associated with increased stiffness of the infection thread wall and in the development of oxidative stress in the symbiotically ineffective mutant SGEFix$^-$-1 (*Pssym40-1*).

8. We demonstrate that the antioxidant system (exemplified by glutathione) and phytohormones (exemplified by trans-zeatin riboside and gibberellic acid GA_3) are involved in the functioning and modification of the symbiotic interface of symbiosomes in *P. sativum* nodules in effective and ineffective interactions.

9. A model of infection thread functioning in indeterminate nodules is proposed, which shows the participation of various components of the symbiotic interface in the construction of the wall and matrix of the infection thread, as well as their participation in the formation of the infection droplet and subsequent bacterial release into the cytoplasm of the plant cell.

MAIN PUBLICATIONS RELEVANT FOR THE THESIS

1. Tsyganova A. V., Seliverstova E. V., Gorshkov A. P., Tsyganov V. E. Analysis of *Glycine max* and *Galega orientalis* nodules revealed specific features of symbiotic interface organization in determinate and indeterminate nodules. // Russian Journal of Plant Physiology. 2023. 70: 192. doi: 10.1134/S1021443723602495
2. Tsyganova A.V., Seliverstova E.V., Tsyganov V.E. Comparison of the formation of plant–microbial interface in *Pisum sativum* L. and *Medicago truncatula* Gaertn. nitrogen-fixing nodules. // International Journal of Molecular Sciences. 2023. 24: 13850. doi: 10.3390/ijms241813850
3. Ivanova K.A., Chernova E.N., Kulaeva O.A., Tsyganova A.V., Kusakin P.G., Russkikh I.V., Tikhonovich I.A., Tsyganov V.E. The regulation of pea (*Pisum sativum* L.) symbiotic nodule infection and defense responses by glutathione, homoglutathione, and their ratio // Frontiers in Plant Science. 2022. 13: 843565. doi: 10.3389/fpls.2022.843565
4. Tsyganova A.V., Brewin N.J., Tsyganov V.E. Structure and development of the legume-rhizobial symbiotic interface in infection threads (review) // Cells. 2021. 10: 1050. doi: 10.3390/cells10051050
5. Dolgikh E.A., Kusakin P.G., Kitaeva A.B., Tsyganova A.V., Kirienko A.N., Leppyanen I.V., Dolgikh A.V., Ilina E.L., Demchenko K.N., Tikhonovich I.A., Tsyganov V.E. Mutational analysis indicates that abnormalities in rhizobial infection and subsequent plant cell and bacteroid differentiation in pea (*Pisum sativum*) nodules coincide with abnormal cytokinin responses and localization // Annals of Botany. 2020. 125 (6): 905-923. doi: 10.1093/aob/mcaa022
6. Tsyganov V.E., Tsyganova A.V. Symbiotic regulatory genes controlling nodule development in *Pisum sativum* L. (review) // Plants. 2020. 9 (12): 1741. doi: 10.3390/plants9121741

7. Serova T.A., Tsyganova A.V., Tikhonovich I.A., Tsyganov V.E. Gibberellins inhibit nodule senescence and stimulate nodule meristem bifurcation in pea (*Pisum sativum* L.) // Frontiers in Plant Science. 2019. 10: 285. doi: 10.3389/fpls.2019.00285
8. Tsyganova A.V., Seliverstova E.V., Brewin N.J., Tsyganov V.E. Comparative analysis of remodelling of the plant–microbe interface in *Pisum sativum* and *Medicago truncatula* symbiotic nodules // Protoplasma. 2019. 256 (4): 983-996. doi: 10.1007/s00709-019-01355-5
9. Tsyganova A.V., Seliverstova E.V., Brewin N.J., Tsyganov V.E. Bacterial release is accompanied by ectopic accumulation of cell wall material around the vacuole in nodules of *Pisum sativum sym33-3* allele encoding transcription factor PsCYCLOPS/PsIPD3 // Protoplasma. 2019. 256 (5): 1449-1453. doi: 10.1007/s00709-019-01383-1
10. Tsyganova A.V., Tsyganov V.E. Plant cell wall in symbiotic interactions. Pectins (review) // Agricultural Biology (Sel'skokhozyaistvennaya Biologiya). 2019. 54 (3): 446-457. doi: 10.15389/agrobiology.2019.3.446rus
11. Tsyganova A.V., Brewin N.J., Tsyganov V.E. Analysis of epitope distribution of arabinogalactan protein-extensins in pea (*Pisum sativum*) nodules of wild-type and mutants impaired in infection thread growth // Ecological genetics. 2019. 17 (3): 5-12. doi: 10.17816/ecogen1735-12
12. Tsyganova A.V., Tsyganov V.E. Organization of the endoplasmic reticulum in cells of effective and ineffective pea nodules (*Pisum sativum* L.) // Ecological genetics. 2019. 17 (4): 5-14. doi: 10.17816/ecogen1745-14
13. Tsyganova A.V., Ivanova K.A., Tsyganov V.E. Histological and ultrastructural nodule organization of the pea (*Pisum sativum*) mutant SGEFix^{-}-5 in the *Sym33* gene encoding the transcription factor PsCYCLOPS/PsIPD3 // Ecological genetics. 2019. 17 (1): 65-70. doi: 10.17816/ecogen17165-70
14. Tsyganova A.V., Tsyganov V.E. Plant genetic control over infection thread development during legume-*Rhizobium* symbiosis (review) // In: Symbiosis (Ed. Rigobelo, E.C.), IntechOpen: London, UK. 2018. P. 23-52. doi: 10.5772/intechopen.70689

15. Serova T.A., Tsyganova A.V., Tsyganov V.E. Early nodule senescence is activated in symbiotic mutants of pea (*Pisum sativum* L.) forming ineffective nodules blocked at different nodule developmental stages //Protoplasma. 2018. 255 (5): 1443-1459. doi: 10.1007/s00709-018-1246-9
16. Tsyganova A.V., Kitaeva A.B., Tsyganov V.E. Cell differentiation in nitrogen–fixing nodules hosting symbiosomes (review) // Functional Plant Biology. 2018. 45: 47–57. doi: 10.1071/FP16377
17. Ivanova K.A., Tsyganova A.V., Brewin N.J., Tikhonovich I.A., Tsyganov V.E. Induction of host defences by *Rhizobium* during ineffective nodulation of pea (*Pisum sativum* L.) carrying symbiotically defective mutations *sym40* (*PsEFD*), *sym33* (*PsIPD3/PsCYCLOPS*) and *sym42* // Protoplasma. 2015. 252: 1505–1517. doi: 10.1007/s00709-015-0780-y
18. Provorov N.A., Tsyganova A.V., Brewin N.J., Tsyganov V.E., Vorobyov N.I. Evolution of symbiotic bacteria within the extra– and intracellular plant compartments: experimental evidence and mathematical simulation (Mini–review) // Symbiosis. 2013. 58: 39–50. doi: 10.1007/s13199-012-0220-0
19. Цыганова В.А., Цыганов В.Е. Роль поверхностных компонентов ризобий в симбиотических взаимодействиях с бобовыми растениями (обзор) // Успехи современной биологии. 2012. 132(2): 211–222.
20. Tsyganov V.E., Tsyganova A.V., Voroshilova V.A., Borisov A.Yu., Tikhonovich I.A. Analysis of the interaction of pea (*Pisum sativum* L.) symbiotic genes *Sym33* and *Sym42* whose mutations result in abnormalities during infection thread development // Russian Journal of Genetics: Applied Research. 2014. 4 (2): 83–87. doi: 10.1134/S2079059714020105
21. Цыганова А.В., Китаева А.Б., Бревин Н.Дж., Цыганов В.Е. Клеточные механизмы развития симбиотических клубеньков у бобовых растений (обзор) // Сельскохозяйственная биология. 2011. 3: 34–40.
22. Tsyganov V.E., Seliverstova E.V., Voroshilova V.A., Tsyganova A.V., Pavlova Z.B., Lebskii V.K., Borisov A.Yu., Brewin N.J., Tikhonovich I.A. Double mutant analysis of sequential functioning of pea (*Pisum sativum* L.) genes *Sym13*, *Sym33*, and *Sym40*

during symbiotic nodule development // Russian Journal of Genetics: Applied Research. 2011. 1 (5): 343–348. doi: 10.1134/S2079059711050145

23. Tsyganova A.V., Tsyganov V.E., Findlay K.C., Borisov A.Y., Tikhonovich I.A., Brewin N.J. Distribution of legume arabinogalactan protein-extensin (AGPE) glycoproteins in symbiotically defective pea mutants with abnormal infection threads. // Cell and Tissue Biology. 2009. 3 (1): 93–102. doi: 10.1134/S1990519X09010131
24. Цыганова А.В., Цыганов В.Е., Борисов А.Ю., Тихонович И.А., Бревин Н. Дж. Сравнительный цитохимический анализ распределения перекиси водорода у неэффективного мутанта гороха SGEFix⁻-1 (*sym40*) и исходной линии SGE // Экологическая генетика. 2009. VII (3): 3–9. doi: 10.17816/ecogen733-9
25. Brewin N., Khodorenko (Tsyganova) A., Tsyganov V.E., Borisov A.Y., Tikhonovich I.A., Rathbun E. Legume AGP-extensins in *Rhizobium* infection // In: Biological Nitrogen Fixation: Towards Poverty Alleviation through Sustainable Agriculture. Eds. F. D. Dakora et al., Springer Science + Business Media B.V., 2008. P. 185-187. doi: 10.1007/978-1-4020-8252-8_70

DESIGNATIONS AND ABBREVIATIONS

CCRC-M	Antibodies from the series «Complex Carbohydrate Research Center-Monoclonal»
JIM	Antibodies from the series «John Innes Monoclonal»
LM	Antibodies from the series «Leeds Monoclonal»
MAC	Monoclonal antibodies from the series ECACC («European collection of authenticated cell cultures»)
SNARE	Soluble NSF attachment receptor
AGP	Arabinogalactan protein
AGPE	Arabinogalactan-protein extensin
ROS	Reactive oxygen species
HG	Homogalacturonan
GPI	Glycosylphosphatidylinositol
XG	Xyloglucan
WAI	Week after inoculation
KPS	Capsular (K-) polysaccharide
LPS	Lipopolysaccharide
RG-I	Rhamnogalacturonan I
EPR	Endoplasmic reticulum
EPS	Exopolysaccharide

REFERENCES

1. Adams M.A., Buchmann N., Sprent J., Buckley T.N., Turnbull T.L. Crops, nitrogen, water: are legumes friend, foe, or misunderstood ally? // Trends in Plant Science. — 2018. — V. 23, № 6. — P. 539-550.

2. Anderson C.T. We be jammin': an update on pectin biosynthesis, trafficking and dynamics // Journal of Experimental Botany. — 2015. — V. 67, № 2. — P. 495-502.

3. Bapaume L., Reinhardt D. How membranes shape plant symbioses: signaling and transport in nodulation and arbuscular mycorrhiza // Frontiers in Plant Science. — 2012. — V. 3.

4. Bellincampi D., Cervone F., Lionetti V. Plant cell wall dynamics and wall-related susceptibility in plant–pathogen interactions // Frontiers in Plant Science. — 2014. — V. 5. — P. 228.

5. Benaben V., Duc G., Lefebvre V., Huguet T. TE7, an inefficient symbiotic mutant of *Medicago truncatula* Gaertn. cv Jemalong // Plant Physiology. — 1995. — V. 107, № 1. — P. 53-62.

6. Bestwick C.S., Brown I.R., Bennett M.H., Mansfield J.W. Localization of hydrogen peroxide accumulation during the hypersensitive reaction of lettuce cells to *Pseudomonas syringae* pv *phaseolicola* // The Plant Cell. — 1997. — V. 9, № 2. — P. 209-221.

7. Bolaños L., Cebrián A., Redondo-Nieto M., Rivilla R., Bonilla I. Lectin-like glycoprotein PsNLEC-1 is not correctly glycosylated and targeted in boron-deficient pea nodules // Molecular Plant-Microbe Interactions. — 2001. — V. 14, № 5. — P. 663-670.

8. Bolaños L., Redondo-Nieto M., Rivilla R., Brewin N.J., Bonilla I. Cell surface interactions of *Rhizobium* bacteroids and other bacterial strains with symbiosomal and peribacteroid membrane components from pea nodules // Molecular Plant-Microbe Interactions. — 2004. — V. 17, № 2. — P. 216-223.

9. Borisov A.Y., Rozov S.M., Tsyganov V.E., Morzhina E.V., Lebsky V.K., Tikhonovich I.A. Sequential functioning of *Sym-13* and *Sym-31*, two genes affecting

symbiosome development in root nodules of pea (*Pisum sativum* L) // Molecular and General Genetics. — 1997. — V. 254, № 5. — P. 592-598.

10. Bourassa D.V., Kannenberg E.L., Sherrier D.J., Buhr R.J., Carlson R.W. The lipopolysaccharide lipid A long-chain fatty acid is important for *Rhizobium leguminosarum* growth and stress adaptation in free-living and nodule environments // Molecular Plant-Microbe Interactions. — 2017. — V. 30, № 2. — P. 161-175.

11. Bradley D.J., Wood E.A., Larkins A.P., Galfre G., Butcher G.W., Brewin N.J. Isolation of monoclonal antibodies reacting with peribacteriod membranes and other components of pea root nodules containing *Rhizobium leguminosarum* // Planta. — 1988. — V. 173, № 2. — P. 149-160.

12. Brewin N., Khodorenko A., Tsyganov V.E., Borisov A.Y., Tikhonovich I.A., Rathbun E. Legume AGP-extensins in *Rhizobium* infection // Biological Nitrogen Fixation: Towards Poverty Alleviation through Sustainable Agriculture / Dakora F. D. et al., 2008. — P. 185-187.

13. Brewin N.J. Development of the legume root nodule // Annual Review of Cell Biology. — 1991. — V. 7, № 1. — P. 191-226.

14. Brewin N.J. Plant cell wall remodelling in the *Rhizobium*–legume symbiosis // Critical Reviews in Plant Sciences. — 2004. — V. 23, № 4. — P. 293-316.

15. Cameron C., Geitmann A. Cell mechanics of pollen tube growth // Current Opinion in Genetics & Development. — 2018. — V. 51. — P. 11-17.

16. Campbell G.R.O., Reuhs B.L., Walker G.C. Chronic intracellular infection of alfalfa nodules by *Sinorhizobium meliloti* requires correct lipopolysaccharide core // Proceedings of the National Academy of Sciences. — 2002. — V. 99, № 6. — P. 3938-3943.

17. Cantu D., Vicente A.R., Labavitch J.M., Bennett A.B., Powell A.L.T. Strangers in the matrix: plant cell walls and pathogen susceptibility // Trends in Plant Science. — 2008. — V. 13, № 11. — P. 610-617.

18. Cao L., Lu W., Mata A., Nishinari K., Fang Y. Egg-box model-based gelation of alginate and pectin: A review // Carbohydrate Polymers. — 2020. — V. 242. — P. 116389.

19. Carol R.J., Dolan L. Building a hair: tip growth in *Arabidopsis thaliana* root hairs // Philosophical Transactions of the Royal Society of London. Section B: Biological Sciences. — 2002. — V. 357, № 1422. — P. 815-821.

20. Cassab G.I. Plant cell wall proteins // Annual Review of Plant Physiology and Plant Molecular Biology. — 1998. — V. 49, № 1. — P. 281-309.

21. Catalano C.M., Lane W.S., Sherrier D.J. Biochemical characterization of symbiosome membrane proteins from *Medicago truncatula* root nodules // Electrophoresis. — 2004. — V. 25, № 3. — P. 519-531.

22. Cho E., Kwon C., Lee S., Tahir M.N., Park S., Jung S. Biotinylation of the rhizobial cyclic β-glucans and succinoglycans crucial for symbiosis with legumes // Carbohydrate Research. — 2014. — V. 389. — P. 141-146.

23. Clarke V.C., Loughlin P.C., Gavrin A., Chen C., Brear E.M., Day D.A., Smith P.M.C. Proteomic analysis of the soybean symbiosome identifies new symbiotic proteins // Molecular & Cellular Proteomics. — 2015. — V. 14, № 5. — P. 1301-1322.

24. Coba de la Peña T., Fedorova E., Pueyo J.J., Lucas M.M. The symbiosome: legume and rhizobia co-evolution toward a nitrogen-fixing organelle? // Frontiers in Plant Science. — 2018. — V. 8, № 2229.

25. Collmer A., Keen N.T. The role of pectic enzymes in plant pathogenesis // Annual Review of Phytopathology. — 1986. — V. 24. — P. 383-409.

26. Combier J.-P., Frugier F., de Billy F., Boualem A., El-Yahyaoui F., Moreau S., Vernié T., Ott T., Gamas P., Crespi M., Niebel A. *MtHAP2-1* is a key transcriptional regulator of symbiotic nodule development regulated by microRNA169 in *Medicago truncatula* // Genes and Development. — 2006. — V. 20, № 22. — P. 3084-3088.

27. Considine M.J., Siddique K.H.M., Foyer C.H. Nature’s pulse power: legumes, food security and climate change // Journal of Experimental Botany. — 2017. — V. 68, № 8. — P. 1815-1818.

28. Cosgrove D.J. Growth of the plant cell wall // Nature Reviews Molecular Cell Biology. — 2005. — V. 6, № 11. — P. 850-861.

29. Dahiya P., Brewin N.J. Immunogold localization of callose and other cell wall components in pea nodule transfer cells // Protoplasma. — 2000. — V. 214, № 3. — P. 210-218.

30. Dahiya P., Sherrier D.J., Kardailsky I.V., Borisov A.Y., Brewin N.J. Symbiotic gene *Sym31* controls the presence of a lectinlike glycoprotein in the symbiosome compartment of nitrogen-fixing pea nodules // Molecular Plant-Microbe Interactions. — 1998. — V. 11, № 9. — P. 915-923.

31. Davies H.A., Daniels M.J., Dow J.M. Induction of extracellular matrix glycoproteins in *Brassica* petioles by wounding and in response to *Xanthomonas campestris* // Molecular Plant-Microbe Interactions. — 1997. — V. 10, № 7. — P. 812-820.

32. de Faria S.M., Ringelberg J.J., Gross E., Koenen E.J.M., Cardoso D., Ametsitsi G.K.D., Akomatey J., Maluk M., Tak N., Gehlot H.S., Wright K.M., Teaumroong N., Songwattana P., de Lima H.C., Prin Y., Zartman C.E., Sprent J.I., Ardley J., Hughes C.E., James E.K. The innovation of the symbiosome has enhanced the evolutionary stability of nitrogen fixation in legumes // New Phytologist. — 2022. — V. 235, № 6. — P. 2365-2377.

33. Dixon R., Kahn D. Genetic regulation of biological nitrogen fixation // Nature Reviews Microbiology. — 2004. — V. 2. — P. 621-631.

34. Dolgikh E.A., Kirienko A.N., Leppyanen I.V., Dolgikh A.V. Role of phytohormones in the control of symbiotic nodule development in legume plants. II. Auxins (review) // Sel’skokhozyaistvennaya Biologiya [Agricultural Biology]. — 2016a. — V. 51, № 5. — P. 585-592.

35. Dolgikh E.A., Kirienko A.N., Leppyanen I.V. Dolgikh A.V. Role of phytohormones in the control of symbiotic nodule development in legume plants. I. Cytokinins (review) // Sel’skokhozyaistvennaya Biologiya [Agricultural Biology]. — 2016b. — V. 51, № 3. — P. 285-298.

36. Dolgikh E.A., Kusakin P.G., Kitaeva A.B., Tsyganova A.V., Kirienko A.N., Leppyanen I.V., Dolgikh A.V., Ilina E.L., Demchenko K.N., Tikhonovich I.A., Tsyganov V.E. Mutational analysis indicates that abnormalities in rhizobial infection and

subsequent plant cell and bacteroid differentiation in pea (*Pisum sativum*) nodules coincide with abnormal cytokinin responses and localization // Annals of Botany. — 2020. — V. 125, № 6. — P. 905-923.

37. Emerich D.W., Krishnan H.B. Symbiosomes: temporary moonlighting organelles // Biochemical Journal. — 2014. — V. 460, № 1. — P. 1-11.

38. Engelsdorf T., Hamann T. An update on receptor-like kinase involvement in the maintenance of plant cell wall integrity // Annals of Botany. — 2014. — V. 114, № 6. — P. 1339-1347.

39. Fagard M., Desnos T., Desprez T., Goubet F., Refregier G., Mouille G., McCann M., Rayon C., Vernhettes S., Höfte H. *PROCUSTE1* encodes a cellulose synthase required for normal cell elongation specifically in roots and dark-grown hypocotyls of *Arabidopsis* // The Plant Cell. — 2000. — V. 12, № 12. — P. 2409-2423.

40. Fedorova E.E. Rapid changes to endomembrane system of infected root nodule cells to adapt to unusual lifestyle // International Journal of Molecular Sciences. — 2023. — V. 24, № 5. — P. 4647.

41. Ferguson G.P., Roop R.M., Walker G.C. Deficiency of a *Sinorhizobium meliloti bacA* mutant in alfalfa symbiosis correlates with alteration of the cell envelope // Journal of Bacteriology. — 2002. — V. 184, № 20. — P. 5625-5632.

42. Forest F., Chase M.W. Eurosid i // The timetree of life. — New York: Oxford University Press, 2009. — P. 188-196.

43. Fraysse N., Couderc F., Poinsot V. Surface polysaccharide involvement in establishing the rhizobium–legume symbiosis // European Journal of Biochemistry. — 2003. — V. 270, № 7. — P. 1365-1380.

44. Frendo P., Matamoros M., Alloing G., Becana M. Thiol-based redox signaling in the nitrogen-fixing symbiosis // Frontiers in Plant Science. — 2013. — V. 4. — P. 376.

45. Freshour G., Bonin C.P., Reiter W.-D., Albersheim P., Darvill A.G., Hahn M.G. Distribution of fucose-containing xyloglucans in cell walls of the *mur1* mutant of *Arabidopsis* // Plant Physiology. — 2003. — V. 131, № 4. — P. 1602-1612.

46. Gage D.J. Infection and invasion of roots by symbiotic, nitrogen-fixing rhizobia during nodulation of temperate legumes // Microbiology and Molecular Biology Reviews. — 2004. — V. 68, № 2. — P. 280-300.

47. García-Rodríguez L.J., Gay A.C., Pon L.A. Puf3p, a Pumilio family RNA binding protein, localizes to mitochondria and regulates mitochondrial biogenesis and motility in budding yeast // The Journal of Cell Biology. — 2007. — V. 176, № 2. — P. 197-207.

48. Gavrin A., Chiasson D., Ovchinnikova E., Kaiser B.N., Bisseling T., Fedorova E.E. VAMP721a and VAMP721d are important for pectin dynamics and release of bacteria in soybean nodules // New Phytologist. — 2016. — V. 210, № 3. — P. 1011-1021.

49. Gavrin A., Kulikova O., Bisseling T., Fedorova E.E. Interface symbiotic membrane formation in root nodules of *Medicago truncatula*: the role of synaptotagmins *MtSyt1*, *MtSyt2* and *MtSyt3* // Frontiers in Plant Science. — 2017. — V. 8, № 201.

50. Goodrum L.J., Patel A., Leykam J.F., Kieliszewski M.J. Gum arabic glycoprotein contains glycomodules of both extensin and arabinogalactan-glycoproteins // Phytochemistry. — 2000. — V. 54, № 1. — P. 99-106.

51. Gorshkova T.A., Chemikosova S.B., Lozovaya V.V., Carpita N.C. Turnover of galactans and other cell wall polysaccharides during development of flax plants // Plant Physiology. — 1997. — V. 114, № 2. — P. 723-729.

52. Gucciardo S., Rathbun E.A., Shanks M., Jenkyns S., Mak L., Durrant M.C., Brewin N.J. Epitope tagging of legume root nodule extensin modifies protein structure and crosslinking in cell walls of transformed tobacco leaves // Molecular Plant-Microbe Interactions. — 2005. — V. 18, № 1. — P. 24-32.

53. Guinel F.C. Getting around the legume nodule: I. The structure of the peripheral zone in four nodule types // Botany. — 2009. — V. 87, № 12. — P. 1117-1138.

54. Guinel F.C., Geil R.D. A model for the development of the rhizobial and arbuscular mycorrhizal symbioses in legumes and its use to understand the roles of

ethylene in the establishment of these two symbioses // Canadian Journal of Botany. — 2002. — V. 80, № 7. — P. 695-720.

55. Haag A.F., Arnold M.F.F., Myka K.K., Kerscher B., Dall'Angelo S., Zanda M., Mergaert P., Ferguson G.P. Molecular insights into bacteroid development during *Rhizobium*–legume symbiosis // FEMS Microbiology Reviews. — 2013. — V. 37, № 3. — P. 364-383.

56. Hancock J.T., Desikan R., Clarke A., Hurst R.D., Neill S.J. Cell signalling following plant/pathogen interactions involves the generation of reactive oxygen and reactive nitrogen species // Plant Physiology and Biochemistry. — 2002. — V. 40, № 6. — P. 611-617.

57. Houston K., Tucker M.R., Chowdhury J., Shirley N., Little A. The plant cell wall: a complex and dynamic structure as revealed by the responses of genes under stress conditions // Frontiers in Plant Science. — 2016. — V. 7. — P. 984.

58. Huang R., Liu M., Gong G., Wu P., Patra B., Yuan L., Qin H., Wang X., Wang G., Liao H., Gao L., Yang C., Li H., Zhang S. The Pumilio RNA-binding protein APUM24 regulates seed maturation by fine-tuning the BPM-WRI1 module in *Arabidopsis* // Journal of Integrative Plant Biology. — 2021. — V. 63, № 7. — P. 1240-1259.

59. Hückelhoven R. Cell wall–associated mechanisms of disease resistance and susceptibility // Annual Review of Phytopathology. — 2007. — V. 45, № 1. — P. 101-127.

60. Ibáñez F., Wall L., Fabra A. Starting points in plant-bacteria nitrogen-fixing symbioses: intercellular invasion of the roots // Journal of Experimental Botany. — 2016. — V. 68, № 8. — P. 1905-1918.

61. Ivanov S., Fedorova E.E., Limpens E., De Mita S., Genre A., Bonfante P., Bisseling T. *Rhizobium*–legume symbiosis shares an exocytotic pathway required for arbuscule formation // Proceedings of the National Academy of Sciences of the United States of America. — 2012. — V. 109, № 21. — P. 8316-8321.

62. Ivanova K.A., Chernova E.N., Kulaeva O.A., Tsyganova A.V., Kusakin P.G., Russkikh I.V., Tikhonovich I.A., Tsyganov V.E. The regulation of pea (*Pisum*

sativum L.) symbiotic nodule infection and defense responses by glutathione, homoglutathione, and their ratio // Frontiers in Plant Science. — 2022. — V. 13. — P. 843565.

63. Ivanova K.A., Tsyganov V.E. Antioxidant defense system in symbiotic nodules of legumes (review) // Sel'skokhozyaistvennaya Biologiya [Agricultural Biology]. — 2017. — T. 52, № 5. — C. 878-894.

64. Ivanova K.A., Tsyganova A.V., Brewin N.J., Tikhonovich I.A., Tsyganov V.E. Induction of host defences by *Rhizobium* during ineffective nodulation of pea (*Pisum sativum* L.) carrying symbiotically defective mutations *sym40* (*PsEFD*), *sym33* (*PsIPD3/PsCYCLOPS*) and *sym42* // Protoplasma. — 2015. — V. 252, № 6. — P. 1505-1517.

65. Jamet A., Mandon K., Puppo A., Hérouart D. H_2O_2 is required for optimal establishment of the *Medicago sativa/Sinorhizobium meliloti* symbiosis // Journal of Bacteriology. — 2007. — V. 189, № 23. — P. 8741-8745.

66. Kardailsky I.V., Sherrier D.J., Brewin N.J. Identification of a new pea gene, *PsNlec1*, encoding a lectin-like glycoprotein isolated from the symbiosomes of root nodules // Plant Physiology. — 1996. — V. 111, № 1. — P. 49-60.

67. Keating D.H., Willits M.G., Long S.R. A *Sinorhizobium meliloti* lipopolysaccharide mutant altered in cell surface sulfation // Journal of Bacteriology. — 2002. — V. 184, № 23. — P. 6681-6689.

68. Keegstra K. Plant cell walls // Plant Physiology. — 2010. — V. 154, № 2. — P. 483-486.

69. Kelly S., Mun T., Stougaard J., Ben C., Andersen S.U. Distinct *Lotus japonicus* transcriptomic responses to a spectrum of bacteria ranging from symbiotic to pathogenic // Frontiers in Plant Science. — 2018. — V. 9. — P. 1218.

70. Kiss E., Kereszt A., Barta F., Stephens S., Reuhs B.L., Kondorosi Á., Putnoky P. The *rkp-3* gene region of *Sinorhizobium meliloti* Rm41 contains strain-specific genes that determine K antigen structure // Molecular Plant-Microbe Interactions. — 2001. — V. 14, № 12. — P. 1395-1403.

71. Kitaeva A.B., Demchenko K.N., Tikhonovich I.A., Timmers A.C.J., Tsyganov V.E. Comparative analysis of the tubulin cytoskeleton organization in nodules of *Medicago truncatula* and *Pisum sativum*: bacterial release and bacteroid positioning correlate with characteristic microtubule rearrangements // New Phytologist. — 2016. — V. 210, № 1. — P. 168-183.

72. Komalavilas P., Mort A.J. The acetylation of O-3 of galacturonic acid in the rhamnose-rich portion of pectins // Carbohydrate Research. — 1989. — V. 189. — P. 261-272.

73. Kusakin P.G., Serova T.A., Gogoleva N.E., Gogolev Y.V., Tsyganov V.E. Laser microdissection of *Pisum sativum* L. nodules followed by RNA-seq analysis revealed crucial transcriptomic changes during infected cell differentiation // Agronomy. — 2021. — V. 11, № 12. — P. 2504.

74. Le Quéré A.J.L., Deakin W.J., Schmeisser C., Carlson R.W., Streit W.R., Broughton W.J., Forsberg L.S. Structural characterization of a K-antigen capsular polysaccharide essential for normal symbiotic infection in *Rhizobium* sp. NGR234: Deletion of the rkpMNO locus prevents synthesis of 5,7-diacetamido-3,5,7,9-tetradeoxy-non-2-ulosonic acid // Journal of Biological Chemistry. — 2006. — V. 281, № 39. — P. 28981-28992.

75. Levesque-Tremblay G., Pelloux J., Braybrook S.A., Müller K. Tuning of pectin methylesterification: consequences for cell wall biomechanics and development // Planta. — 2015. — V. 242, № 4. — P. 791-811.

76. Li Y.-Y., Chen X.-M., Zhang Y., Cho Y.-H., Wang A.-R., Yeung E.C., Zeng X., Guo S.-X., Lee Y.-I. Immunolocalization and changes of hydroxyproline-rich glycoproteins during symbiotic germination of *Dendrobium officinale* // Frontiers in Plant Science. — 2018. — V. 9. — P. 552.

77. Lievens S., Goormachtig S., Herman S., Holsters M. Patterns of pectin methylesterase transcripts in developing stem nodules of *Sesbania rostrata* // Molecular Plant-Microbe Interactions. — 2002. — V. 15, № 2. — P. 164-168.

78. Limpens E., Ivanov S., van Esse W., Voets G., Fedorova E., Bisseling T. *Medicago* N_2-fixing symbiosomes acquire the endocytic identity marker Rab7 but delay

the acquisition of vacuolar identity // The Plant Cell. — 2009. — V. 21, № 9. — P. 2811-2828.

79. Lionetti V., Cervone F., Bellincampi D. Methyl esterification of pectin plays a role during plant–pathogen interactions and affects plant resistance to diseases // Journal of Plant Physiology. — 2012. — V. 169, № 16. — P. 1623-1630.

80. Madsen L.H., Tirichine L., Jurkiewicz A., Sullivan J.T., Heckmann A.B., Bek A.S., Ronson C.W., James E.K., Stougaard J. The molecular network governing nodule organogenesis and infection in the model legume *Lotus japonicus* // Nature Communications. — 2010. — V. 1. — P. 10.

81. Matamoros M.A., Becana M. Redox control of the legume-Rhizobium symbiosis // Advances in Botanical Research / Frendo P. et al.Academic Press, 2020. — P. 67-96.

82. Matamoros M.A., Clemente M.R., Sato S., Asamizu E., Tabata S., Ramos J., Moran J.F., Stiller J., Gresshoff P.M., Becana M. Molecular analysis of the pathway for the synthesis of thiol tripeptides in the model legume *Lotus japonicus* // Molecular Plant-Microbe Interactions. — 2003. — V. 16, № 11. — P. 1039-1046.

83. Matamoros M.A., Fernández-García N., Wienkoop S., Loscos J., Saiz A., Becana M. Mitochondria are an early target of oxidative modifications in senescing legume nodules // New Phytologist. — 2013. — V. 197, № 3. — P. 873-885.

84. Mathesius U. Hormonal interactions in the regulation of the nitrogen-fixing legume-*Rhizobium* symbiosis // Advances in Botanical Research / Frendo P. et al.Academic Press, 2020. — P. 41-66.

85. Mbengue M.D., Hervé C., Debellé F. Nod factor signaling in symbiotic nodulation // Advances in Botanical Research / Frendo P. et al.Academic Press, 2020. — P. 1-39.

86. McAdam E.L., Reid J.B., Foo E. Gibberellins promote nodule organogenesis but inhibit the infection stages of nodulation // Journal of Experimental Botany. — 2018. — V. 69, № 8. — P. 2117-2130.

87. McCartney L., Ormerod A.P., Gidley M.J., Knox J.P. Temporal and spatial regulation of pectic (1→4)-β-D-galactan in cell walls of developing pea cotyledons:

implications for mechanical properties // The Plant Journal. — 2000. — V. 22, № 2. — P. 105-113.

88. McCartney L., Steele-King C.G., Jordan E., Knox J.P. Cell wall pectic (1→4)-β-$_D$-galactan marks the acceleration of cell elongation in the Arabidopsis seedling root meristem // The Plant Journal. — 2003. — V. 33, № 3. — P. 447-454.

89. Miedes E., Vanholme R., Boerjan W., Molina A. The role of the secondary cell wall in plant resistance to pathogens // Frontiers in Plant Science. — 2014. — V. 5. — P. 358.

90. Mohnen D. Pectin structure and biosynthesis // Current Opinion in Plant Biology. — 2008. — V. 11, № 3. — P. 266-277.

91. Monahan-Giovanelli H., Pinedo C.A., Gage D.J. Architecture of infection thread networks in developing root nodules induced by the symbiotic bacterium *Sinorhizobium meliloti* on *Medicago truncatula* // Plant Physiology. — 2006. — V. 140, № 2. — P. 661-670.

92. Muñoz J.A., Coronado C., Pérez-Hormaeche J., Kondorosi A., Ratet P., Palomares A.J. *MsPG3*, a *Medicago sativa* polygalacturonase gene expressed during the alfalfa–*Rhizobium meliloti* interaction // Proceedings of the National Academy of Sciences of the United States of America. — 1998. — V. 95, № 16. — P. 9687-9692.

93. Newcomb W. A correlated light and electron microscopic study of symbiotic growth and differentiation in *Pisum sativum* root nodules // Canadian Journal of Botany. — 1976. — V. 54, № 18. — P. 2163-2186.

94. Nezamivand-Chegini M., Metzger S., Moghadam A., Tahmasebi A., Koprivova A., Eshghi S., Mohammadi-Dehchesmeh M., Kopriva S., Niazi A., Ebrahimie E. Nitrogen and phosphorus deficiencies alter primary and secondary metabolites of soybean roots // bioRxiv. — 2022. — V. 03, № 14. — P. 484309.

95. Nguema-Ona E., Bannigan A., Chevalier L., Baskin T.I., Driouich A. Disruption of arabinogalactan proteins disorganizes cortical microtubules in the root of *Arabidopsis thaliana* // The Plant Journal. — 2007. — V. 52, № 2. — P. 240-251.

96. Nguema-Ona E., Vicré-Gibouin M., Cannesan M.-A., Driouich A. Arabinogalactan proteins in root–microbe interactions // Trends in Plant Science. — 2013. — V. 18, № 8. — P. 440-449.

97. Niehaus K., Kapp D., Pühler A. Plant defence and delayed infection of alfalfa pseudonodules induced by an exopolysaccharide (EPS I)-deficient *Rhizobium meliloti* mutant // Planta. — 1993. — V. 190, № 3. — P. 415-425.

98. Oldroyd G.E.D., Murray J.D., Poole P.S., Downie J.A. The rules of engagement in the legume-rhizobial symbiosis // Annual Review of Genetics. — 2011. — V. 45, № 1. — P. 119-144.

99. Ovchinnikova E., Journet E.-P., Chabaud M., Cosson V., Ratet P., Duc G., Fedorova E., Liu W., den Camp R.O., Zhukov V., Tikhonovich I., Borisov A., Bisseling T., Limpens E. IPD3 controls the formation of nitrogen-fixing symbiosomes in pea and *Medicago* Spp. // Molecular Plant-Microbe Interactions. — 2011. — V. 24, № 11. — P. 1333-1344.

100. Palin R., Geitmann A. The role of pectin in plant morphogenesis // Biosystems. — 2012. — V. 109, № 3. — P. 397-402.

101. Parada M., Vinardell J.M., Ollero F.J., Hidalgo Á., Gutiérrez R., Buendía-Clavería A.M., Lei W., Margaret I., López-Baena F.J., Gil-Serrano A.M., Rodríguez-Carvajal M.A., Moreno J., Ruiz-Sainz J.E. *Sinorhizobium fredii* HH103 mutants affected in capsular polysaccharide (KPS) are impaired for nodulation with soybean and *Cajanus cajan* // Molecular Plant-Microbe Interactions. — 2006. — V. 19, № 1. — P. 43-52.

102. Parniske M. Arbuscular mycorrhiza: the mother of plant root endosymbioses // Nature Reviews Microbiology. — 2008. — V. 6, № 10. — P. 763-775.

103. Pawlowski K., Sirrenberg A. Symbiosis between *Frankia* and actinorhizal plants: root nodules of non-legumes // Indian Journal Of Experimental Biology. — 2003. — V. 41, № 10. — P. 1165-1183.

104. Pedersen H.L., Fangel J.U., McCleary B., Ruzanski C., Rydahl M.G., Ralet M.-C., Farkas V., von Schantz L., Marcus S.E., Andersen M.C.F., Field R., Ohlin M., Knox J.P., Clausen M.H., Willats W.G.T. Versatile high resolution oligosaccharide

microarrays for plant glycobiology and cell wall research // Journal of Biological Chemistry. — 2012. — V. 287, № 47. — P. 39429-39438.

105. Perotto S., Donovan N., Drobak B.K., Brewin N.J. Differential expression of a glycosyl inositol phospholipid antigen on the peribacteroid membrane during pea nodule development // Molecular Plant-Microbe Interactions. — 1995. — V. 8, № 4. — P. 560-568.

106. Perotto S., Vandenbosch K.A., Butcher G.W., Brewin N.J. Molecular composition and development of the plant glycocalyx associated with the peribacteroid membrane of pea root-nodules // Development. — 1991. — V. 112, № 3. — P. 763-773.

107. Pogorelko G., Lionetti V., Bellincampi D., Zabotina O. Cell wall integrity: Targeted post-synthetic modifications to reveal its role in plant growth and defense against pathogens // Plant Signaling & Behavior. — 2013. — V. 8, № 9. — P. e25435.

108. Prasad A., Porter D.F., Kroll-Conner P.L., Mohanty I., Ryan A.R., Crittenden S.L., Wickens M., Kimble J. The PUF binding landscape in metazoan germ cells // RNA. — 2016. — V. 22, № 7. — P. 1026-1043.

109. Provorov N.A., Tsyganova A.V., Brewin N.J., Tsyganov V.E., Vorobyov N.I. Evolution of symbiotic bacteria within the extra- and intra-cellular plant compartments: experimental evidence and mathematical simulation (Mini-review) // Symbiosis. — 2012. — V. 58, № 1-3. — P. 39-50.

110. Pumplin N., Harrison M.J. Live-cell imaging reveals periarbuscular membrane domains and organelle location in *Medicago truncatula* roots during arbuscular mycorrhizal symbiosis // Plant Physiology. — 2009. — V. 151, № 2. — P. 809-819.

111. Puppo A., Pauly N., Boscari A., Mandon K., Brouquisse R. Hydrogen peroxide and nitric oxide: key regulators of the legume–*Rhizobium* and mycorrhizal symbioses // Antioxidants and Redox Signaling. — 2013. — V. 18, № 16. — P. 2202-2219.

112. Rae A., Perotto S., Knox J., Kannenberg E., Brewin N. Expression of extracellular glycoproteins in the uninfected cells of developing pea nodule tissue // Molecular Plant-Microbe Interactions. — 1991. — V. 4, № 6. — P. 563-570.

113. Rae A.L., Bonfante-Fasolo P., Brewin N.J. Structure and growth of infection threads in the legume symbiosis with *Rhizobium leguminosarum* // The Plant Journal. — 1992. — V. 2, № 3. — P. 385-395.

114. Ramu S.K., Peng H.-M., Cook D.R. Nod factor induction of reactive oxygen species production is correlated with expression of the early nodulin gene *rip1* in *Medicago truncatula* // Molecular Plant-Microbe Interactions. — 2002. — V. 15, № 6. — P. 522-528.

115. Rathbun E.A., Brewin N.J. Gum arabic glycoprotein and the infection of legumes by *Rhizobium*: evidence for tyrosine cross-linking by peroxidase and by inorganic catalysis // Aspects of Applied Biology. — 2009. — V. 96. — P. 241-246.

116. Rathbun E.A., Naldrett M.J., Brewin N.J. Identification of a family of extensin-like glycoproteins in the lumen of *Rhizobium*-induced infection threads in pea root nodules // Molecular Plant-Microbe Interactions. — 2002. — V. 15, № 4. — P. 350-359.

117. Redondo-Nieto M., Reguera M., Bonilla I., Bolaños L. Boron dependent membrane glycoproteins in symbiosome development and nodule organogenesis // Plant Signaling & Behavior. — 2008. — V. 3, № 5. — P. 298-300.

118. Reguera M., Abreu I., Brewin N.J., Bonilla I., Bolaños L. Borate promotes the formation of a complex between legume AGP-extensin and rhamnogalacturonan II and enhances production of *Rhizobium* capsular polysaccharide during infection thread development in *Pisum sativum* symbiotic root nodules // Plant, Cell & Environment. — 2010. — V. 33, № 12. — P. 2112-2120.

119. Reiter W.-D., Chapple C.C.S., Somerville C.R. Altered growth and cell walls in a fucose-deficient mutant of *Arabidopsis* // Science. — 1993. — V. 261, № 5124. — P. 1032-1035.

120. Rich M.K., Schorderet M., Reinhardt D. The role of the cell wall compartment in mutualistic symbioses of plants // Frontiers in Plant Science. — 2014. — V. 5. — P. 238.

121. Robledo M., Jiménez-Zurdo J.I., Velázquez E., Trujillo M.E., Zurdo-Piñeiro J.L., Ramírez-Bahena M.H., Ramos B., Díaz-Mínguez J.M., Dazzo F., Martínez-Molina

E., Mateos P.F. *Rhizobium* cellulase CelC2 is essential for primary symbiotic infection of legume host roots // Proceedings of the National Academy of Sciences. — 2008. — V. 105, № 19. — P. 7064-7069.

122. Rodríguez-Llorente I.D., Pérez-Hormaeche J., Dary M., Caviedes M.A., Kondorosi A., Ratet P., Palomares A.J. Expression of MsPG3-GFP fusions in *Medicago truncatula* 'hairy roots' reveals preferential tip localization of the protein in root hairs // European Journal of Biochemistry. — 2003. — V. 270, № 2. — P. 261-269.

123. Rodríguez-Llorente I.D., Pérez-Hormaeche J., Mounadi K.E., Dary M., Caviedes M.A., Cosson V., Kondorosi A., Ratet P., Palomares A.J. From pollen tubes to infection threads: recruitment of *Medicago* floral pectic genes for symbiosis // The Plant Journal. — 2004. — V. 39, № 4. — P. 587-598.

124. Roth L., Stacey G. Bacterium release into host cells of nitrogen-fixing soybean nodules: the symbiosome membrane comes from three sources // European Journal of Cell Biology. — 1989. — V. 49, № 1. — P. 13-23.

125. Rubio M.C., James E.K., Clemente M.R., Bucciarelli B., Fedorova M., Vance C.P., Becana M. Localization of superoxide dismutases and hydrogen peroxide in legume root nodules // Molecular Plant-Microbe Interactions. — 2004. — V. 17, № 12. — P. 1294-1305.

126. Rydahl M.G., Hansen A.R., Kračun S.K., Mravec J. Report on the current inventory of the toolbox for plant cell wall analysis: proteinaceous and small molecular probes // Frontiers in Plant Science. — 2018. — V. 9. — P. 581.

127. Santos R., Hérouart D., Puppo A., Touati D. Critical protective role of bacterial superoxide dismutase in *Rhizobium*–legume symbiosis // Molecular Microbiology. — 2000. — V. 38, № 4. — P. 750-759.

128. Santos R., Hérouart D., Sigaud S., Touati D., Puppo A. Oxidative burst in alfalfa-*Sinorhizobium meliloti* symbiotic interaction // Molecular Plant-Microbe Interactions. — 2001. — V. 14, № 1. — P. 86-89.

129. Schreiber L., Hartmann K., Skrabs M., Zeier J. Apoplastic barriers in roots: chemical composition of endodermal and hypodermal cell walls // Journal of Experimental Botany. — 1999. — V. 50, № 337. — P. 1267-1280.

130. Seifert G.J., Roberts K. The biology of arabinogalactan proteins // Annual Review of Plant Biology. — 2007. — V. 58, № 1. — P. 137-161.

131. Serova T.A., Tsyganova A.V., Tikhonovich I.A., Tsyganov V.E. Gibberellins inhibit nodule senescence and stimulate nodule meristem bifurcation in pea (*Pisum sativum* L.) // Frontiers in Plant Science. — 2019. — V. 10, № 285. — P. 285.

132. Serova T.A., Tsyganova A.V., Tsyganov V.E. Early nodule senescence is activated in symbiotic mutants of pea (*Pisum sativum* L.) forming ineffective nodules blocked at different nodule developmental stages // Protoplasma. — 2018. — V. 255, № 5. — P. 1443-1459.

133. Sherrier D.J., Borisov A.Y., Tikhonovich I.A., Brewin N.J. Immunocytological evidence for abnormal symbiosome development in nodules of the pea mutant line Sprint-2Fix$^-$ (*sym31*) // Protoplasma. — 1997. — V. 199, № 1. — P. 57-68.

134. Sherrier D.J., Prime T.A., Dupree P. Glycosylphosphatidylinositol-anchored cell-surface proteins from *Arabidopsis* // Electrophoresis. — 1999. — V. 20, № 10. — P. 2027-2035.

135. Showalter A.M., Basu D. Extensin and arabinogalactan-protein biosynthesis: glycosyltransferases, research challenges, and biosensors // Frontiers in Plant Science. — 2016. — V. 7.

136. Silva I.R., Jers C., Meyer A.S., Mikkelsen J.D. Rhamnogalacturonan I modifying enzymes: an update // New Biotechnology. — 2016. — V. 33, № 1. — P. 41-54.

137. Singh S., Katzer K., Lambert J., Cerri M., Parniske M. CYCLOPS, a DNA-binding transcriptional activator, orchestrates symbiotic root nodule development // Cell Host and Microbe. — 2014. — V. 15, № 2. — P. 139-152.

138. Skorupska A., Janczarek M., Marczak M., Mazur A., Król J. Rhizobial exopolysaccharides: genetic control and symbiotic functions // Microbial Cell Factories. — 2006. — V. 5, № 1. — P. 7.

139. Smallwood M., Martin H., Knox J.P. An epitope of rice threonine- and hydroxyproline-rich glycoprotein is common to cell wall and hydrophobic plasma-membrane glycoproteins // Planta. — 1995. — V. 196, № 3. — P. 510-522.

140. Sprent J.I., Ardley J., James E.K. Biogeography of nodulated legumes and their nitrogen-fixing symbionts // New Phytologist. — 2017. — V. 215, № 1. — P. 40-56.

141. Su C. Pectin modifications at the symbiotic interface // New Phytologist. — 2023. — V. 238, № 1. — P. 25-32.

142. Su C., Zhang G., Rodriguez-Franco M., Hinnenberg R., Wietschorke J., Liang P., Yang W., Uhler L., Li X., Ott T. Transcellular progression of infection threads in *Medicago truncatula* roots is associated with locally confined cell wall modifications // Current Biology. — 2023. — V. 33, № 3. — P. 533-542.e535.

143. Su S., Higashiyama T. Arabinogalactan proteins and their sugar chains: functions in plant reproduction, research methods, and biosynthesis // Plant Reproduction. — 2018. — V. 31, № 1. — P. 67-75.

144. Sujkowska-Rybkowska M., Borucki W. Accumulation and localization of extensin protein in apoplast of pea root nodule under aluminum stress // Micron. — 2014. — V. 67. — P. 10-19.

145. Sujkowska M., Górska-Czekaj M., Bederska M., Borucki W. Vacuolar organization in the nodule parenchyma is important for the functioning of pea root nodules // Symbiosis. — 2011. — V. 54, № 1. — P. 1-16.

146. Tatsukami Y., Ueda M. Rhizobial gibberellin negatively regulates host nodule number // Scientific Reports. — 2016. — V. 6. — P. 27998.

147. Thordal-Christensen H., Zhang Z., Wei Y., Collinge D.B. Subcellular localization of H_2O_2 in plants. H_2O_2 accumulation in papillae and hypersensitive response during the barley—powdery mildew interaction // The Plant Journal. — 1997. — V. 11, № 6. — P. 1187-1194.

148. Timmers A.C., Auriac M.C., Truchet G. Refined analysis of early symbiotic steps of the *Rhizobium-Medicago* interaction in relationship with microtubular

cytoskeleton rearrangements // Development. — 1999. — V. 126, № 16. — P. 3617-3628.

149. Timmers A.C.J., Soupène E., Auriac M.-C., de Billy F., Vasse J., Boistard P., Truchet G. Saprophytic intracellular rhizobia in alfalfa nodules // Molecular Plant-Microbe Interactions. — 2000. — V. 13, № 11. — P. 1204-1213.

150. Tirichine L.l., de Billy F., Huguet T. *Mtsym6*, a gene conditioning *Sinorhizobium* strain-specific nitrogen fixation in *Medicago truncatula* // Plant Physiology. — 2000. — V. 123, № 3. — P. 845-852.

151. Tsyganov V.E., Morzhina E.V., Stefanov S.Y., Borisov A.Y., Lebsky V.K., Tikhonovich I.A. The pea (*Pisum sativum* L.) genes *sym33* and *sym40* control infection thread formation and root nodule function // Molecular and General Genetics. — 1998. — V. 259, № 5. — P. 491-503.

152. Tsyganov V.E., Seliverstova E., Voroshilova V., Tsyganova A., Pavlova Z., Lebskii V., Borisov A.Y., Brewin N., Tikhonovich I. Double mutant analysis of sequential functioning of pea (*Pisum sativum* L.) genes *Sym13*, *Sym33*, and *Sym40* during symbiotic nodule development // Russian Journal of Genetics: Applied Research. — 2011. — V. 1, № 5. — P. 343.

153. Tsyganov V.E., Tsyganova A.V. Symbiotic regulatory genes controlling nodule development in *Pisum sativum* L // Plants. — 2020. — V. 9, № 12. — P. 1741.

154. Tsyganov V.E., Tsyganova A.V., Voroshilova V.A., Borisov A.Yu., Tikhonovich I.A. Analysis of the interaction of pea (*Pisum sativum* L.) symbiotic genes *Sym33* and *Sym42* whose mutations result in abnormalities during infection thread development. // Russian Journal of Genetics: Applied Research. — 2014. — V.4, № 2. — P. 83–87.

155. Tsyganov V.E., Voroshilova V.A., Herrera-Cervera J.A., Sanjuan-Pinilla J.M., Borisov A.Y., Tikhonovich I.A., Priefer U.B., Olivares J., Sanjuan J. Developmental downregulation of rhizobial genes as a function of symbiosome differentiation in symbiotic root nodules of *Pisum sativum* // New Phytologist. — 2003. — V. 159, № 2. — P. 521-530.

156. Tsyganov V.E., Voroshilova V.A., Priefer U.B., Borisov A.Y., Tikhonovich I.A. Genetic dissection of the initiation of the infection process and nodule tissue development in the *Rhizobium*-pea (*Pisum sativum* L.) symbiosis // Annals of Botany. — 2002. — V. 89, № 4. — P. 357-366.

157. Tsyganova A.V., Brewin N., Tsyganov V.E. Analysis of epitope distribution of arabinogalactan protein-extensins in pea *(Pisum sativum*) nodules of wild-type and mutants impaired in infection thread growth // Ecological genetics. — 2019a. — V. 17, № 3. — P. 5-12.

158. Tsyganova A.V., Brewin N.J., Tsyganov V.E. Structure and development of the legume-rhizobial symbiotic interface in infection threads // Cells. — 2021. — V. 10, № 5.

159. Tsyganova A.V., Ivanova K.A., Tsyganov V.E. Histological and ultrastructural nodule organization of the pea (*Pisum sativum*) mutant SGEFix^{-}-5 in the *Sym33* gene encoding the transcription factor PsCYCLOPS/PsIPD3. // Ecological genetics. — 2019. — T. 17, № 1. — C. 65-70.

160. Tsyganova A.V., Kitaeva A.B., Brewin N.J., Tsyganov V.E. Cellular mechanisms of nodule development in legume plants (rewiew) // Sel'skokhozyaistvennaya Biologiya [Agricultural Biology]. — 2011. № 3. — P. 34-40. [In Russian]

161. Tsyganova A.V., Kitaeva A.B., Tsyganov V.E. Cell differentiation in nitrogen-fixing nodules hosting symbiosomes // Functional Plant Biology. — 2018. — V. 45, № 2. — P. 47-57.

162. Tsyganova A.V., Seliverstova E.V., Brewin N.J., Tsyganov V.E. Bacterial release is accompanied by ectopic accumulation of cell wall material around the vacuole in nodules of *Pisum sativum sym33-3* allele encoding transcription factor PsCYCLOPS/PsIPD3 // Protoplasma. — 2019b. — V. 256, № 5. — P. 1449-1453.

163. Tsyganova A.V., Seliverstova E.V., Brewin N.J., Tsyganov V.E. Comparative analysis of remodelling of the plant–microbe interface in *Pisum sativum* and *Medicago truncatula* symbiotic nodules // Protoplasma. — 2019c. — V. 256, № 4. — P. 983-996.

164. Tsyganova A.V., Seliverstova E.V., Gorshkov A.P., Tsyganov V.E. Analysis of *Glycine max* and *Galega orientalis* nodules revealed specific features of symbiotic interface organization in determinate and indeterminate nodules // Russian Journal of Plant Physiology. — 2023a. — V. 70, № 8. — P. 192.

165. Tsyganova A.V., Seliverstova E.V., Tsyganov V.E. Comparison of the formation of plant-microbial interface in *Pisum sativum* L. and *Medicago truncatula* Gaertn. nitrogen-fixing nodules // International Journal of Molecular Sciences. — 2023b. — V. 24, № 18. — P. 13850.

166. Tsyganova A.V., Tsyganov V.E. Plant genetic control over infection thread development during legume-*Rhizobium* symbiosis // Symbiosis / Rigobelo E. C. — London: IntechOpen, 2018. — P. 23-52.

167. Tsyganova A.V., Tsyganov V.E. Role of surface components of rhizobia in symbiotic interactions with legumes // Uspehi sovremennoj biologii. — 2012. — T. 132, № 2. — C. 211-222. [In Russian]

168. Tsyganova, A.V.; Tsyganov V.E. Negative hormonal regulation of symbiotic nodule development. I. Ethylene (review). // Sel'skokhozyaĭstvennaya Biologiya [Agricultural Biology]. — 2015. — V. 50, № 3. — P. 267-277.

169. Tsyganova, A.V.; Tsyganov V.E. Negative hormonal regulation of symbiotic nodule development. II. Salicilic, jasmonic and abscisic acids (review) // Sel'skokhozyaĭstvennaya Biologiya [Agricultural Biology]. — 2018. — T. 53, № 1. — C. 3-14.

170. Tsyganova A.V., Tsyganov V.E. Organization of the endoplasmic reticulum in cells of effective and ineffective pea nodules (Pisum sativum L.). // Ecological genetics. — 2019a. — T. 17, № 4. — C. 5-14.

171. Tsyganova A.V., Tsyganov V.E. Plant cell wall in symbiotic interactions. Pectins (review) // Sel'skokhozyaĭstvennaya Biologiya [Agricultural Biology]. — 2019b. — V. 54, № 3. — P. 446-457.

172. Tsyganova A.V., Tsyganov V.E., Borisov A.Y., Tikhonovich I.A., Brewin N.J. Comparative cytochemical analysis of hydrogen peroxide distribution in pea

ineffective mutant SGEFix⁻-1 (*sym40*) and initial line SGE // Ecological genetics. — 2009. — V. 7, № 3. — P. 3-9.

173. Tsyganova A.V., Tsyganov V.E., Findlay K.C., Borisov A.Y., Tikhonovich I.A., Brewin N.J. Distribution of legume arabinogalactan protein-extensin (AGPE) glycoproteins in symbiotically defective pea mutants with abnormal infection threads // Cell and Tissue Biology. — 2009. — V. 3, № 1. — P. 93-102.

174. Van de Velde W., Guerra J.C.P., Keyser A.D., De Rycke R., Rombauts S., Maunoury N., Mergaert P., Kondorosi E., Holsters M., Goormachtig S. Aging in legume symbiosis. A molecular view on nodule senescence in *Medicago truncatula* // Plant Physiology. — 2006. — V. 141, № 2. — P. 711-720.

175. Van de Velde W., Zehirov G., Szatmari A., Debreczeny M., Ishihara H., Kevei Z., Farkas A., Mikulass K., Nagy A., Tiricz H., Satiat-Jeunemaître B., Alunni B., Bourge M., Kucho K.-i., Abe M., Kereszt A., Maroti G., Uchiumi T., Kondorosi E., Mergaert P. Plant peptides govern terminal differentiation of bacteria in symbiosis // Science. — 2010. — V. 327, № 5969. — P. 1122-1126.

176. van Rhijn P., Vanderleyden J. The *Rhizobium*-plant symbiosis // Microbiological Reviews. — 1995. — V. 59, № 1. — P. 124-142.

177. van Spronsen P.C., Grønlund M., Bras C.P., Spaink H.P., Kijne J.W. Cell biological changes of outer cortical root cells in early determinate nodulation // Molecular Plant-Microbe Interactions. — 2001. — V. 14, № 7. — P. 839-847.

178. VandenBosch K.A., Bradley D.J., Knox J.P., Perotto S., Butcher G.W., Brewin N.J. Common components of the infection thread matrix and the intercellular space identified by immunocytochemical analysis of pea nodules and uninfected roots // The EMBO Journal. — 1989. — V. 8, № 2. — P. 335-341.

179. Vasse J., de Billy F., Camut S., Truchet G. Correlation between ultrastructural differentiation of bacteroids and nitrogen fixation in alfalfa nodules // Journal of Bacteriology. — 1990. — V. 172, № 8. — P. 4295-4306.

180. Verhertbruggen Y., Walker J.L., Guillon F., Scheller H.V. A comparative study of sample preparation for staining and immunodetection of plant cell walls by light microscopy // Frontiers in Plant Science. — 2017. — V. 8. — P. 1505.

181. Vernié T., Moreau S., de Billy F., Plet J., Combier J.-P., Rogers C., Oldroyd G., Frugier F., Niebel A., Gamas P. EFD is an ERF transcription factor involved in the control of nodule number and differentiation in *Medicago truncatula* // The Plant Cell. — 2008. — V. 20, № 10. — P. 2696-2713.

182. Vincken J.-P., Schols H.A., Oomen R.J., McCann M.C., Ulvskov P., Voragen A.G., Visser R.G. If homogalacturonan were a side chain of rhamnogalacturonan I. Implications for cell wall architecture // Plant Physiology. — 2003. — V. 132, № 4. — P. 1781-1789.

183. Voroshilova V.A., Boesten B., Tsyganov V.E., Borisov A.Y., Tikhonovich I.A., Priefer U.B. Effect of mutations in *Pisum sativum* L. genes blocking different stages of nodule development on the expression of late symbiotic genes in *Rhizobium leguminosarum* bv. *viciae* // Molecular Plant-Microbe Interactions. — 2001. — V. 14, № 4. — P. 471-476.

184. Voroshilova V.A., Demchenko K.N., Brewin N.J., Borisov A.Y., Tikhonovich I.A. Initiation of a legume nodule with an indeterminate meristem involves proliferating host cells that harbour infection threads // New Phytologist. — 2009. — V. 181, № 4. — P. 913-923.

185. Wang D., Dong X. A highway for war and peace: The secretory pathway in plant-microbe interactions // Molecular Plant. — 2011. — V. 4, № 4. — P. 581-587.

186. Wang J., Ling L., Cai H., Guo C. Gene-wide identification and expression analysis of the PMEI family genes in soybean (*Glycine max*) // 3 Biotech. — 2020. — V. 10, № 8. — P. 335.

187. Wang L., Gao Y., Wang S., Zhang Q., Yang S. Genome-wide identification of PME genes, evolution and expression analyses in soybean (*Glycine max* L.) // BMC Plant Biology. — 2021. — V. 21, № 1. — P. 578.

188. Wang T., Park Y.B., Caporini M.A., Rosay M., Zhong L., Cosgrove D.J., Hong M. Sensitivity-enhanced solid-state NMR detection of expansin's target in plant cell walls // Proceedings of the National Academy of Sciences. — 2013. — V. 110, № 41. — P. 16444-16449.

189. Willats W.G., Steele-King C.G., Marcus S.E., Knox J.P. Side chains of pectic polysaccharides are regulated in relation to cell proliferation and cell differentiation // The Plant Journal. — 1999. — V. 20, № 6. — P. 619-628.

190. Wilmowicz E., Kućko A., Alché J.D.D., Czeszewska-Rosiak G., Florkiewicz A.B., Kapusta M., Karwaszewski J. Remodeling of cell wall components in root nodules and flower abscission zone under drought in yellow lupine // International Journal of Molecular Sciences. — 2022. — V. 23, № 3. — P. 1680.

191. Wisniewski J.-P., Rathbun E.A., Knox J.P., Brewin N.J. Involvement of diamine oxidase and peroxidase in insolubilization of the extracellular matrix: Implications for pea nodule Initiation by *Rhizobium leguminosarum* // Molecular Plant-Microbe Interactions. — 2000. — V. 13, № 4. — P. 413-420.

192. Wolf S., Greiner S. Growth control by cell wall pectins // Protoplasma. — 2012. — V. 249, № 2. — P. 169-175.

193. Wolf S., Mouille G., Pelloux J. Homogalacturonan methyl-esterification and plant development // Molecular Plant. — 2009. — V. 2, № 5. — P. 851-860.

194. Wormit A., Usadel B. The multifaceted role of pectin methylesterase inhibitors (PMEIs) // International Journal of Molecular Sciences. — 2018. — V. 19, № 10. — P. 2878.

195. Xie F., Murray J.D., Kim J., Heckmann A.B., Edwards A., Oldroyd G.E.D., Downie J.A. Legume pectate lyase required for root infection by rhizobia // Proceedings of the National Academy of Sciences of the United States of America. — 2012. — V. 109, № 2. — P. 633-638.

196. Yang L., El Msehli S., Benyamina S., Lambert A., Hopkins J., Cazareth J., Pierre O., Hérouart D., Achi-Smiti S., Boncompagni E., Frendo P. Glutathione deficiency in *Sinorhizobium meliloti* does not impair bacteroid differentiation but induces early senescence in the interaction with *Medicago truncatula* // Frontiers in Plant Science. — 2020. — V. 11, № 137.

197. Zgadzaj R., James E.K., Kelly S., Kawaharada Y., de Jonge N., Jensen D.B., Madsen L.H., Radutoiu S. A legume genetic framework controls infection of nodules by

symbiotic and endophytic bacteria // PLOS Genetics. — 2015. — V. 11, № 6. — P. e1005280.

198. Zipfel C., Oldroyd G.E.D. Plant signalling in symbiosis and immunity // Nature. — 2017. — V. 543. — P. 328-336.

ACKNOWLEDGEMENTS

I express my most sincere and deepest gratitude to my scientific advisor, Victor Evgenyevich Tsyganov, for his many years of guidance and direction of research as head of the laboratory where I work, for critical reading of my articles and thesis. I express my deep gratitude to Professor Nicholas Brevin (John Innes Center, UK), thanks in many respects to whom the present work took place.

I express great gratitude to all teachers of the Faculty of Biology of Kazakh National University and first of all to the Department of Cytology, Histology and Embryology. I express special gratitude to one of my scientific supervisors Tamara Minazhevna Shalakhmetova, who taught me not to give up in my scientific search.

I am extremely grateful to the staff of my first research laboratory, the electron microscopy laboratory at the Scientific Center of Surgery, Evgeny Leonidovich Zumerov, Alexey Ivanovich Zharikov, Nina Efimovna Zhirnova, and Anastasia Mikhailovna Sokolova, who opened for me the world of microscopy and scientific research. I am extremely grateful for many years of guidance and friendship to Galina Vasilievna Fedotovskikh, who opened for me the beauty and logic of morphology.

I am deeply grateful to international colleagues Peter Calo, Ward Capoen, Anne Heckmann, and Anne Edwards for their cooperation and warm environment during my work in the Plant-Microbial Relations Laboratory at the John Innes Center under the supervision of Giles Oldroyd and Allan Downey. Many thanks also go to the technical staff of the John Innes Center's Cell Biology Department, Kim Findlay, Grant Calder, and Sue Bunnewell, for helping me learn new techniques.

I am grateful to my colleagues with whom I had the pleasure to work within the laboratories of molecular and cell biology, first of all: Elena Valentinovna Seliverstova, Anna Borisovna Kitaeva, Tatiana Alexandrovna Serova, Kira Andreyevna Ivanova, Petr Glebovich Kusakin, Artemiy Pavlovich Gorshkov and all others.

I express my sincere gratitude to Kirill Nikolaevich Demchenko, thanks to whose invaluable experience some of the studies were carried out, and also for critical comments that helped to make my work better.

I express my sincere gratitude to the staff of the SPbSU Resource Center "Development of Molecular and Cellular Technologies", especially Alexandra Nikolaevna Ivanova, Maxim Germanovich Vorobyev and Yaroslav Gennadyevich Borisov, who provided the most convenient work in the center, where most of the research was conducted.

I am eternally grateful to my parents Victor Georgievich Neverdovsky, to whose memory I dedicate my work, and Zhanna Anatolievna Svetysheva, who not only gave me her love and care, but also opened the road to science for me.

I am immensely grateful to my husband for all-round care and love, which he gives me every day. I am grateful to my children Valentina and Yuri for the fact that I have them.

APPENDIX A

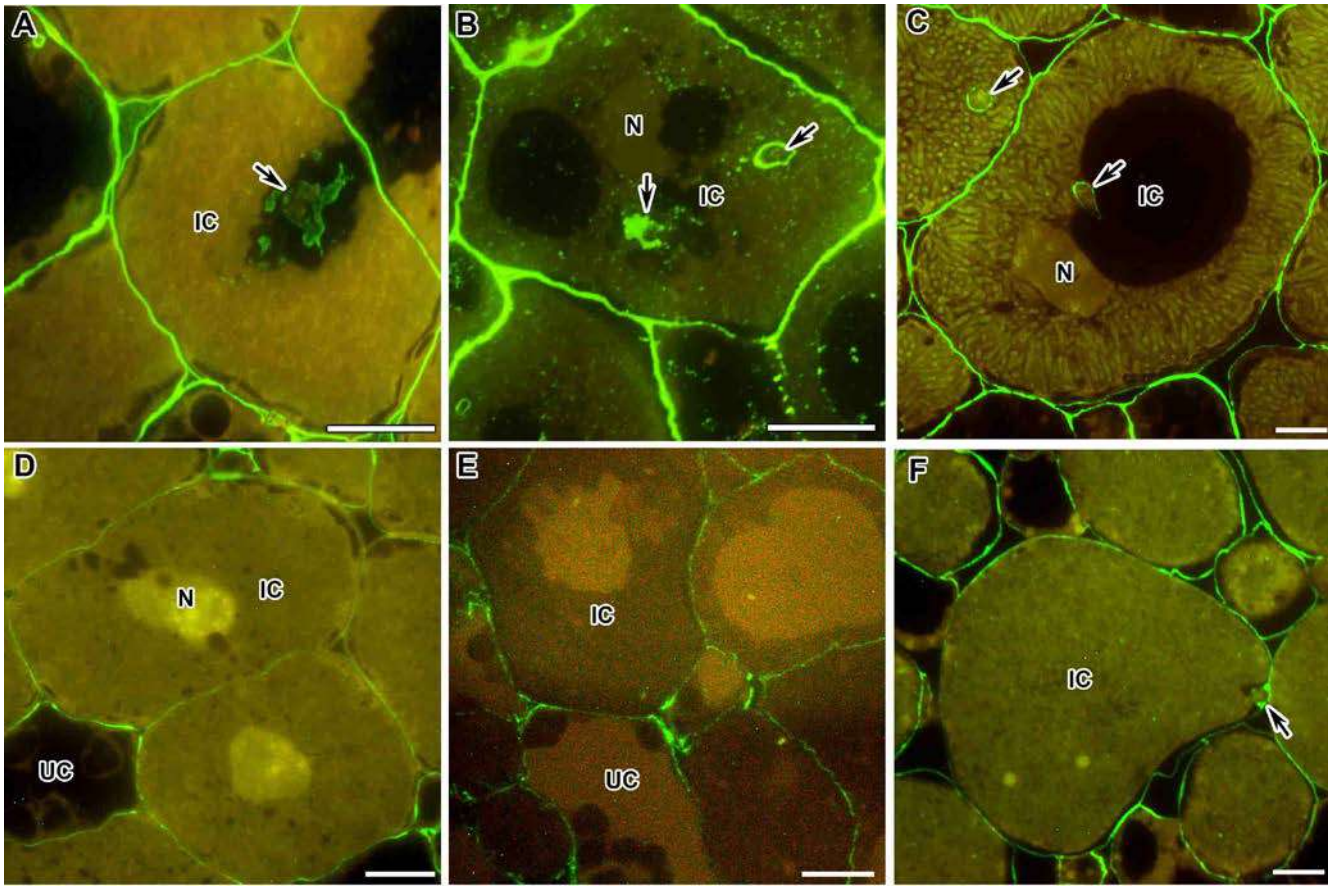

Fluorescent immunolocalization with the JIM7 antibody in nodules of *Pisum sativum* (A), *Medicago truncatula* (B), *Galega orientalis* (C), *Vavilovia formosa* (D), *Vicia villosa* (E) and *Glycine max* (F). The secondary antibody used was goat anti-rat IgG MAb conjugated with Alexa Fluor 488. IC — infected cell, UC — uninfected cell, N — nucleus; arrows indicate infection threads. Scale bar = 20 μm (A,B), 10 μm (C-F).

Figure A.1 — High methyl-esterified homogalacturonan in legume nodules

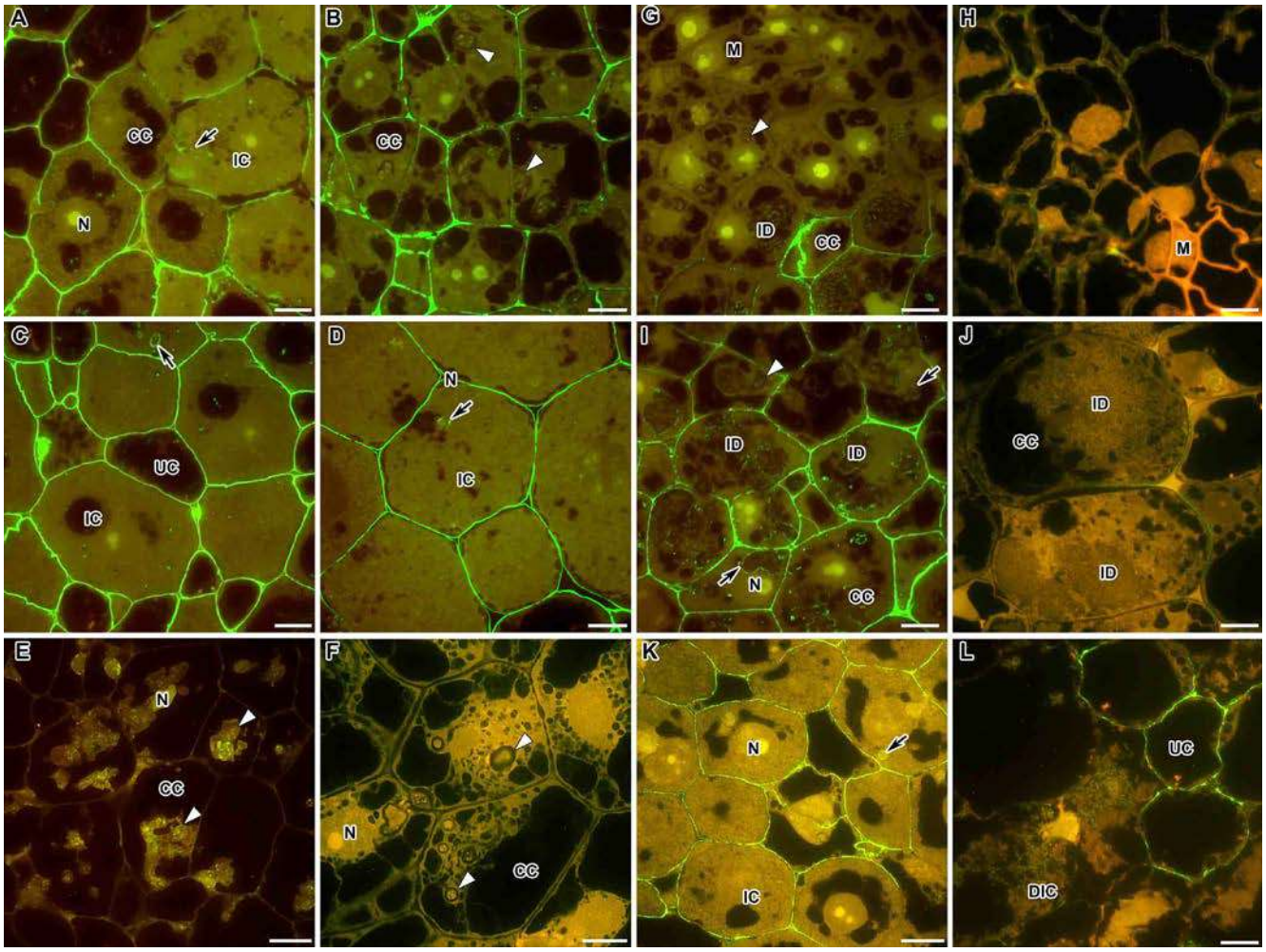

Fluorescent immunolocalisation with the LM20 antibody in nodules from wild-type and mutants *Medicago truncatula* (A,C,E,G,I) and *Pisum sativum* (B,D,F,H,J-L). The secondary antibody used was the goat anti-rat IgG monoclonal antibody conjugated with Alexa Fluor 488. (A) Infection zone of the wild-type A17. (B) Infection zone of the wild-type SGE. (C) Nitrogen fixation zone of the wild-type A17. (D) Nitrogen fixation zone of the wild-type SGE. (E) Colonized cells of the mutant TR3 (*Mtipd3*). (F) Colonized cells of the mutant SGEFix$^-$-2 (*Pssym33*). (G) Meristem of the mutant *Mtefd–1*. (H) Meristem of the mutant SGEFix$^-$-1 (*Pssym40*). (I) Infection zone of the mutant *Mtefd–1*. (J) Infection zone of the mutant SGEFix$^-$-1 (*Pssym40*). (K) Zone corresponding to nitrogen fixation zone of the wild type in the mutant SGEFix$^-$-3 (*Pssym26*). (L) Senescence zone of the mutant SGEFix$^-$-3 (*Pssym26*). M — meristematic cell, CC — colonized cell, IC — infected cell, UC — uninfected cell, DIC — degraded infected cell, N — nucleus, ID — infection droplet; arrows indicate infection threads, triangles indicate infection threads without signal. Bar = 10 μm.

Figure A.2 — High methyl-esterified homogalacturonan in nodules from wild-type and mutant *Medicago truncatula* and *Pisum sativum*

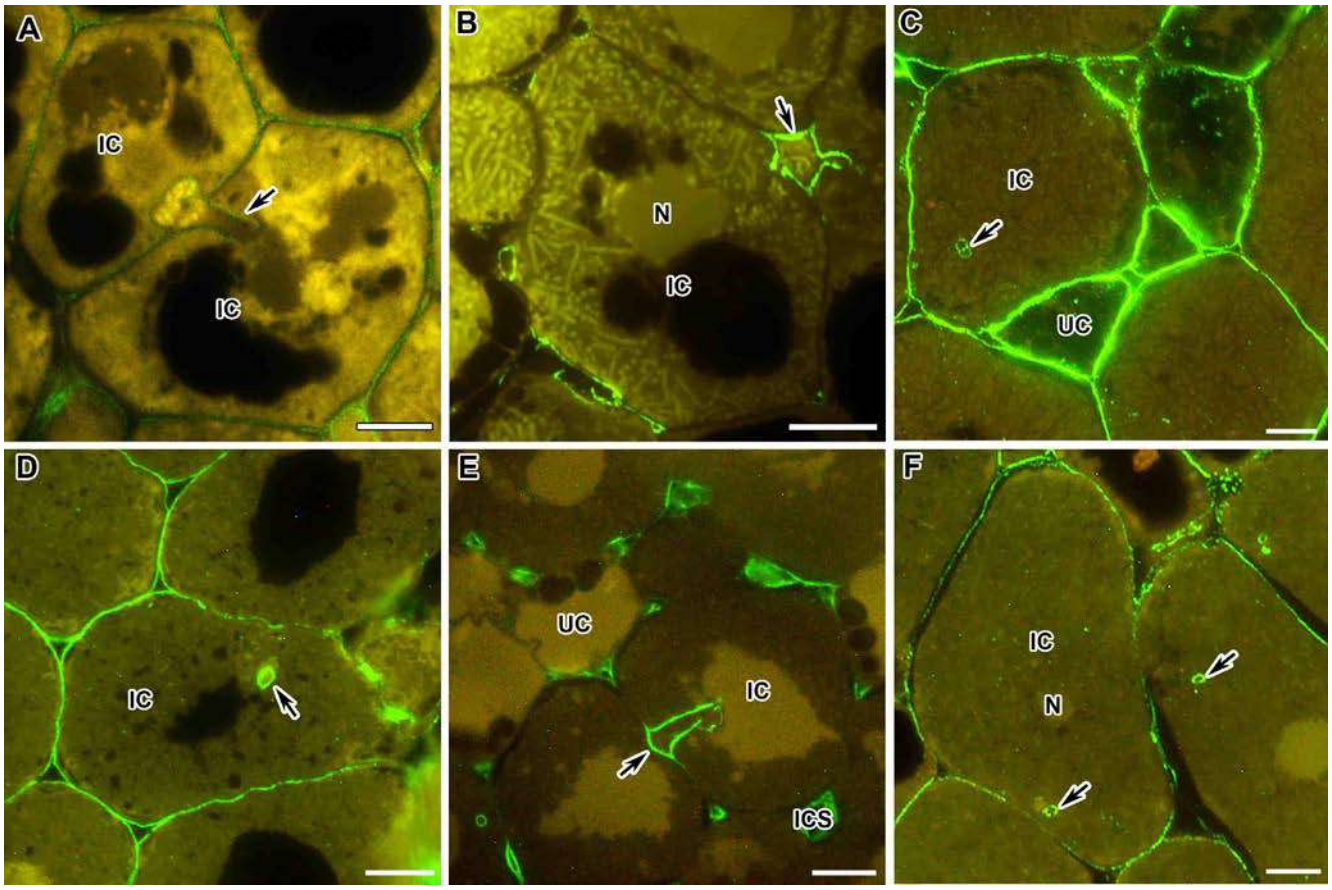

Fluorescent immunolocalization with the JIM5 antibody in nodules of *Pisum sativum* (A), *Medicago truncatula* (B), *Galega orientalis* (C), *Vavilovia formosa* (D), *Vicia villosa* (E) and *Glycine max* (F). The secondary antibody used was goat anti-rat IgG MAb conjugated with Alexa Fluor 488. IC — infected cell, UC — uninfected cell, ICS — intercellular space, N — nucleus; arrows indicate infection threads. Scale bar = 20 μm (A,B), 10 μm (C-F).

Figure A.3 — Low methyl-esterified homogalacturonan in legume nodules

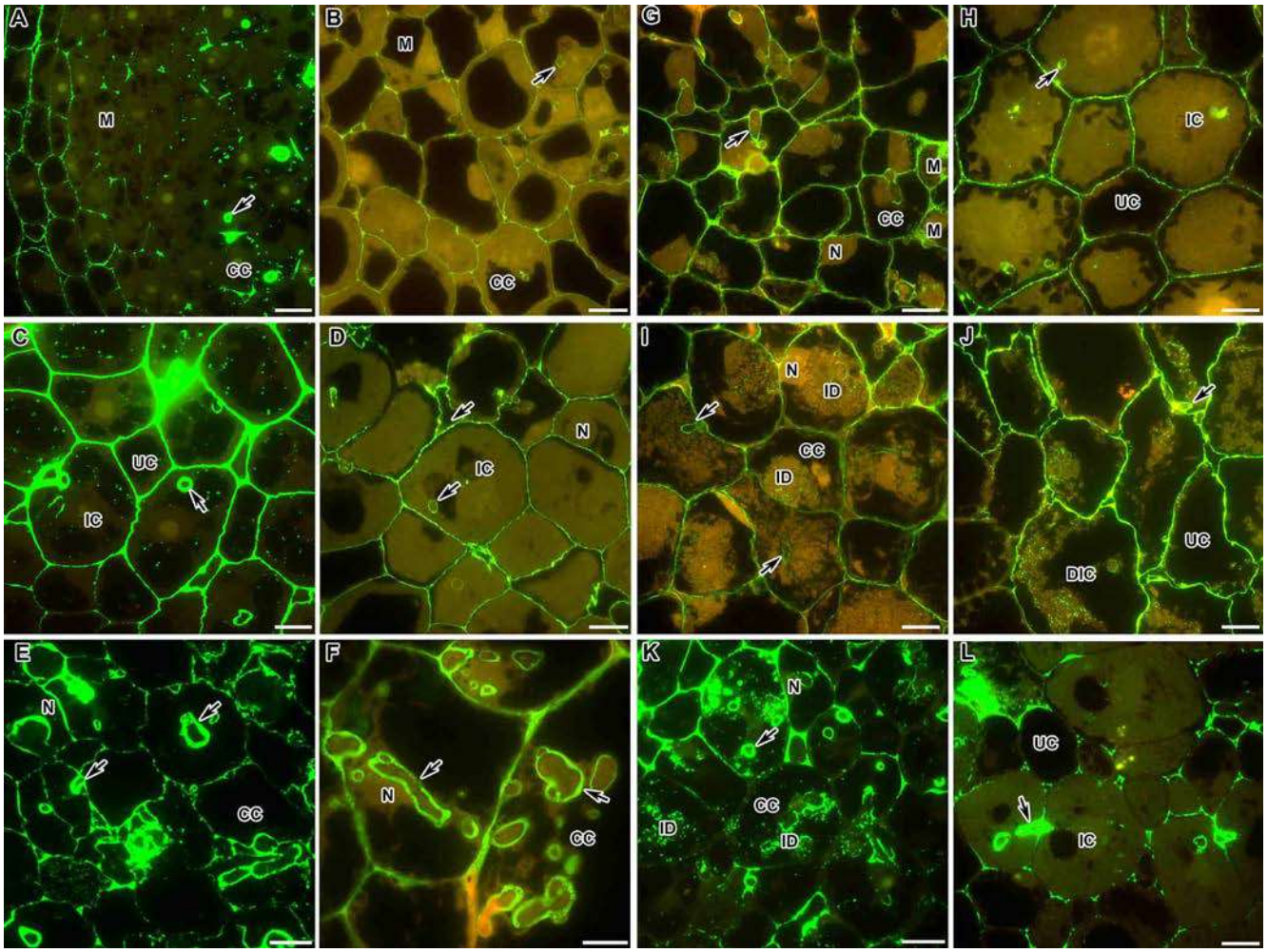

Fluorescent immunolocalisation with the LM19 antibody in nodules from wild-type and mutant *Medicago truncatula* (A,C,E,K,L) and *Pisum sativum* (B,D,F-J). The secondary antibody used was the goat anti-rat IgG monoclonal antibody conjugated with Alexa Fluor 488. (A) Meristem and infection zone of the wild-type A17. (B) Meristem and infection zone of the wild-type SGE. (C) Nitrogen fixation zone of the wild-type A17. (D) Nitrogen fixation zone of the wild-type SGE. (E) Colonized cells of the mutant TR3 (*Mtipd3*). (F) Colonized cells of the mutant SGEFix$^-$-2 (*Pssym33-3*). (G) Meristem and early infection zone of the mutant SGEFix$^-$-1 (*Pssym40-1*). (H) Zone corresponding to the nitrogen fixation zone of the wild type in the mutant SGEFix$^-$-3 (*Pssym26*). (I) Infection zone of the mutant SGEFix$^-$-1 (*Pssym40-1*). (J) Senescence zone of the mutant SGEFix$^-$-3 (*Pssym26*). (K) Infection zone of the mutant *Mtefd–1*. (L) Infection zone of the mutant *Mtdnf1–1*. M — meristematic cell, CC — colonized cell, IC — infected cell, UC — uninfected cell, DIC — degraded infected cell, N — nucleus, ID — infection droplet; arrows indicate infection threads. Bar = 10 μm.

Figure A.4 — Low methyl-esterified homogalacturonan in nodules from wild-type and mutant *Medicago truncatula* and *Pisum sativum*

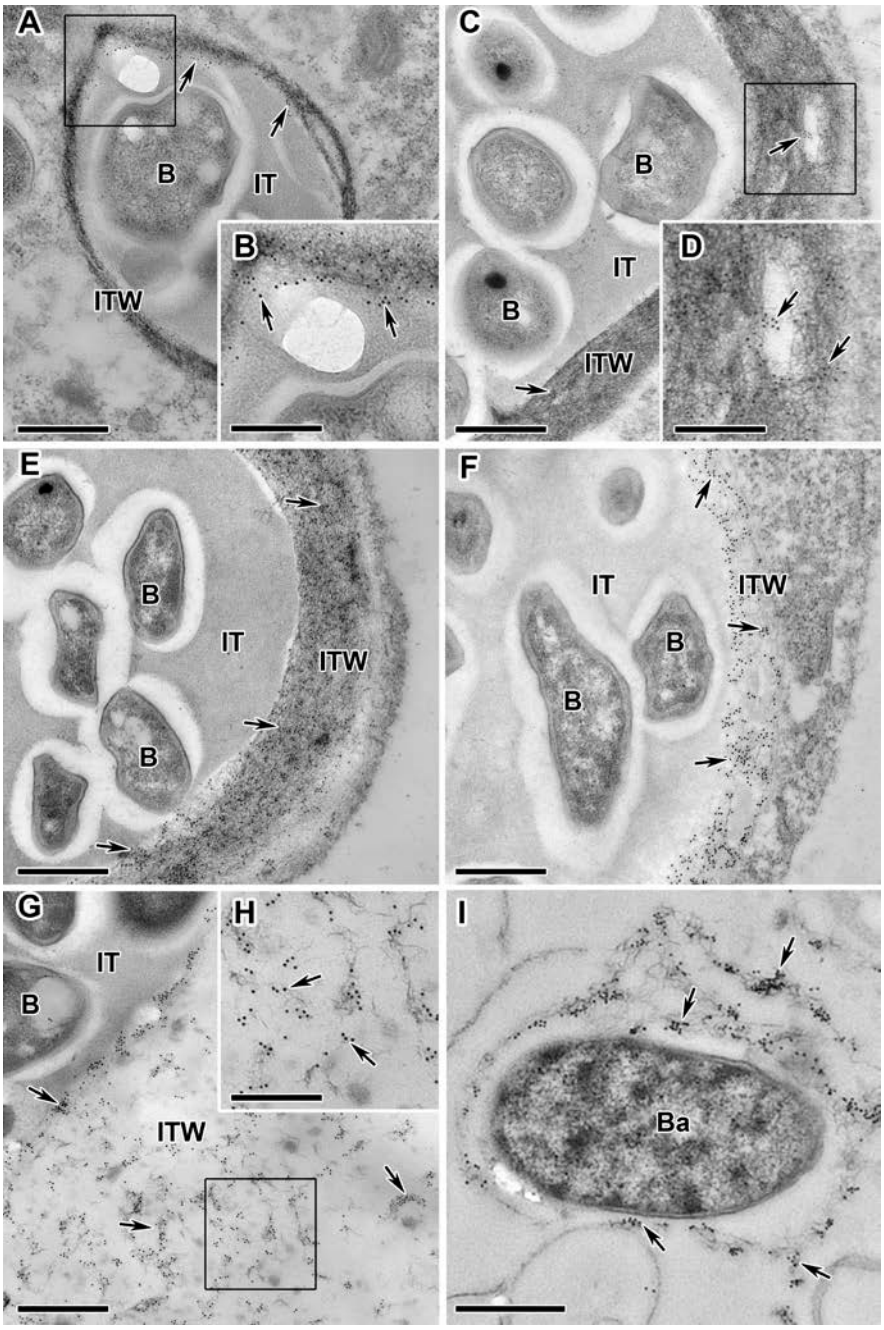

Immunogold localization with JIM5 antibody in 2-week-old nodules of wild-type and mutant *Pisum sativum*. (A) Wild-type SGE. (B) High magnification of the boxed area in (A). (C) Mutant SGEFix^{-}-2 (*Pssym33-3*). (D) High magnification of the boxed area in (C). (E) Double mutant RBT3 (*Pssym33-3*, *Pssym40-1*). (F) Double mutant RBT4 (*Pssym33-3*, *Pssym42*). (G,I) Mutant RisFixV (*Pssym42*). (H) High magnification of the boxed area in (G). IT — infection thread, ITW — infection thread wall, B — bacterium, Ba — bacteroid; arrows indicate gold particles. Bar = 500 nm (A,C,E,F,G,I), = 250 nm (B,D,H).

Figure A.5 — Low methyl-esterified homogalacturonan in nodules from wild-type and mutant *Pisum sativum*

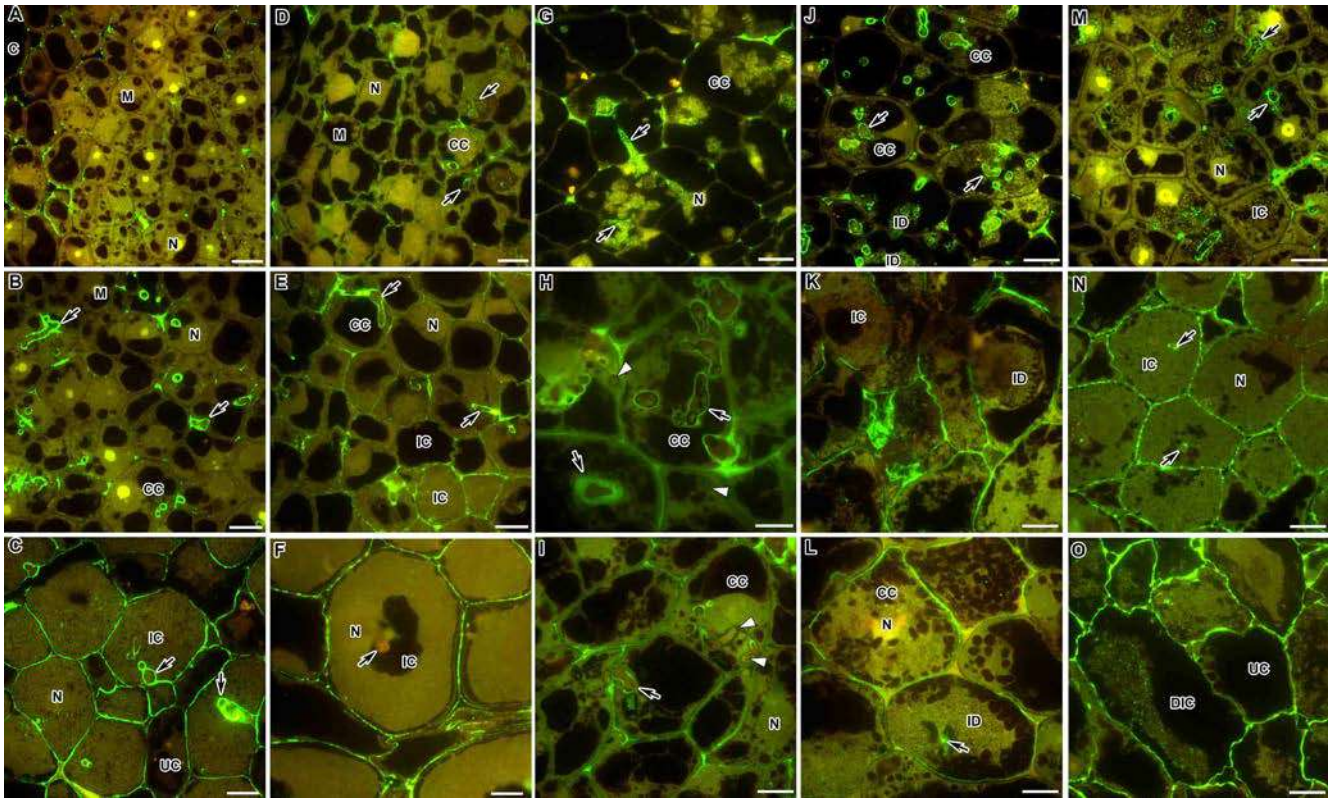

Fluorescent immunolocalisation with the 2F4 antibody in nodules from wild-type and mutant *Medicago truncatula* (A-C,G,J,M) and *Pisum sativum* (D-F,H,I,K,L,N,O). The secondary antibody used was the goat anti-mouse IgG monoclonal antibody conjugated with Alexa Fluor 488. (A) Meristem of the wild-type A17. (B) Infection zone of the wild-type A17. (C) Nitrogen fixation zone of the wild-type A17. (D) Meristem of the wild-type SGE. (E) Infection zone of the wild-type SGE. (F) Nitrogen fixation zone of the wild-type SGE. (G) Colonized cells of the mutant TR3 (*Mtipd3*). (H,I) Colonized cells of the mutant SGEFix$^-$-2 (*Pssym33-3*). (J) Infection zone in the mutant *Mtefd–1*. (K) Early infection zone of the mutant SGEFix$^-$-1 (*Pssym40-1*). (L) Late infection zone of the mutant SGEFix$^-$-1 (*Pssym40-1*). (M) Infection zone in the mutant *Mtdnf1–1*. (N) Zone corresponding to the nitrogen fixation zone of the wild type in the mutant SGEFix$^-$-3 (*Pssym26*). (O) Senescence zone of the mutant SGEFix$^-$-3 (*Pssym26*). M — meristematic cell, CC — colonized cell, IC — infected cell, UC — uninfected cell, DIC — degraded infected cell, N — nucleus, ID — infection droplet; arrows indicate infection threads, triangles indicate infection thread without signal. Bar = 10 μm.

Figure A.6 — Dimeric association of homogalacturonan chains through Ca^{2+} ions labelled in nodules from wild-type and mutant *Medicago truncatula* and *Pisum sativum*

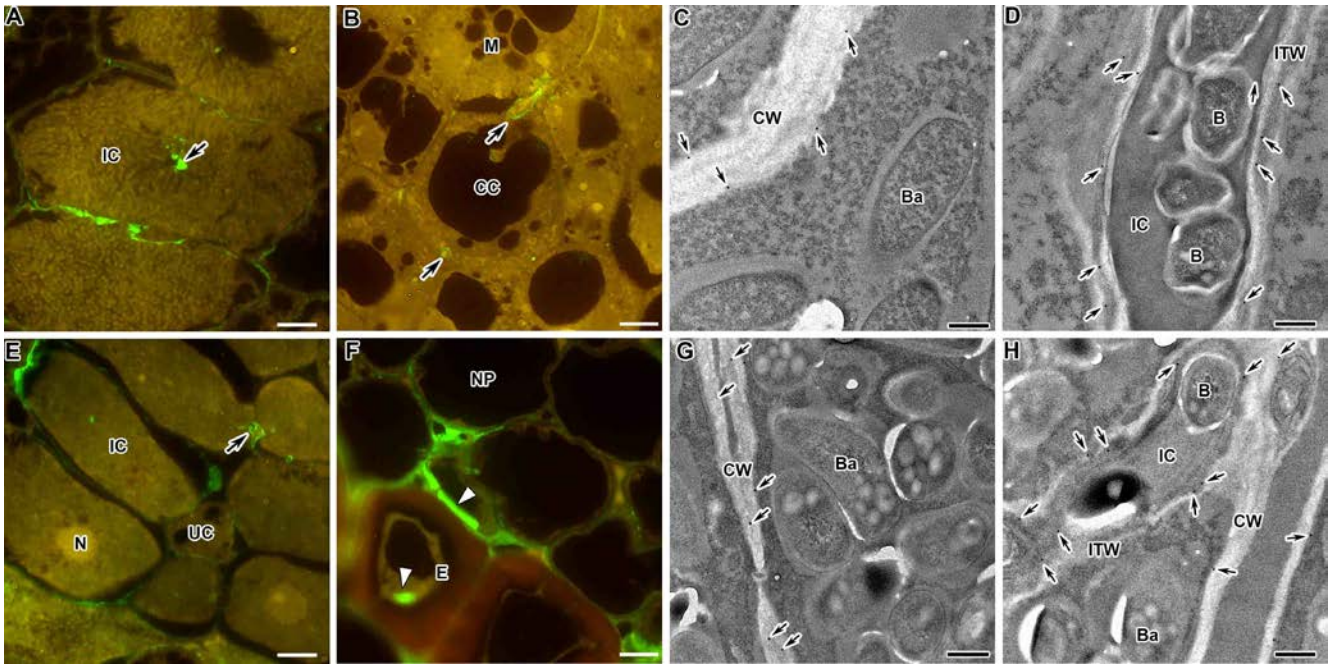

Fluorescence immunolocalization (A,B,E,F) and immunogold localization (C,D,G,H) with the 2F4 antibody in nodules of *Galega orientalis* (A-D) and *Glycine max* (E-H). The secondary antibody used were the goat anti-mouse IgG monoclonal antibody conjugated with Alexa Fluor 488 (A,B,E,F) and conjugated to 10 nm diameter colloidal gold (C,D,G,H). (A) Infected cells from the nitrogen fixation zone. (B) Colonized cells from the early infection zone. (C,G) Cell walls of infected cells. (D,H) Infection threads. (E) Infected cells. (E) Endoderm. E — endodermal cell, NP — nodule parenchyma cells, M — meristematic cell, CC — colonized cell, IC — infected cell, UC — uninfected cell, N — nucleus, CW — cell wall, IT — infection thread, ITW — infection thread wall, B — bacterium, Ba — bacteroid; arrows indicate infection threads, triangles indicate signal, small arrows indicate gold particles. Scale bar = 10 μm (A,B,E,D), = 500 nm (C,D,G,H).

Figure A.7 — Dimeric association of homogalacturonan chains through Ca^{2+} ions labelled in nodules *Galega orientalis* and *Glycine max*

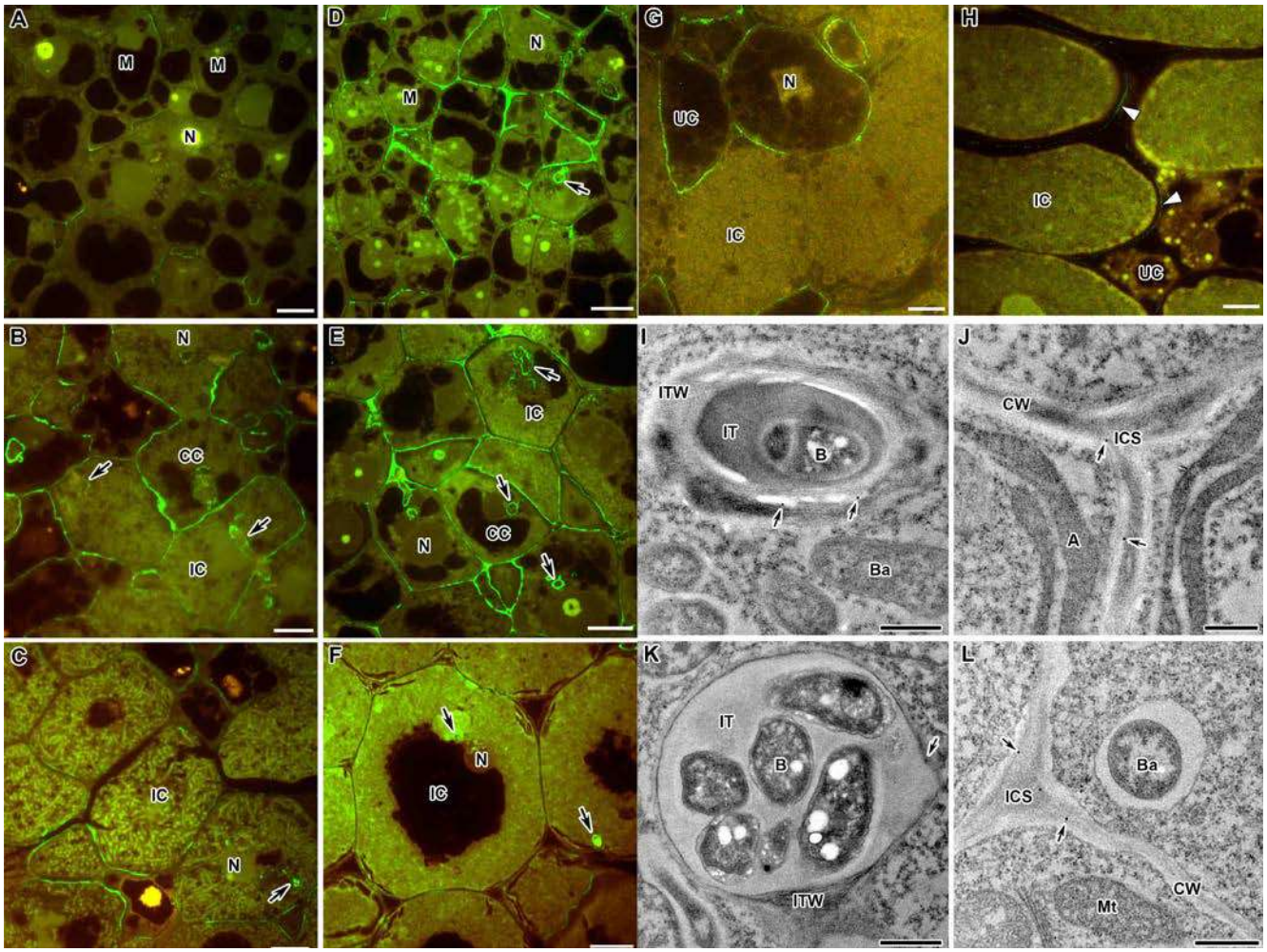

Fluorescence immunolocalization (A-H) and immunogold localization (I-L) with the CCRC-M36 antibody in nodules of *Medicago truncatula* (A-C), *Pisum sativum* (D-F), *Galega orientalis* (G), *Glycine max* (H), *Vavilovia formosa* (I,J) and *Vicia villosa* (K,L). The secondary antibody used were the goat anti-mouse IgG monoclonal antibody conjugated with Alexa Fluor 488 (A-H) and conjugated to 10 nm diameter colloidal gold (I-L). (A,D) Meristem. (B,E) Infection zone. (C,F,G) Nitrogen fixation zone. (H) Infected cells. (I,K) Infection threads. (J,L) Cell walls of infected cells. M — meristematic cell, CC — colonized cell, IC — infected cell, UC — uninfected cell, N — nucleus, A - amyloplast, Mt — mitochondrion, CW — cell wall, ICS — intercellular space, IT — infection thread, ITW — infection thread wall, B — bacterium, Ba — bacteroid; arrows indicate infection threads, triangles indicate signal, small arrows indicate gold particles. Scale bar = 10 μm (A-H), = 500 nm (I-L).

Figure A.8 — Rhamnogalacturonan I backbone in legume nodules

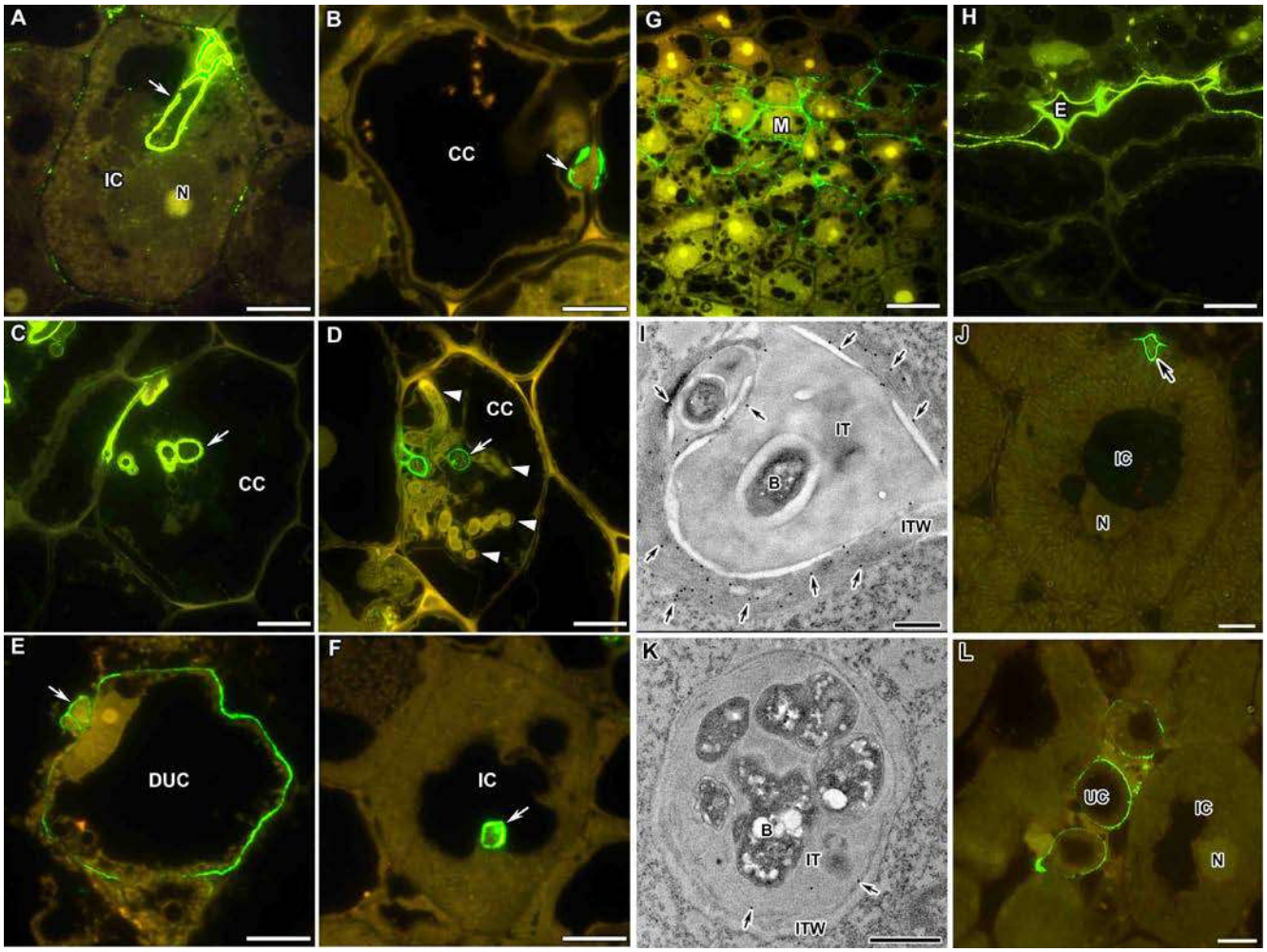

Fluorescence immunolocalization (A-H,J,L) and immunogold localization (I,K) with the LM5 antibody in nodules from wild-type and mutant of *Pisum sativum* (A-F,H), in nodules of *Medicago truncatula* (G), *Vavilovia formosa* (I), *Galega orientalis* (J), *Vicia villosa* (K) and *Glycine max* (L). The secondary antibody used were the goat anti-mouse IgG monoclonal antibody conjugated with Alexa Fluor 488 (A-H,J,L) and conjugated to 10 nm diameter colloidal gold (I,K). (A) Wild type SGE. (B) Mutant SGEFix^{-}-1 (*Pssym40-1*). (C,D) Mutant SGEFix^{-}-2 (*Pssym33-3*). (E) Mutant SGEFix^{-}-3 (*Pssym26*). (F) Mutant Sprint-2Fix^{-}- (*Pssym31*). (G) Meristem. (H) Endoderm. (I,K) Infection threads. (J) Nitrogen fixation zone. (L) Uninfected cells. E — endodermal cell, M — meristematic cell, CC — colonized cell, IC — infected cell, UC — uninfected cell, DUC — degrading uninfected cell, IT — infectious thread, ITW — infectious thread wall, B — bacterium; arrows indicate infection threads, triangles indicate unlabeled infection threads, small arrows indicate gold particles. Scale = 10 µm (A-H,J,L), = 500 nm (I,K).

Figure A.9 — (1→4)-β-D-galactan side chain of rhamnogalacturonan I in legume nodules

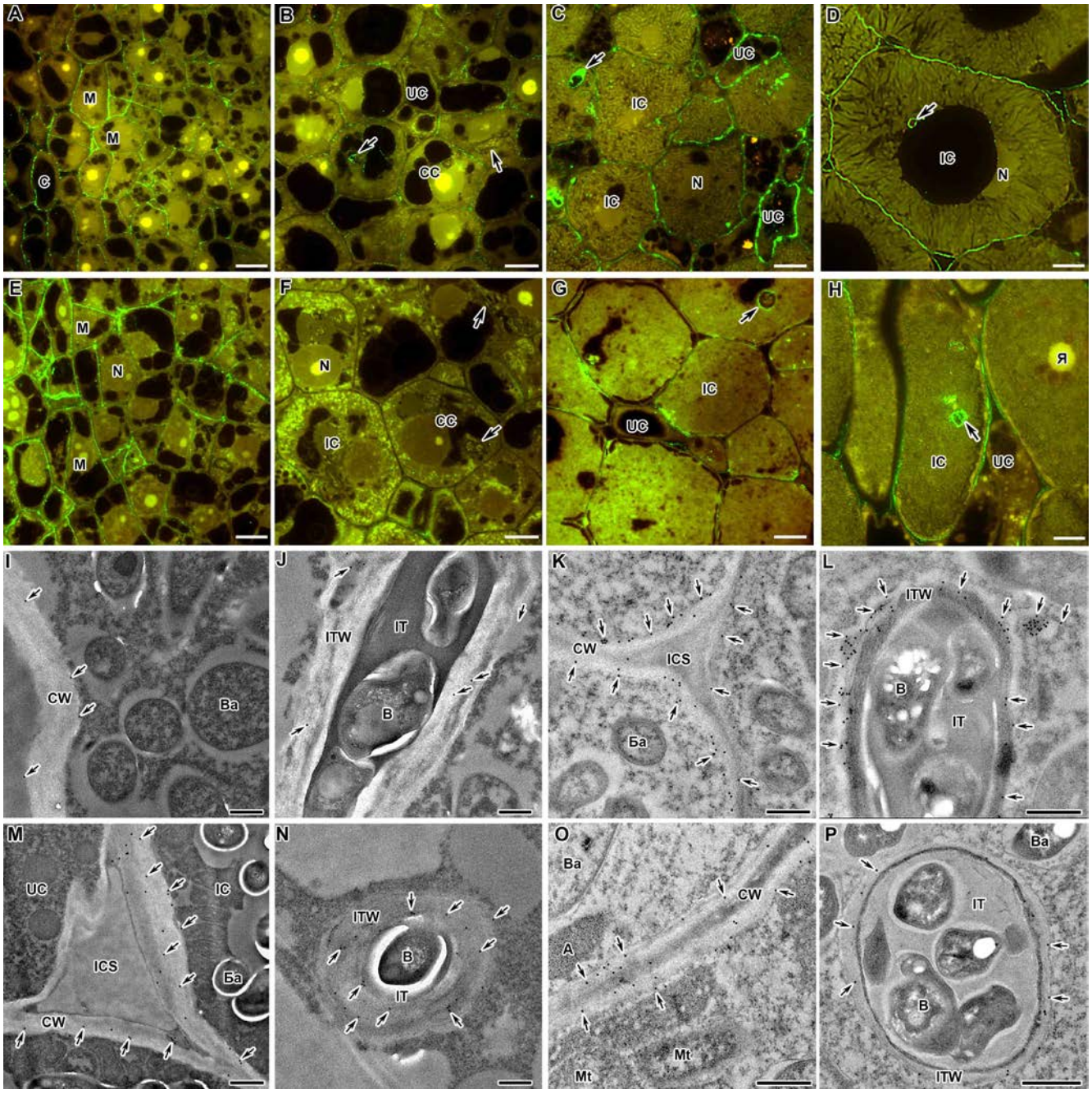

Fluorescence immunolocalization (A-H) and immunogold localization (I-P) with the CCRC-M1 antibody in nodules *Pisum sativum* (A-C), *Galega orientalis* (D,I,J), *Medicago truncatula* (E-G), *Glycine max* (H,M,N), *Vavilovia formosa* (K,L) and *Vicia villosa* (O,P). The secondary antibody used were the goat anti-mouse IgG monoclonal antibody conjugated with Alexa Fluor 488 (A-H) and conjugated to 10 nm diameter colloidal gold (I-P). (A,E) Meristem. (B,F) Infection zone. (C,D,G) Nitrogen fixation zone. (H) Infected cells. (I,K,M,O) Cell walls. (J,L,N,P) Infection threads. C — cortical cell, M — meristematic cell, CC — colonized cell, IC — infected cell, UC — uninfected cell, N — nucleus, A — amyloplast, Mt — mitochondrion, CW — cell wall, IT — infection thread, ITW — infection thread wall, B — bacterium, Ba — bacteroid, arrows indicate infection threads, small arrows indicate gold particles. Scale bar = 10 μm (A-H), = 500 nm (K-M,O,P), = 200 nm (I,J,N).

Figure A.10 — Fucosylated xyloglucan in legume nodules

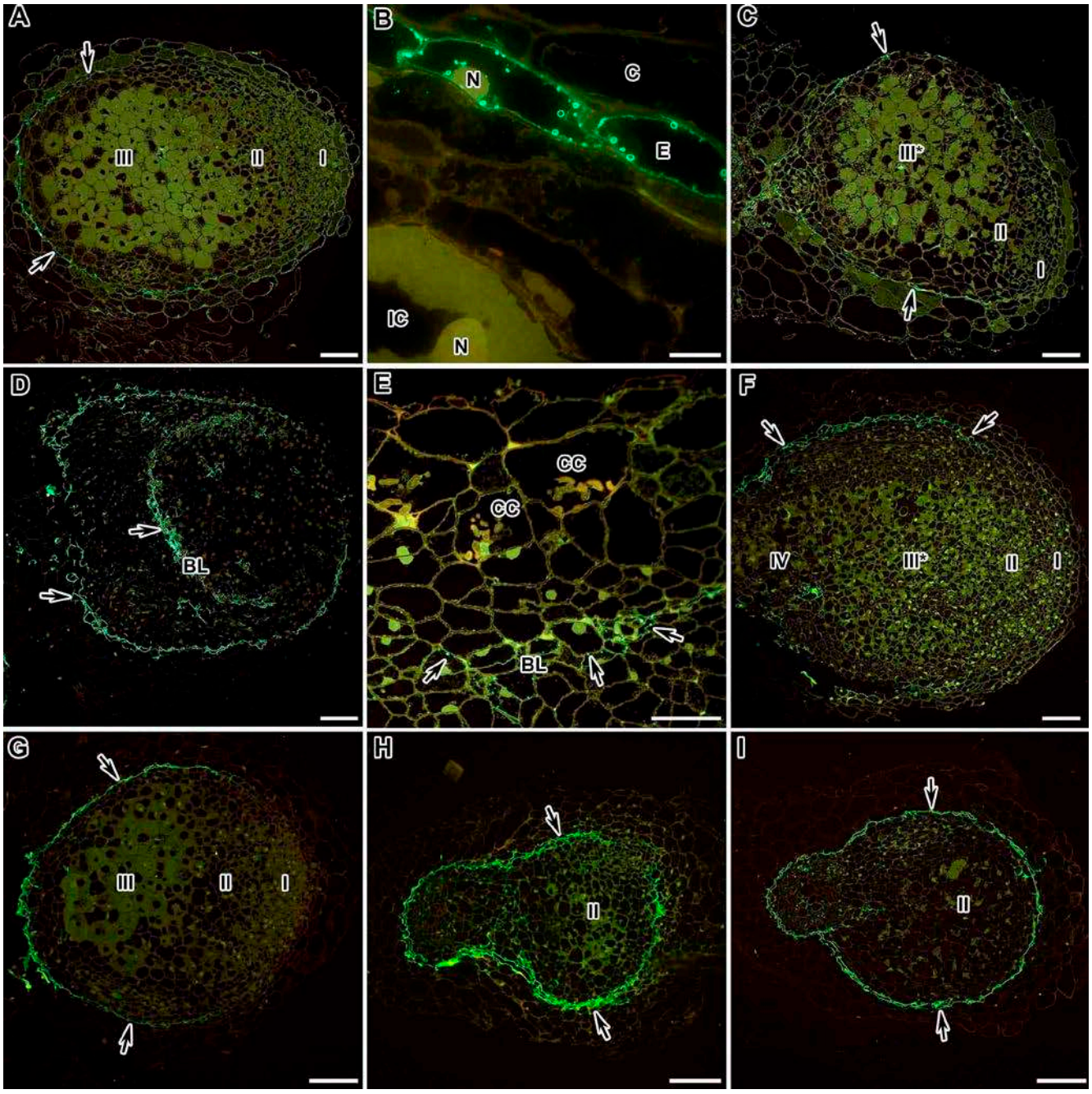

Fluorescent immunolocalisation with the JIM13 antibody in nodules from wild-type and mutant *Pisum sativum* (A-F) and *Medicago truncatula* (G-I). The secondary antibody used was the goat anti-mouse IgG monoclonal antibody conjugated with Alexa Fluor 488. (A) Section of a nodule of the wild-type SGE. (B) Endodermis of the wild-type SGE. (C) Section of a nodule of the mutant SGEFix$^-$-1 (*Pssym40-1*). (D) Section of a nodule of the mutant SGEFix$^-$-2 (*Pssym33-3*). (E) "Barrier layer" in the nodule of the mutant SGEFix$^-$-2 (*Pssym33-3*). (F) Section of a nodule of the mutant SGEFix$^-$-3 (*Pssym26*). (G) Section of a nodule of the wild-type A17. (H) Section of a nodule of the mutant *Mtefd–1*. (I) Section of a nodule of the mutant TR3 *(*Mt*ipd3)*. I — meristem, II — infection zone, III — nitrogen-fixation zone, III* — zone corresponding to the nitrogen fixation zone of the wild type, IV — senescence zone, C — cortex, E – endodermis, CC — colonized cell, IC — infected cell, N — nucleus, BL — "barrier layer"; arrows indicate the signal. Bars (A,C,D,F,G) = 100 μm, (H,I) = 50 μm, (E) = 20 μm, (B) = 5 μm.

Figure A.11 — Arabinogalactan protein in the endoderm of nodules from wild-type and mutant of *Pisum sativum* and *Medicago truncatula*

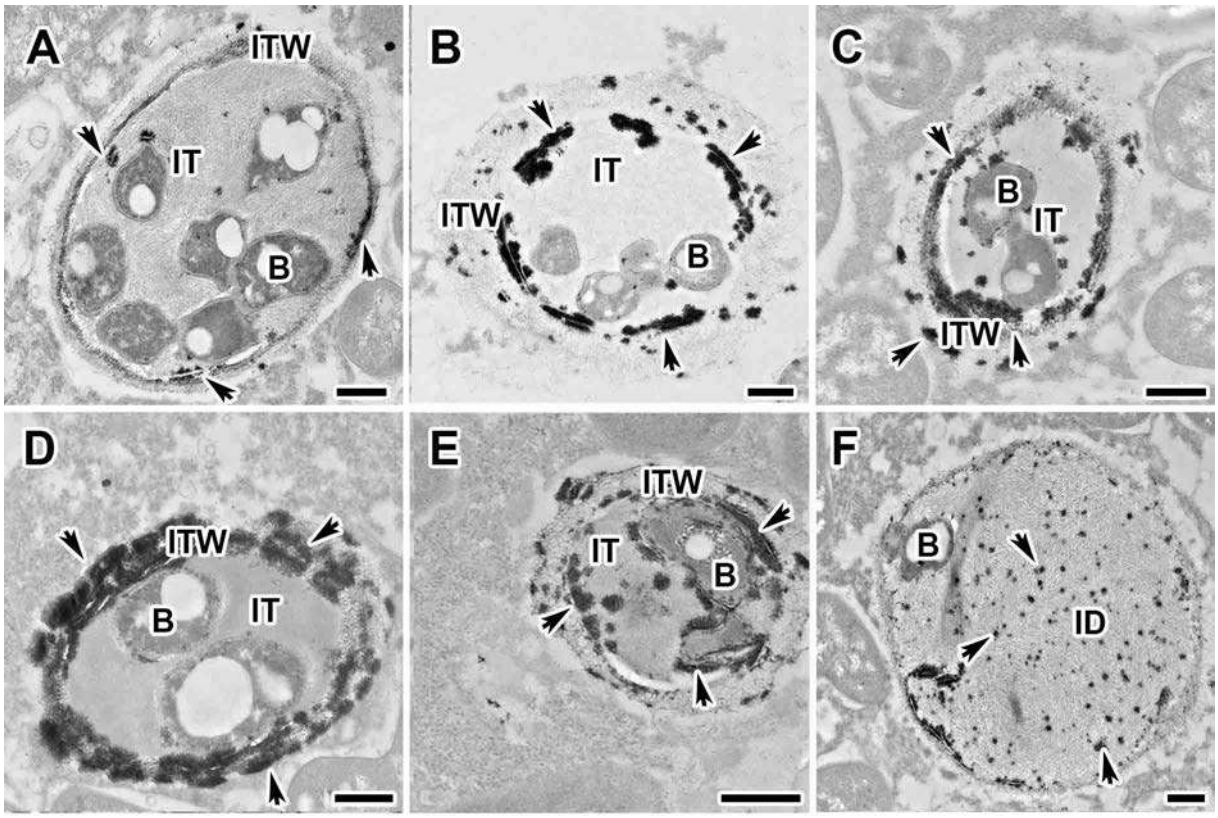

Cytochemical reaction with cerium chloride in 2-week-old nodules of *Pisum sativum* wild type SGE. (A) Initial H_2O_2 deposits on the inner surface of the infection thread wall. (B) Continuous H_2O_2 deposits on the inner surface of the infection thread wall. (C) Appearance of H_2O_2 deposits on the outer surface of the infection thread wall. (D) Complete impregnation of the infection thread wall with H_2O_2. (E) Appearance of cerium perhydroxide precipitates in the matrix of infection threads. (F) Appearance of cerium perhydroxide precipitates in the matrix of infection droplet. IT — infection thread, ITW — infection thread wall, ID — infection droplet, B — bacterium; arrows indicate cerium perhydroxide deposits. Scale bar = 500 nm (B,C,E), = 200 nm (A,D,F).

Figure A.12 — Hydrogen peroxide in the infection thread wall in wild-type *Pisum sativum* nodules SGE

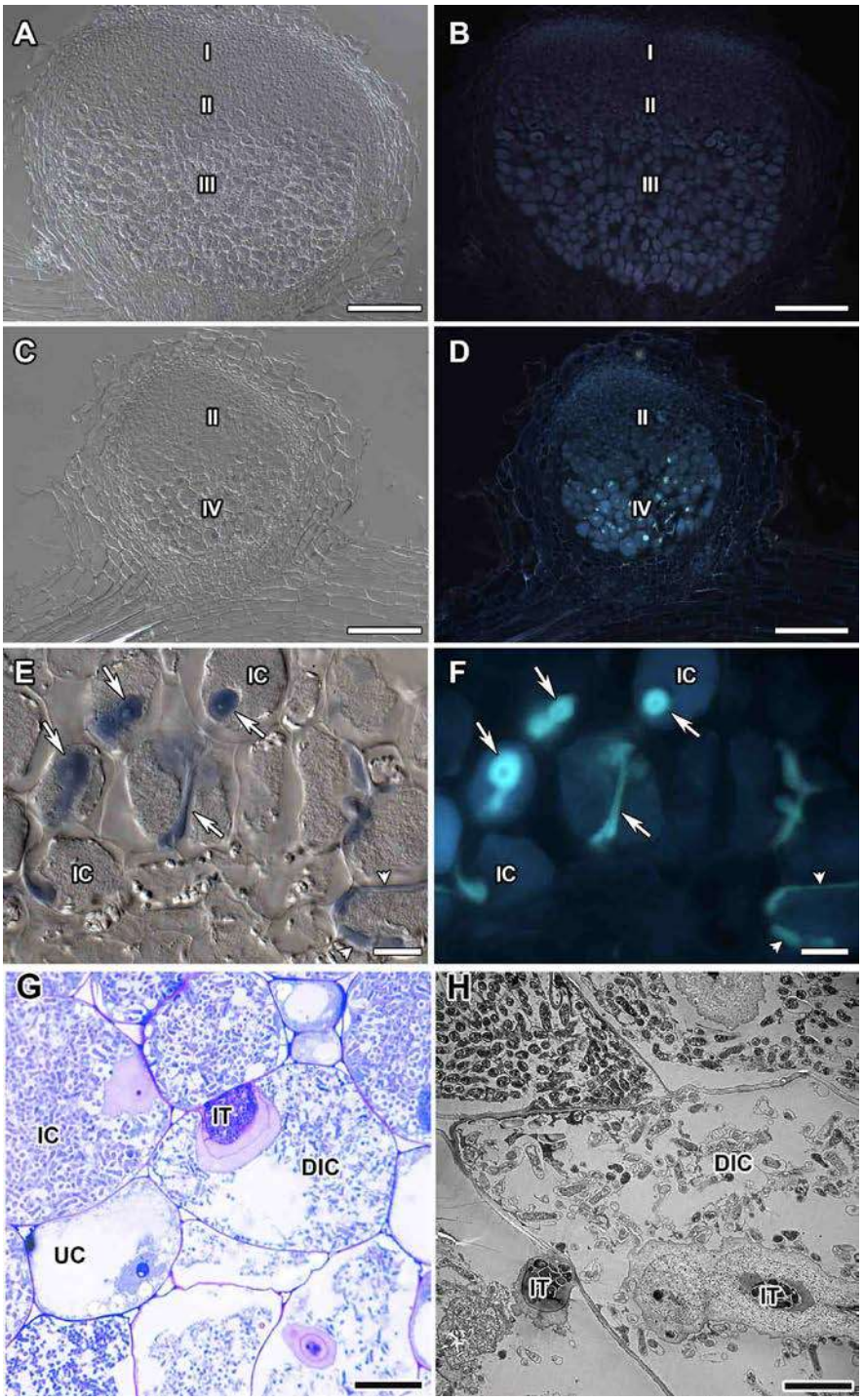

Cytochemical localization of callose (A-F) in 2-week-old nodules of *Pisum sativum* wild-type SGE (A,B) and mutant RisFisV (*Pssym42*) (C-H). Aniline blue staining (B,D,F), differential-interference contrast (A,C,E), methylene blue staining (G), transmission electron microscopy (H). (A-D) Sagittal section of the nodule. (E,F) Accumulation of callose in the infection thread walls and in cell walls. (G,H) Thickened infection thread walls in degenerating infected cells. I — meristem, II — infection zone, III — nitrogen-fixation zone, IV — senescence zone, IC — infected cell, UC — uninfected cell, DIC — degenerating infected cell, IT — infection thread; arrows indicate infection threads with callose accumulation, triangles indicate callose accumulation in the cell wall. Scale bar = 200 μm (A-D), = 20 μm (E-G), = 5 μm (H).

Figure A.13 — Callose in *Pisum sativum* nodules of wild-type SGE and mutant RisFixV (*Pssym42*)

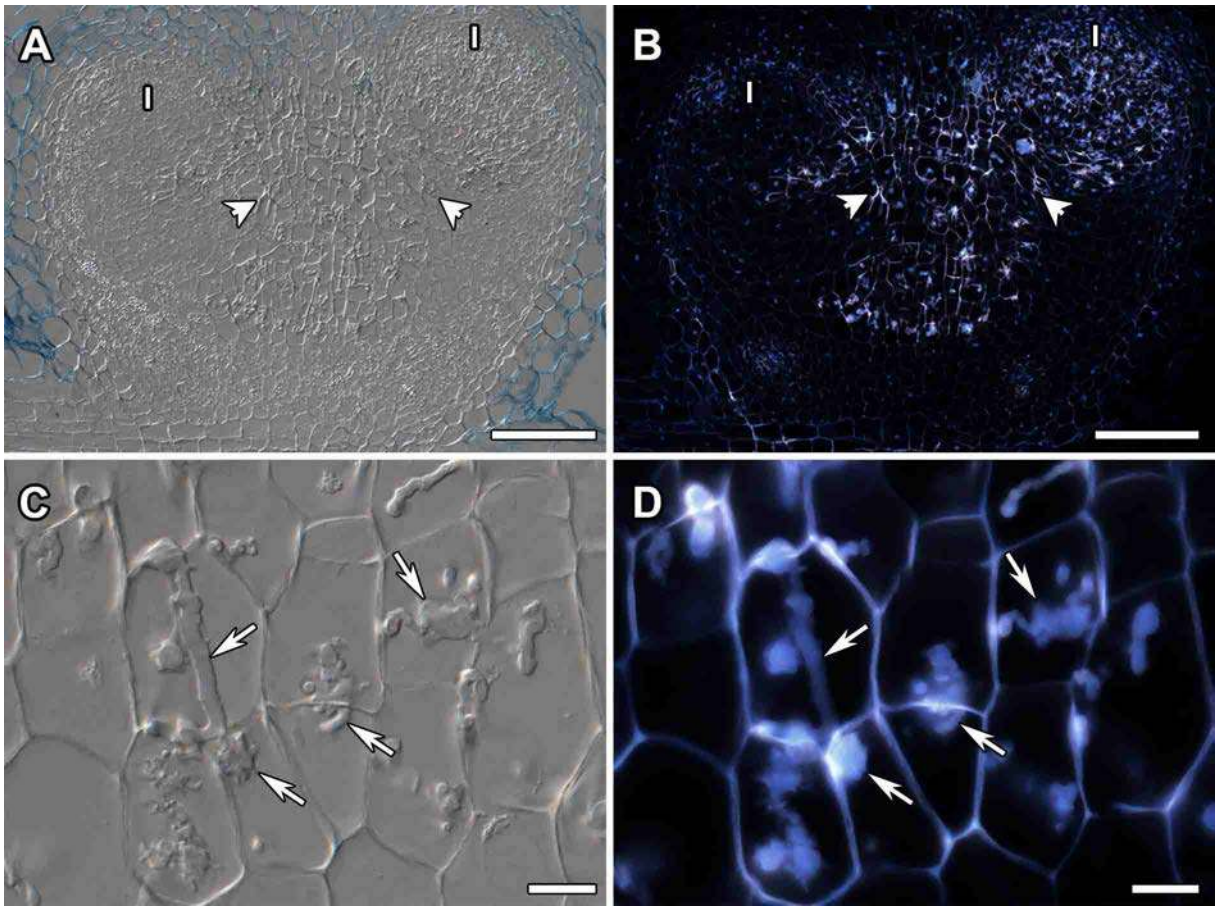

Cytochemical localization of suberin in 3-week-old nodules of the *Pisum sativum* mutant SGEFix⁻-2 (*Pssym33-3*). Neutral red staining (B,D), differential interference contrast (A,C). (A,B) Sagittal section of the nodule. (C,D) Infection zone with twisted infection threads. I — meristem; arrowheads indicate infection threads, arrows indicate the suberized infection thread walls. Scale =200 μm (A,B), =20 μm (C,D).

Figure A.14 — Suberin in nodules of the *Pisum sativum* mutant SGEFix⁻-2 (*Pssym33-3*)

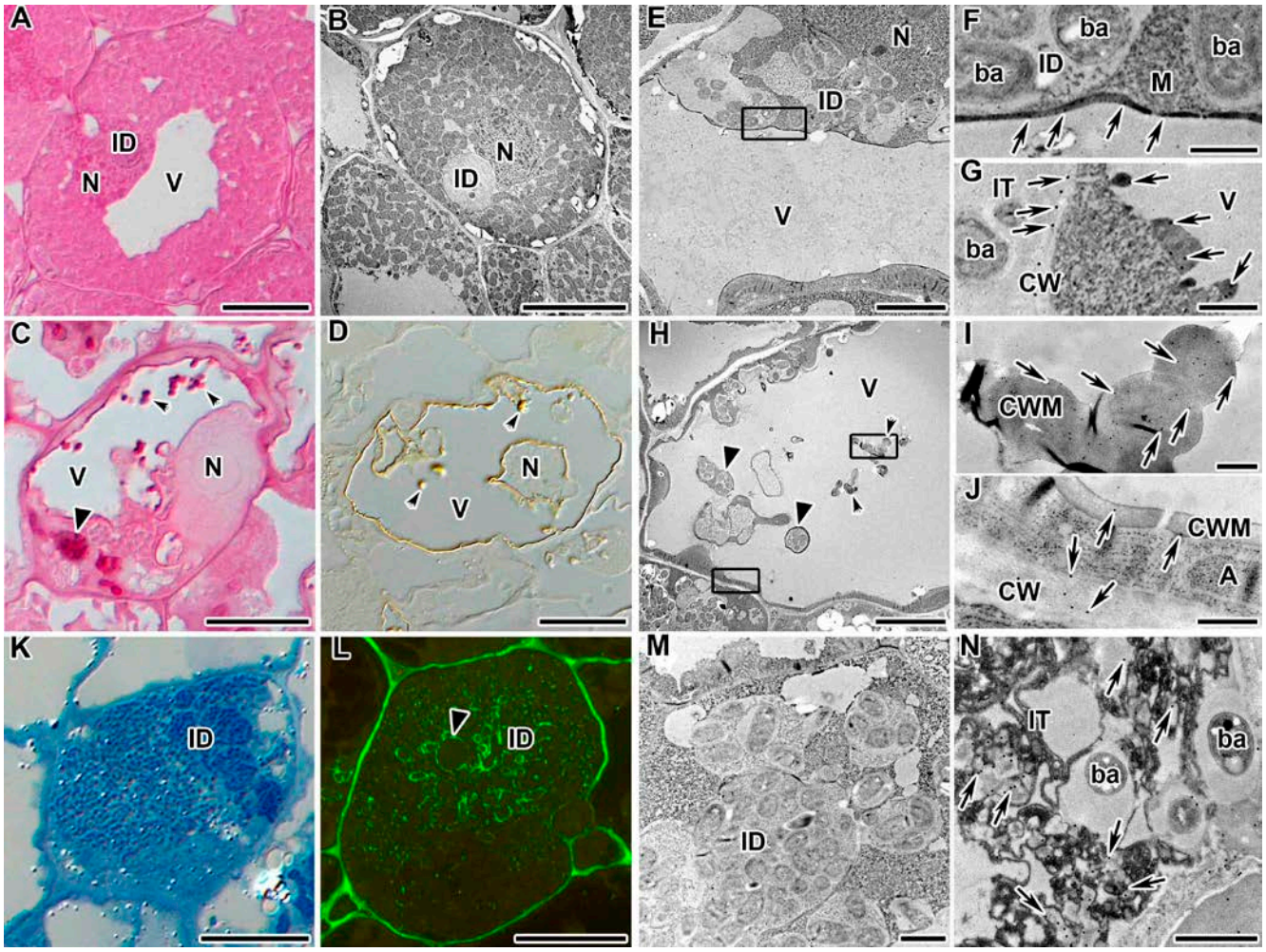

The cell wall material is deposited around the vacuole in the infected cells containing both infection threads and bacteroids and includes additional outgrowths and drops in the lumen of the vacuole. (A) Infected cell from wild type nodule SGE. Histochemical staining with ruthenium red. (B) Transmission electron micrographs of infected cells from wild type nodules SGE. (C,D) Cell wall material around vacuole in the nodules of the mutant line SGEFix^{-}-2 (*Pssym33-3*) indicated with ruthenium red (C) and iodium and sulphuric acid (D). (E-G) Cell wall material deposition around vacuole. Immunogold localisation of highly methyl-esterified homogalacturonan epitope labelled with JIM7 antibody. (F) High magnification of the boxed area in (E). (G) Cell wall material outgrowths into the lumen of the vacuole. (H) Cell wall material deposition around vacuole and in the form of drops in the lumen of a vacuole. Immunogold localisation of galactan sidechain of rhamnogalacturonan I epitope labelled with LM5 antibody. (I,J) High magnification of the boxed areas in (H). (K-M) Hypertrophied infection droplet in the nodules of the mutant line SGEFix^{-}-2 (*Pssym33-3*) observed in semi-thin section (K), by using fluorescent immunolocalization of highly methyl-esterified homogalacturonan epitope labelled with JIM7 antibody (L) and immunogold localisation of rhamnogalacturonan I epitope labelled with LM5 antibody (M). (N) The infection thread with electron-dense matrix where rhizobia are immersed. Immunogold localisation of galactan sidechain of rhamnogalacturonan I epitope labelled with LM5 antibody. N — nucleus, V — vacuole, ID — infection droplet, IT — infection thread, CW — cell wall, CWM — cell wall material, M — mitochondrion, A — amyloplast, ba — bacterium,

arrows indicate gold particles, arrowheads – suberin deposits, triangles – infection threads. Bar = 20 µm (A-D,H,K,L), bar = 5µm (E), bar = 500nm (F,G,I,J,N), bar = 2 µm (M).

Figure A.15 — Defense responses in nodules of the *Pisum sativum* mutant SGEFix⁻-2 (*Pssym33-3*)

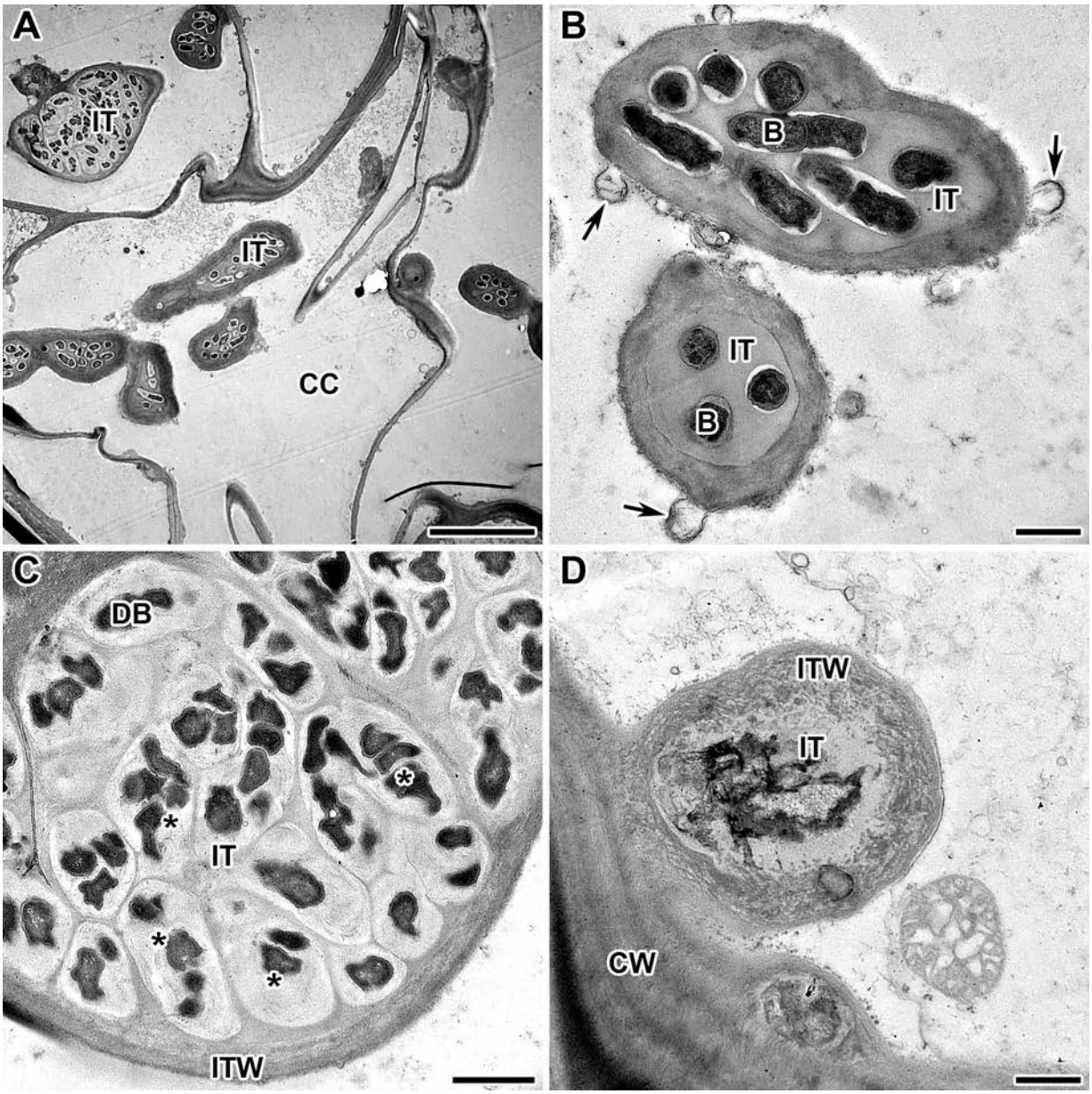

Transmission electron microscopy of nodules of the *Pisum sativum* mutant SGEFix⁻-5 (*Pssym33-2*). (A) Colonized cells. (B) Infection threads with thickened walls and intact bacteria in the matrix. (C) Infection thread with thickened walls and degrading bacteria assembled in clusters. (D) Infection thread with completely degraded bacteria in the lumen. CC — colonized cell, IT — infection thread, ITW — infection thread wall, CW — cell wall, B — bacterium, DB — degrading bacterium, arrows indicate vesicles, asterisks indicate clusters of bacteria within the lumen of infection thread. Scale bar = 10 μm (A), = 1 μm (B-D).

Figure A.16 — Ultrastructural organization of nodules of the *Pisum sativum* mutant SGEFix⁻-5 (*Pssym33-2*)

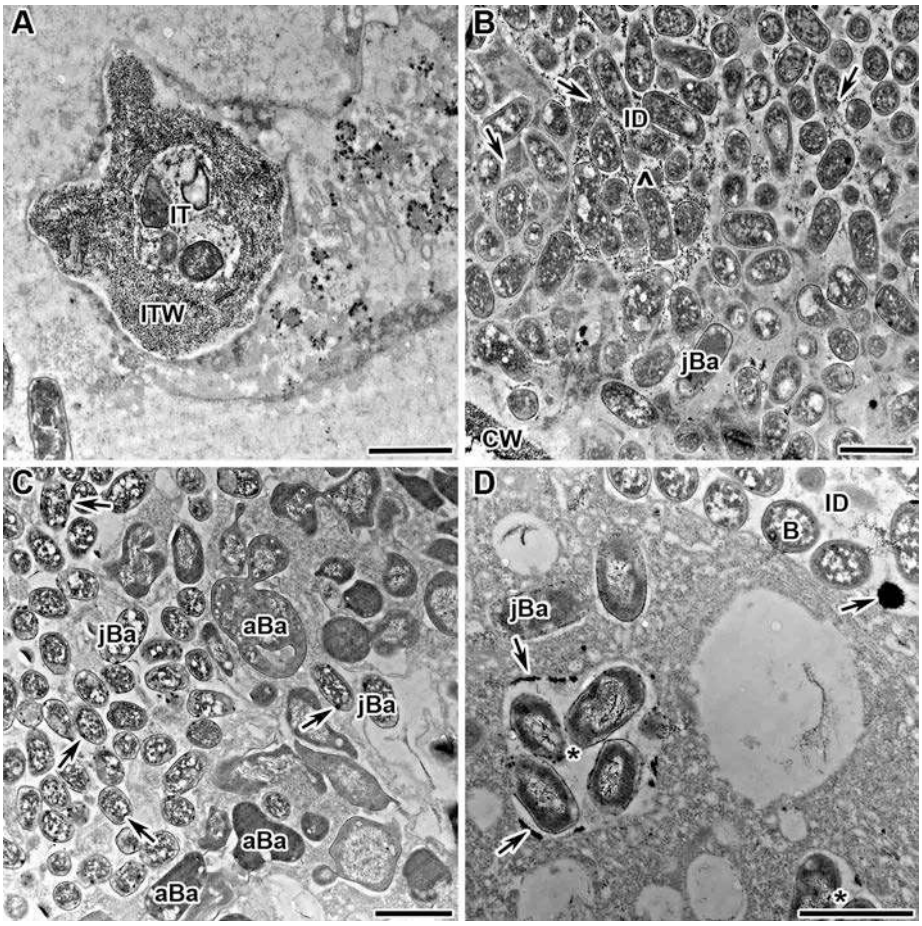

Cytochemical reaction with cerium chloride in 2-week-old nodules of the *Pisum sativum* mutant SGEFix⁻-1 (*Pssym40-1*). (A) Infection thread with intense accumulation of cerium perhydroxide precipitates in the wall and matrix. (B) Infection droplet completely filled with cerium perhydroxide precipitates. (C) Juvenile bacteroids with cerium perhydroxide precipitates. (D) Formation of multibacteroid symbiosomes surrounded by cerium perhydroxide precipitates. CW — cell wall, IT — infection thread, ID — infection droplet, ITW — infection thread wall, B — bacterium, jBa — juvenile bacteroid, aBa — abnormal bacteroid, ^ — infection thread matrix filled with small cerium perhydroxide precipitates, * — multibacteroid symbiosomes, arrows indicate cerium perhydroxide precipitates. Scale bar = 1 μm.

Figure A.17 — Hydrogen peroxide in nodules of the *Pisum sativum* mutant SGEFix⁻-1 (*Pssym40-1*)

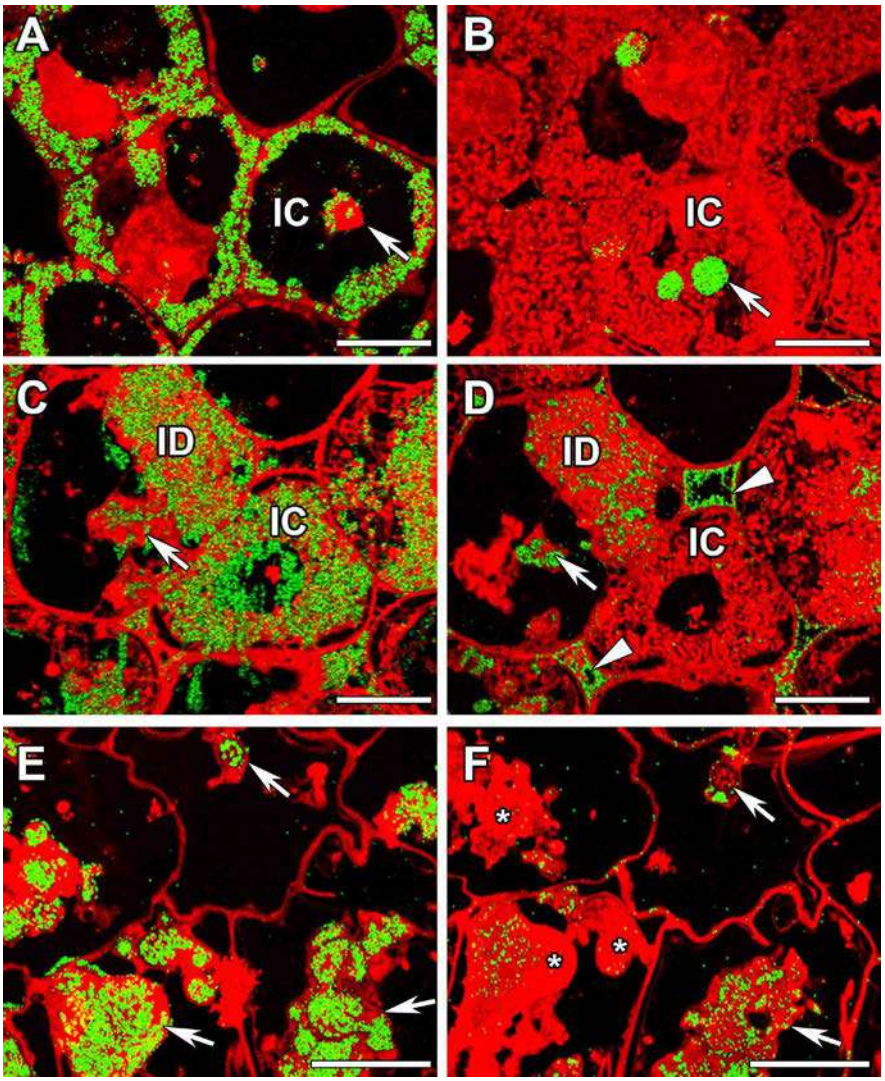

Confocal laser microscopy of 2-week-old nodules of *Pisum sativum* wild-type SGE (A,B) and mutants SGEFix⁻-1 (*Pssym40-1*) (C,D), and RBT3 (*Pssym33-3*, *Pssym40-1*) (E,F). Immunolocalization using the MAC57 antibody (for lipopolysaccharides of *Rhizobium leguminosarum* bv. *viceae* 3841) (A,B,D) and the MAC265 antibody (for arabinogalactan-protein extensin) (B,G,E). The secondary antibody used were the goat anti-rat IgG monoclonal antibody conjugated to 10 nm diameter colloidal gold followed by silver enhancing. IC — infected cell, ID — infection droplet, arrows indicate infection threads, asterisk indicates infection threads with relative absence of MAC265 label in the double mutant RBT3, arrowheads indicate localization of MAC265 in the intercellular space in the mutant SGEFix⁻-1. Scale bar = 10 μm.

Figure A.18 — Lipopolysaccharides of *Rhizobium leguminosarum* bv. *viceae* 3841 and arabinogalactan-protein extensin of infection thread matrix in nodules of *Pisum sativum* wild type and mutants

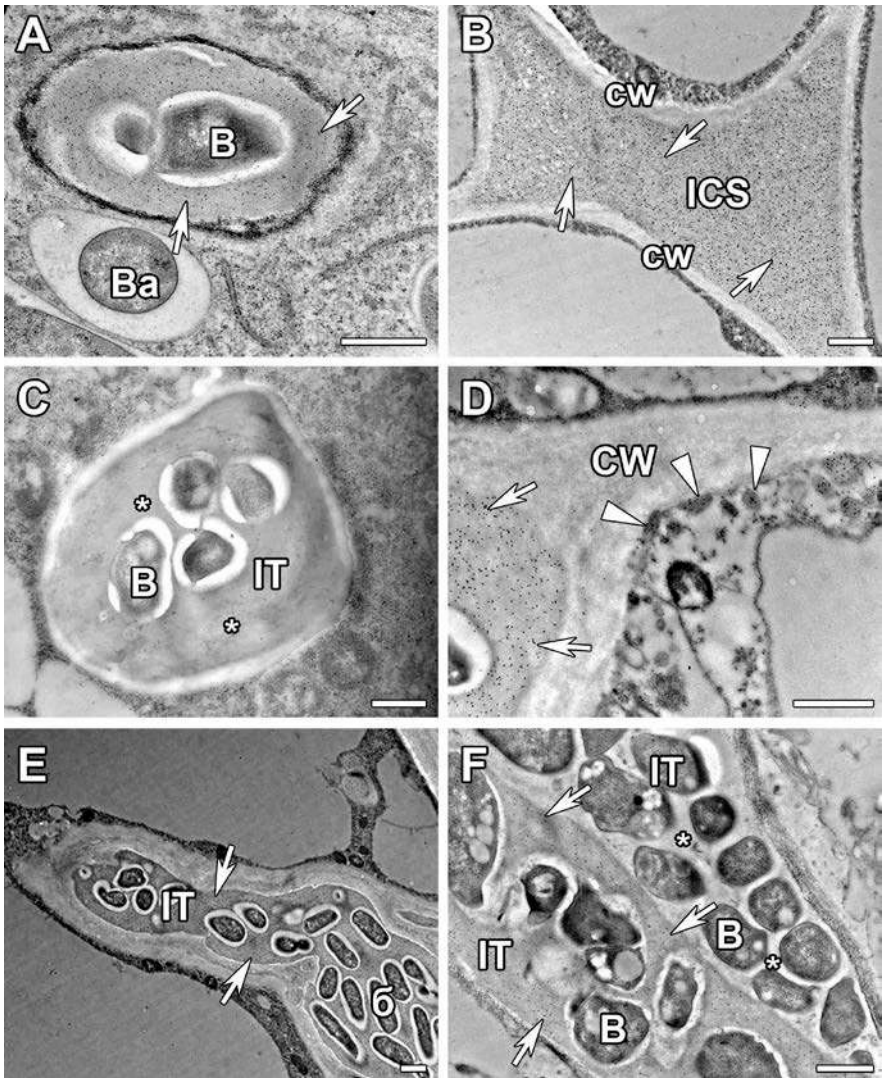

Immunogold localization with the MAC265 antibody in 2-week-old nodules of *Pisum sativum* wild type and mutants. The secondary antibody used were the goat anti-rat IgG monoclonal antibody conjugated to 10 nm diameter colloidal gold. (A) Wild type SGE. (B) Mutant SGEFix⁻-1 (*Pssym40-1*). (C) Mutant SGEFix⁻-2 (*Pssym33-3*). (D) Double mutant RBT3 (*Pssym33-3*, *Pssym40-1*). (E) Double mutant RBT4 (*Pssym33-3*, *Pssym42*). (E) Mutant RisFixV (*Pssym42*). B — bacterium, Ba — bacteroid, CW — cell wall, ICS — intercellular space, IT — infection thread; arrowheads indicate transport vesicles, arrows indicate gold particles, and asterisks indicate the part of the infection thread matrix lacking the MAC265 label. Scale bar = 500 nm.

Figure A.19 — Arabinogalactan-protein extensin of infection thread matrix in nodules of *Pisum sativum* wild type and mutants

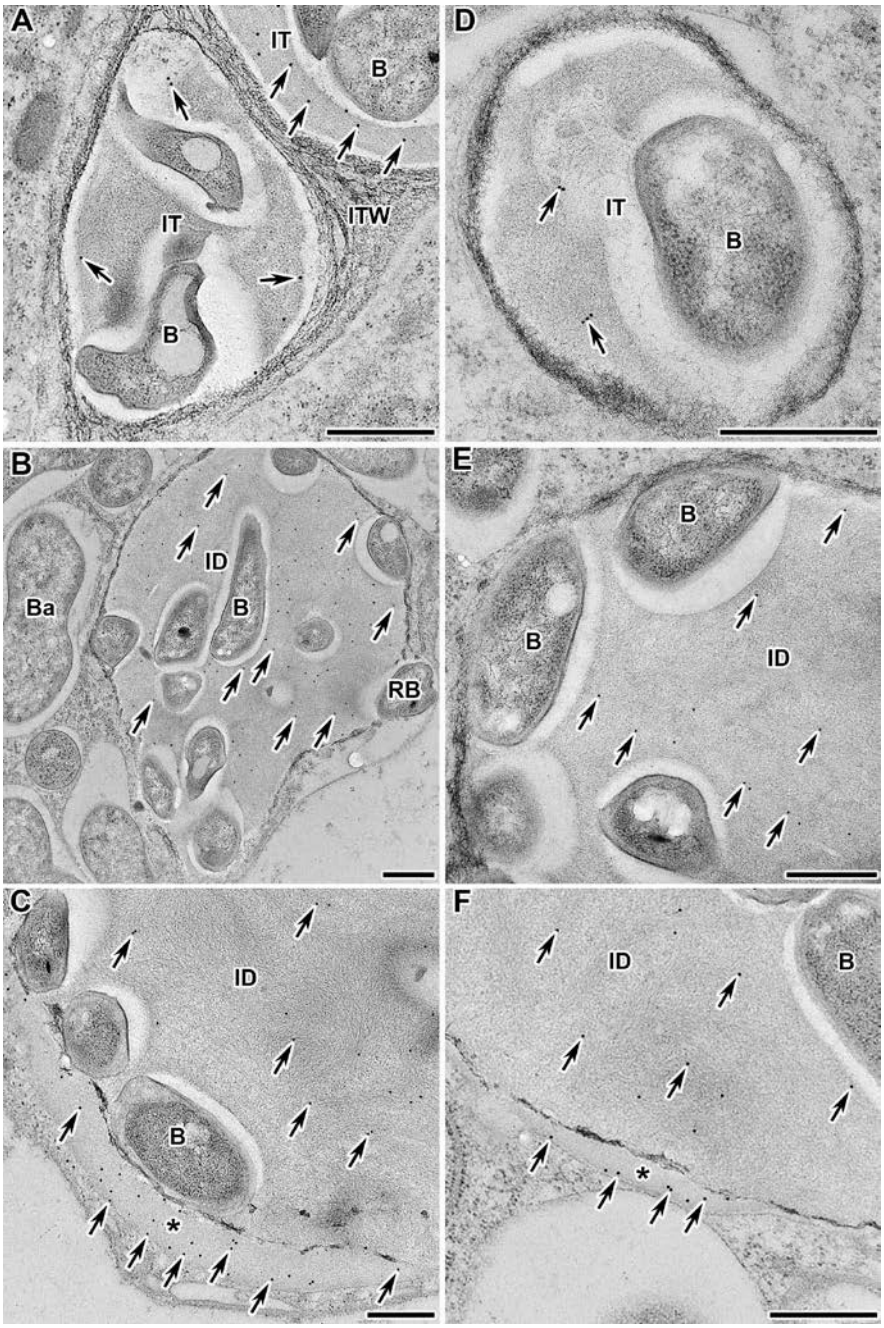

Immunogold localization with the MAC204 (A-B) and the MAC236 (G-E) antibodies in 2-week-old nodules of *Pisum sativum* wild-type SGE. The secondary antibody used were the goat anti-rat IgG monoclonal antibody conjugated to 10 nm diameter colloidal gold. (A, D) Localization in the matrix of the infection thread. (B, D) Localization in the matrix of the infection droplet. (C, E) Localization in the newly synthesized matrix of the infection droplet. IT — infection thread, ID — infection droplet, B — bacterium, RB — released bacterium, Ba — bacteroid; arrows indicate gold particles, * — areas of infection droplet with newly synthesized matrix. Scale = 500 nm.

Figure A.20 — Arabinogalactan-protein extensins of the infection thread matrix in nodules of *Pisum sativum* wild-type SGE

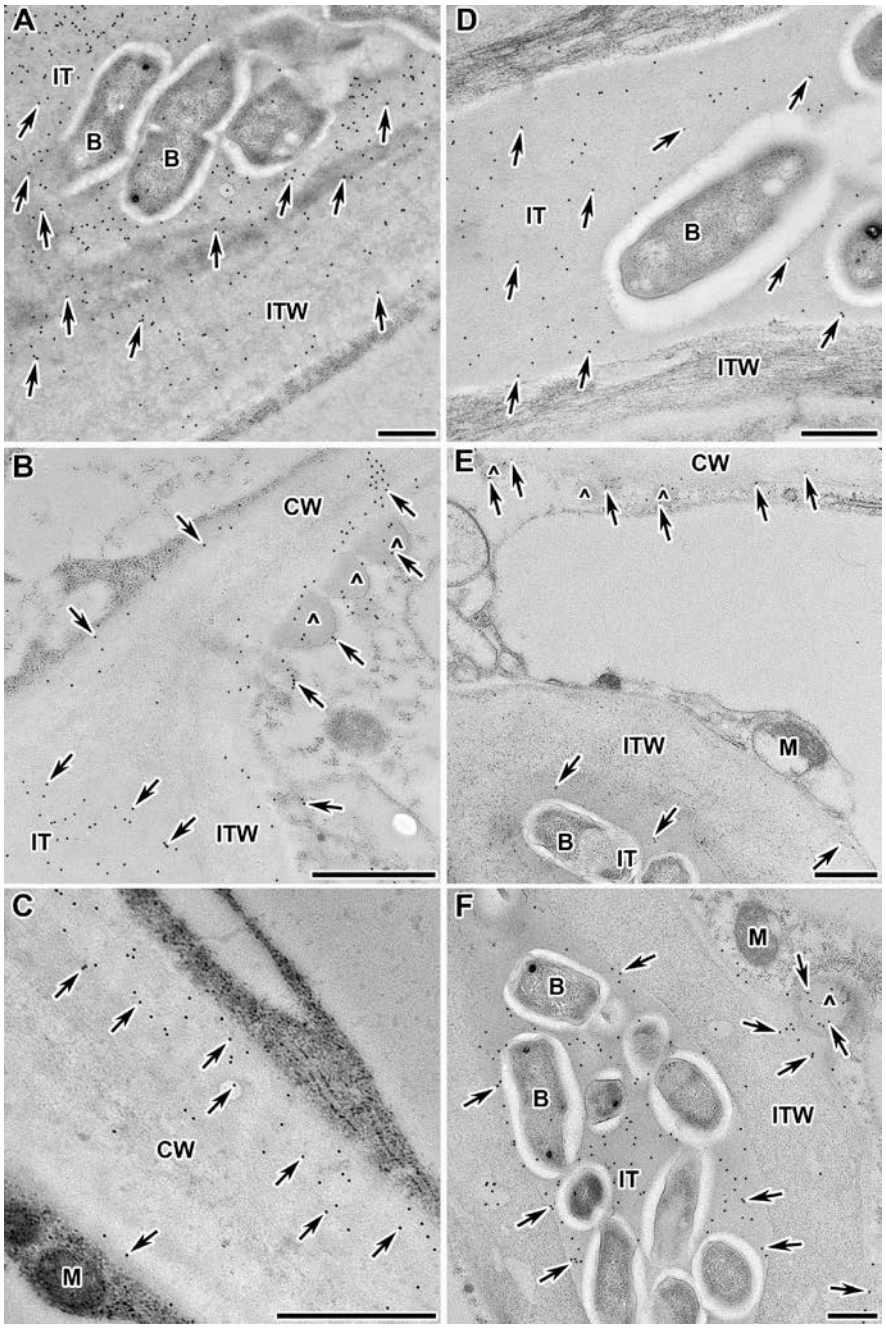

Immunogold localization with the MAC204 (A-B) and the MAC236 (G-E) antibodies in 2-week-old nodules of *Pisum sativum* double mutant RBT3 (*Pssym33-3*, *Pssym40-1*). The secondary antibody used were the goat anti-rat IgG monoclonal antibody conjugated to 10 nm diameter colloidal gold. (A, D) Localization in the matrix of the infection thread. (B, E) Transport vesicles carrying the AGPE label near the cell wall. (C) AGPE epitope in the cell wall. (F) Transport vesicles carrying the AGPE label next to the infection thread wall. IT — infection thread, ITW — infection thread wall, B — bacterium, CW — cell wall, M — mitochondrion, ^ — vesicles labeled to arabinogalactan-protein extensin epitopes; arrows indicate gold particles. Scale bar = 500 nm.

Figure A.21 — Arabinogalactan-protein extensins of the infection thread matrix in nodules of *Pisum sativum* double mutant RBT3 (*Pssym33-3, Pssym40-1*)

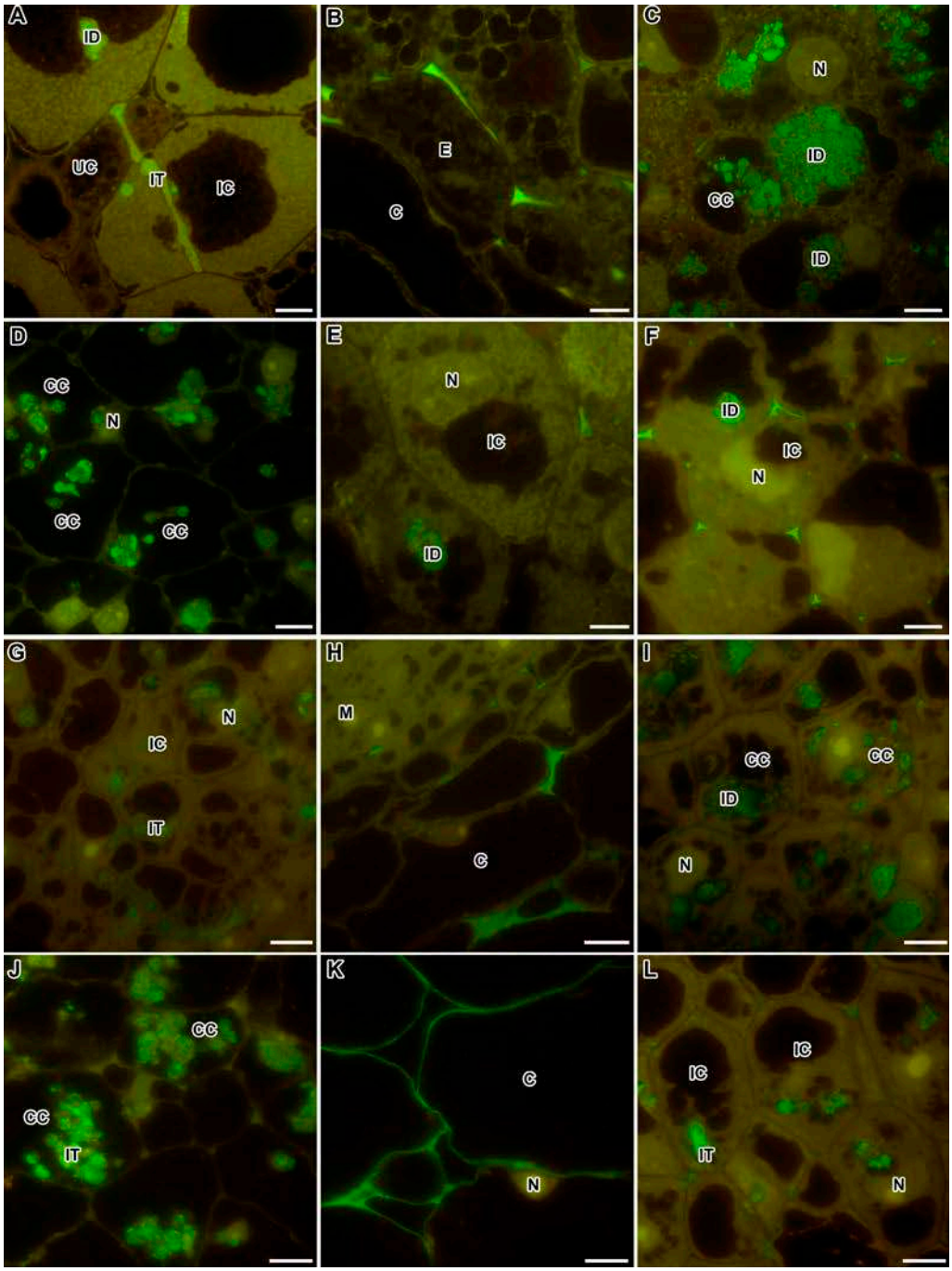

Fluorescent immunolocalisation with JIM11 in nodules from wild-type and mutant *Pisum sativum* (A-F) and *Medicago truncatula* (G-L). The secondary antibody used was the goat anti-rat IgG monoclonal antibody conjugated with Alexa Fluor 488. (A) Nitrogen fixation zone of the wild-type SGE. (B) Endodermis of the wild-type SGE. (C) Infection zone of the mutant SGEFix$^-$-1 (*Pssym40-1*). (D) Colonized cells of the mutant SGEFix$^-$-2 (*Pssym33-3*). (E) Infection zone in the mutant SGEFix$^-$-3 (*Pssym26*). (F) Infection zone of the mutant Sprint-2Fix$^-$ (*Pssym31*). (G) Infection zone of the wild-type A17. (H) Endodermis of the wild-type A17. (I) Infection zone of the mutant *Mtefd–1*. (J) Colonized cells of the mutant TR3 (*Mtipd3*). (K) Cortex of the mutant TR3 (*Mtipd3*). (L) Infection zone in the mutant *Mtdnf1–1*. C — cortex, E — endodermis, CC — colonized cell, IC — infected cell, N — nucleus, ID — infection droplet, IT — infection thread. Bar = 10 μm.

Figure A.22 — Extensin in nodules of wild-type and mutants of *Pisum sativum* and *Medicago truncatula*

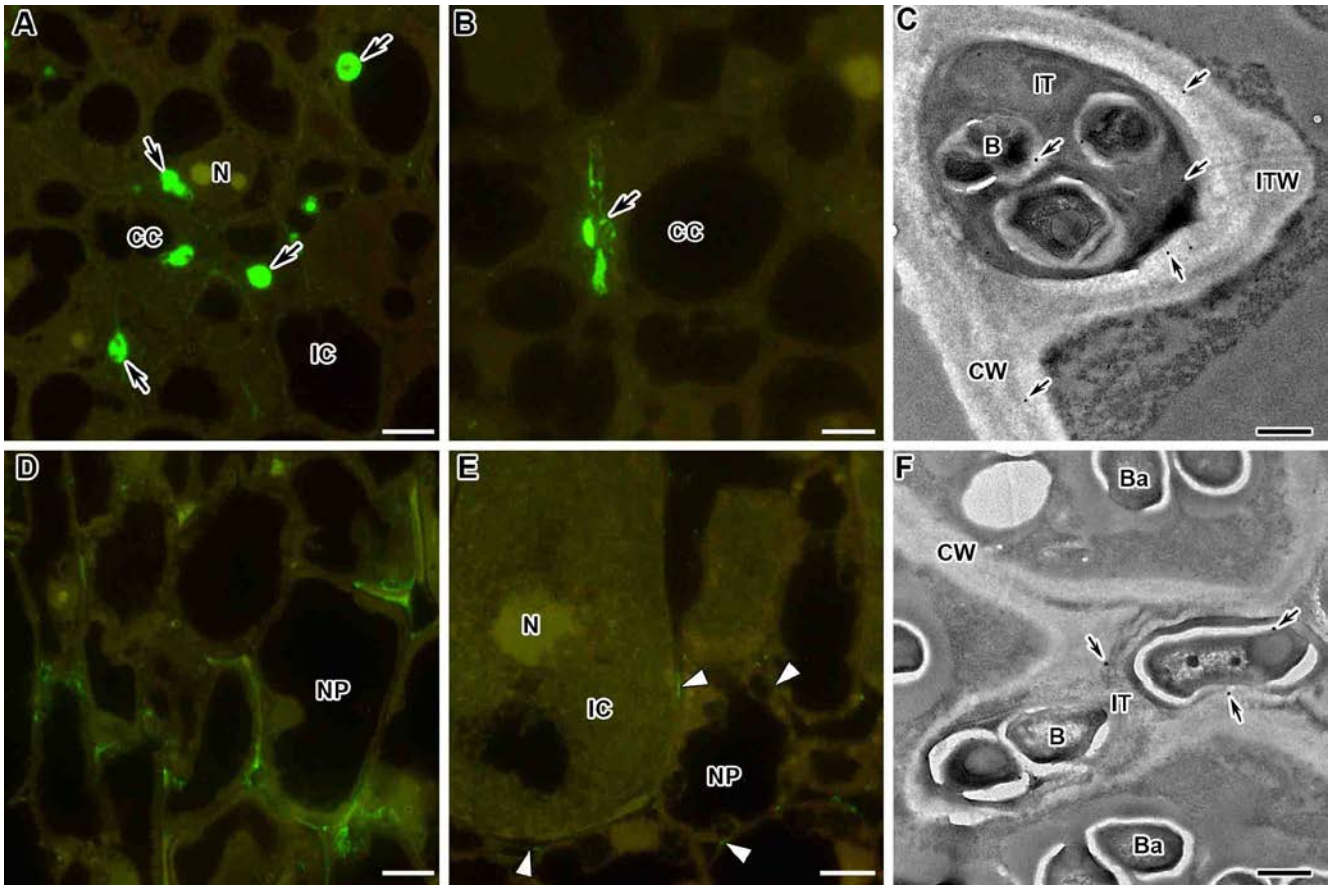

Fluorescence immunolocalization (A,B,D,E) with the MAC265 (A,D), the JIM11 (B,E) antibodies and immunogold localization (C,F) with the JIM19 antibody in *Galega orientalis* (A-C) and *Glycine max* (D-F) nodules. The secondary antibody used were the goat anti-rat IgG monoclonal antibody conjugated with Alexa Fluor 488 (A,B,D,E) and conjugated to 10 nm diameter colloidal gold (C,F). (A,B) Infection zone. (C,F) Infection threads. (D) Parenchyma of the nodule. (E) Infected cells. NP — nodule parenchyma, IC — infected cell, CC — colonized cell, N — nucleus, CW — cell wall, IT — infection thread, ITW — infection thread wall, B — bacterium, Ba — bacteroid; arrows indicate infection threads, triangles indicate signal, small arrows indicate gold particles. Scale bar = 10 μm (A,B,D,E), = 500 nm (C,F).

Figure A.23 — Arabinogalactan-protein extensin and extensins in nodules of *Galega orientalis* and *Glycine max*

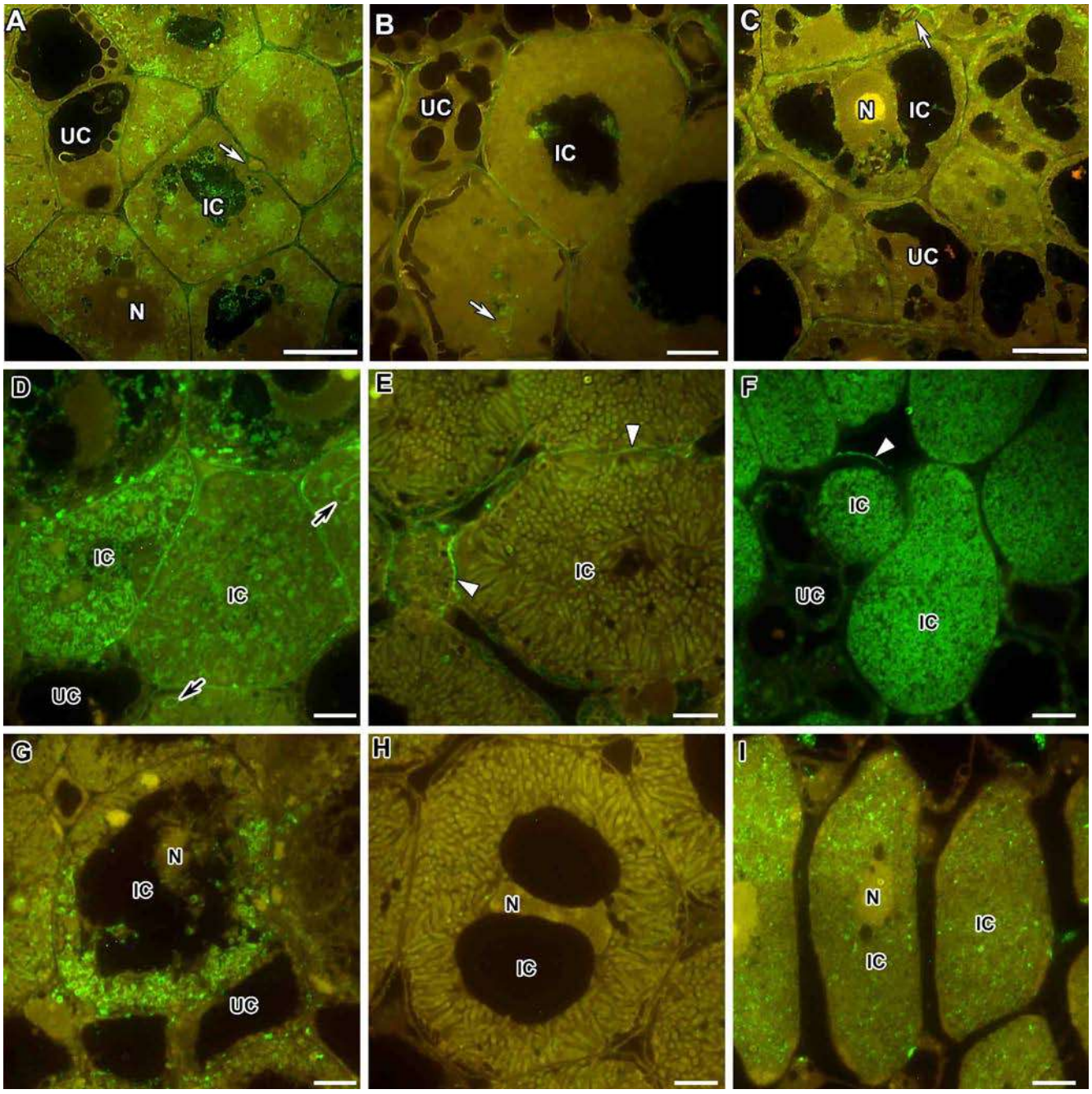

Fluorescence immunolocalization with the LM6-M (A-F) and the LM2 (G-I) antibodies in nodules of *Pisum sativum* (A,B), *Medicago truncatula* (C), *Galega orientalis* (D,E,G,H) and *Glycine max* (F,I). The secondary antibody used were the goat anti-rat IgG monoclonal antibody conjugated with Alexa Fluor 488. (A,C,D,G) Infected cells with juvenile symbiosomes. (B,E,H) Mature infected cells. (F,I) Infected cells. IC — infected cell, UC — uninfected cell, N — nucleus; arrows indicate infection threads, triangles indicate signal in cell walls. Scale bar = 10 μm.

Figure A.24 — Arabinans and arabinogalactan proteins in legume nodules

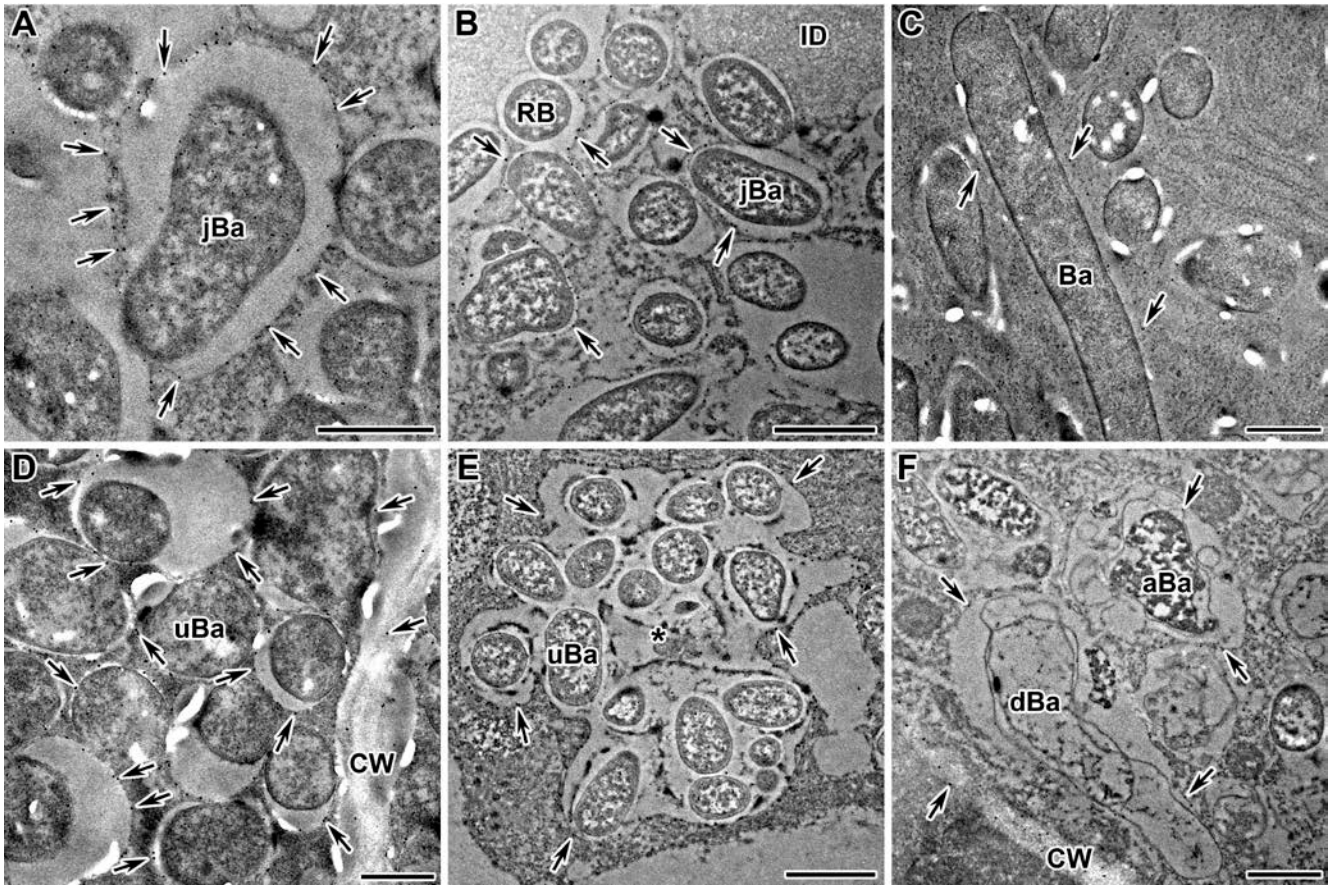

Immunogold localisation with the LM6-M antibody in nodules from wild-type and mutant *Medicago truncatula* (C,D) and *Pisum sativum* (A,B,E,F). The secondary antibody used was the goat anti-rat IgG monoclonal antibody conjugated to 10 nm diameter colloidal gold. (A) Juvenile symbiosomes in the wild-type SGE. (B) Juvenile symbiosomes in the mutant SGEFix⁻-1 (*Pssym40-1*). (C) Mature symbiosomes in the wild-type A17. (D) Undifferentiated symbiosomes in the mutant *Mtdnf1–1*. (E) Multiple symbiosomes in the mutant SGEFix⁻-1 (*Pssym40-1*). (F) Symbiosomes with abnormal and degraded bacteroids in the mutant SGEFix⁻-1 (*Pssym40-1*). CW — cell wall, Ba — mature bacteroid, jBa — juvenile bacteroid, uBa — undifferentiated bacteroid, aBa — abnormal bacteroid, dBa — degraded bacteroid, * — multiple symbiosome; arrows indicate gold particles. Bars (B,E) = 1 μm, (A,C,D,F) = 500 nm.

Figure A.25 — (1→5)-α-L-arabinane side chain of rhamnogalacturonan I in nodules of *Pisum sativum* and *Medicago truncatula* wild types and mutants

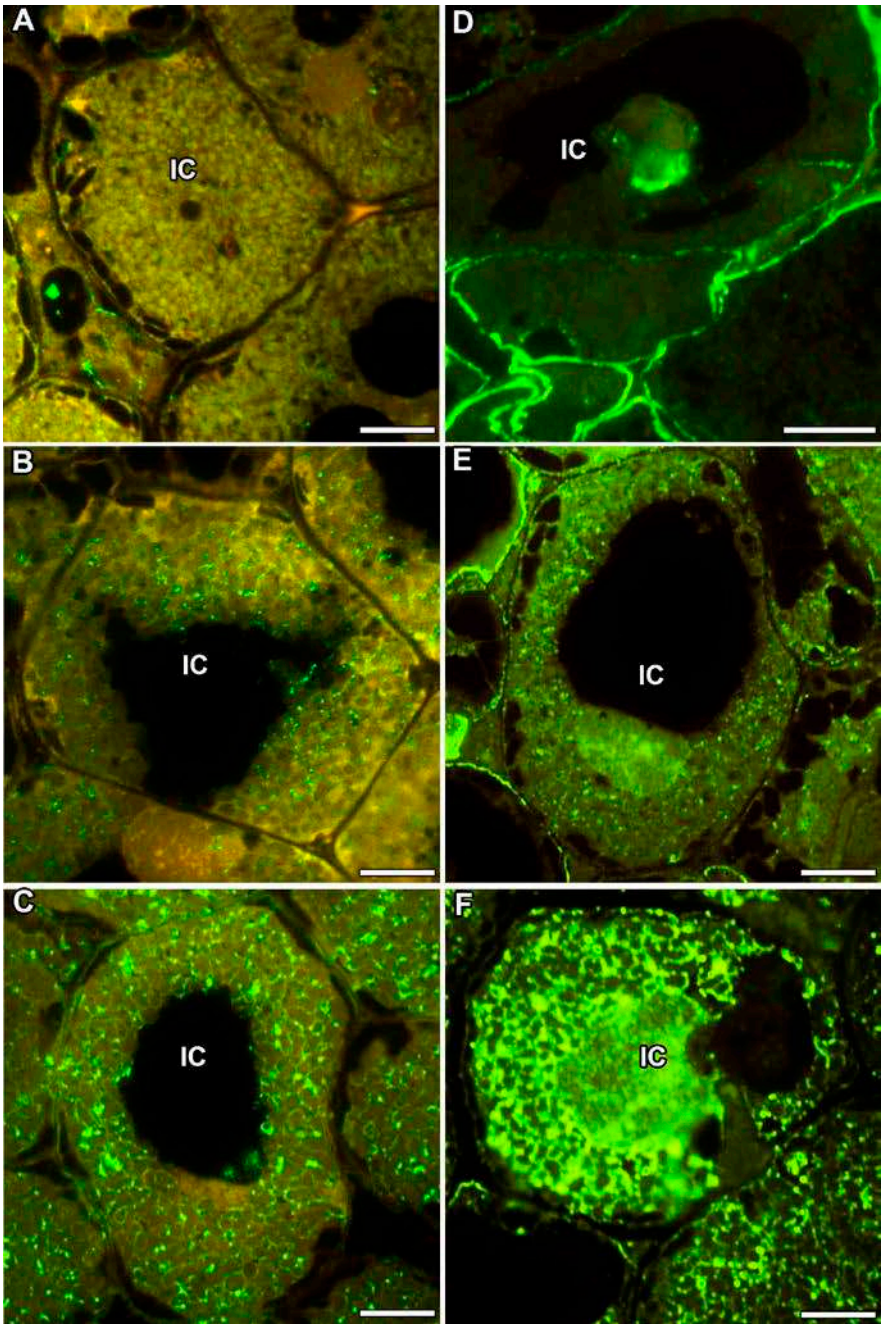

Fluorescent immunolocalization with the JIM1 antibody in the nodules of the *M. truncatula* (A) and *P. sativum* (B-F) wild-types and mutant lines. The secondary antibody used was goat anti-rat IgG MAb conjugated with Alexa Fluor 488. (A) Two-week-old nodule of wild-type A17. (B) Two-week-old nodule of wild-type SGE. (C) Four-week-old nodule of wild-type SGE. (D) Two-week-old nodule of mutant Sprint-2Fix$^-$ (*Pssym31*). (E) Two-week-old nodule of mutant SGEFix$^-$-1 (*Pssym40*). (F) Two-week-old nodule of mutant SGEFix$^-$-3 (*sym26*). IC — infected cell. Bar = 20 µm.

Figure A.26 — Arabinogalactan protein with a glycosylphosphatidylinositol anchor in nodules of wild-type *Medicago truncatula* and wild-type and mutants of *Pisum sativum*

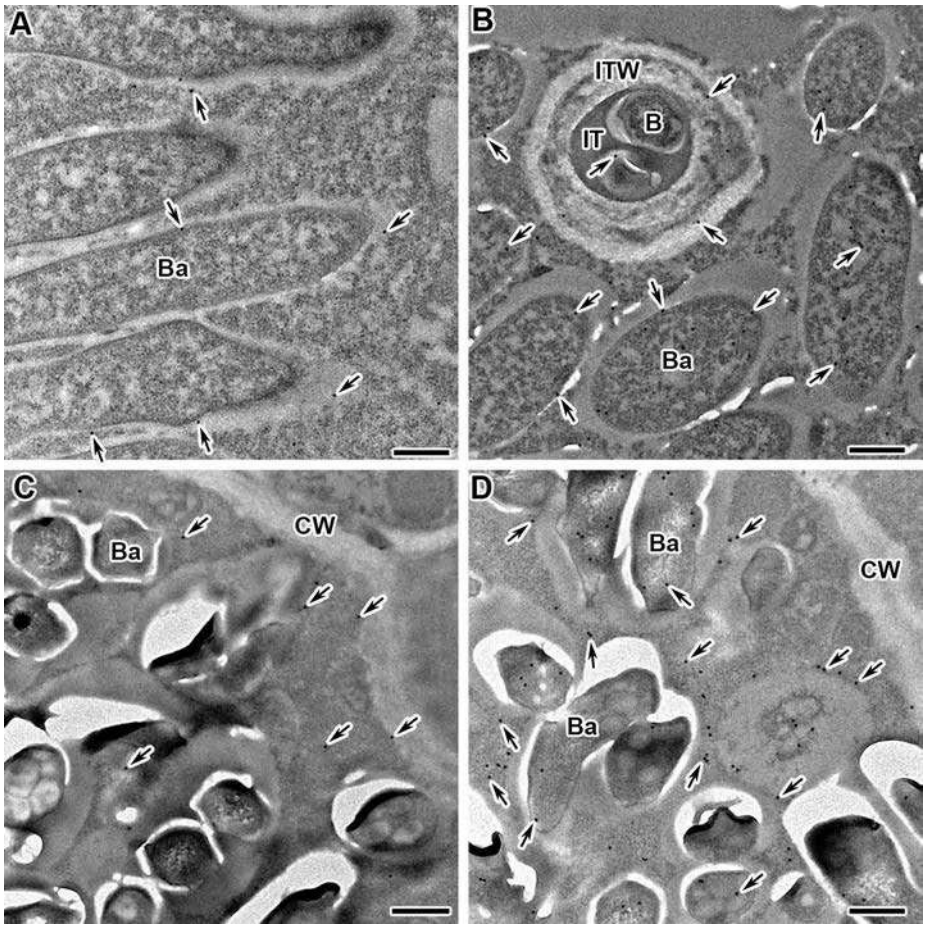

Immunogold localization with the JIM4 (b, e) and with the JIM15 (c, f) antibodies in the nodules of *Galega orientalis* (A,B) and *Glycine max* (C,D). The secondary antibody used was the goat anti-rat IgG monoclonal antibodies conjugated to 10 nm diameter colloidal gold. (A,C,D) Bacteroids in the infected cells. (B) Infection thread in the infected cell. CW — cell wall; IT — infection thread; ITW — infection thread wall; B — bacterium; Ba — bacteroid; small arrows indicate gold particles. Bar = 500 nm.

Figure A.27 — Arabinogalactan proteins in nodules of *Galega orientalis* and *Glycine max*

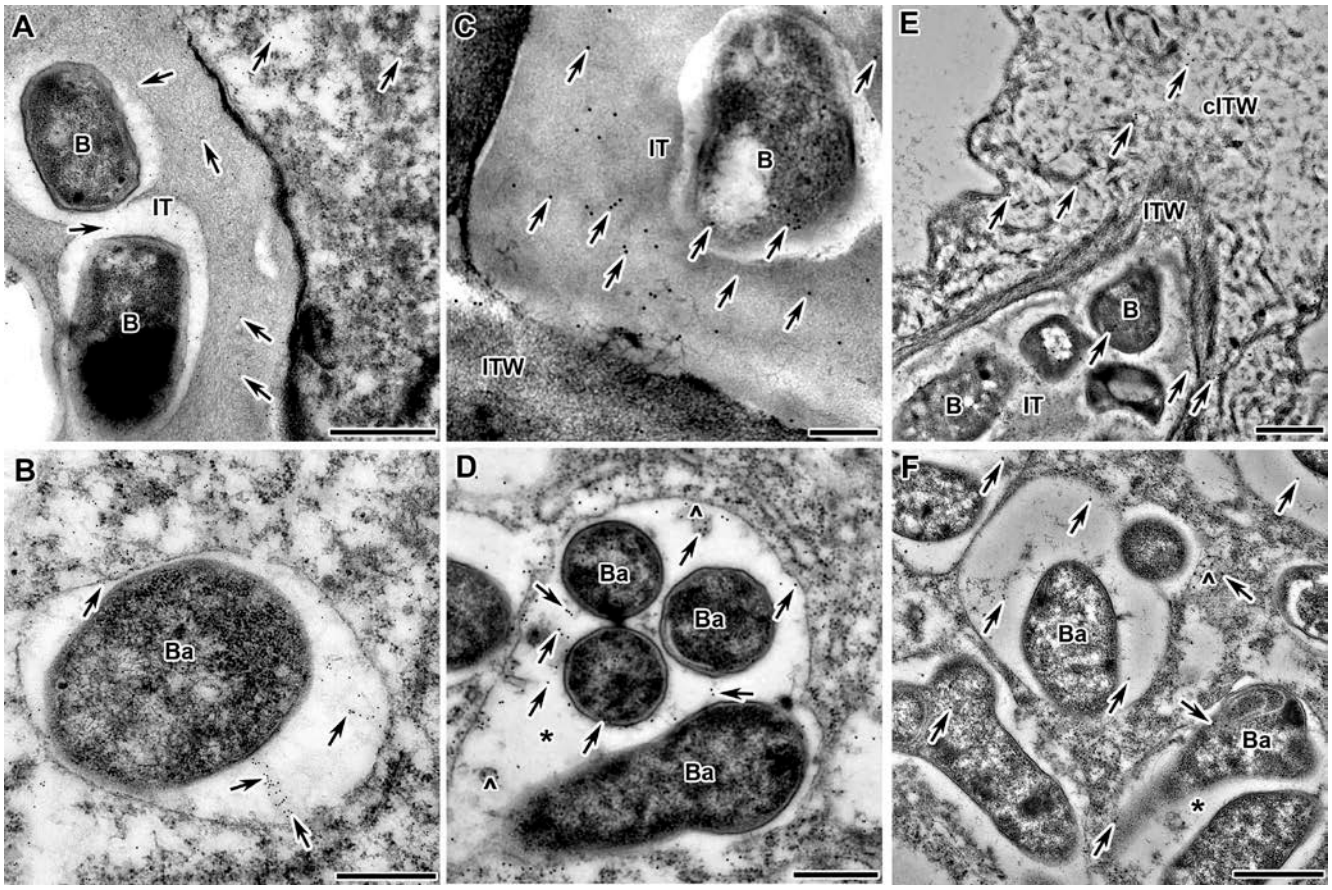

Immunogold localization with a polyclonal antibody to trans-zeatin riboside in nodules of wild-type SGE (A,B) and mutants SGEFix⁻-2 (*Pssym33-3*) (C), SGEFix⁻-1 (*Pssym40-1*) (D), and RisFixV (*Pssym42*) (E,E). The secondary antibody used was the goat anti-rabbit IgG monoclonal antibodies conjugated to 10 nm diameter colloidal gold. IT — infection thread, ITW — infection thread wall, cITW — callose-impregnated infection thread wall, B — bacteria, Ba — bacteroidetes, * — multibacteroid symbiosomes, ^ — vesicles carrying a trans-zeatin riboside label; arrows indicate gold particles. Scale = 500 nm (A, D-F), = 200 nm (B, C).

Figure A.28 — Trans-zeatin riboside in wild-type and mutant nodules of *Pisum sativum*

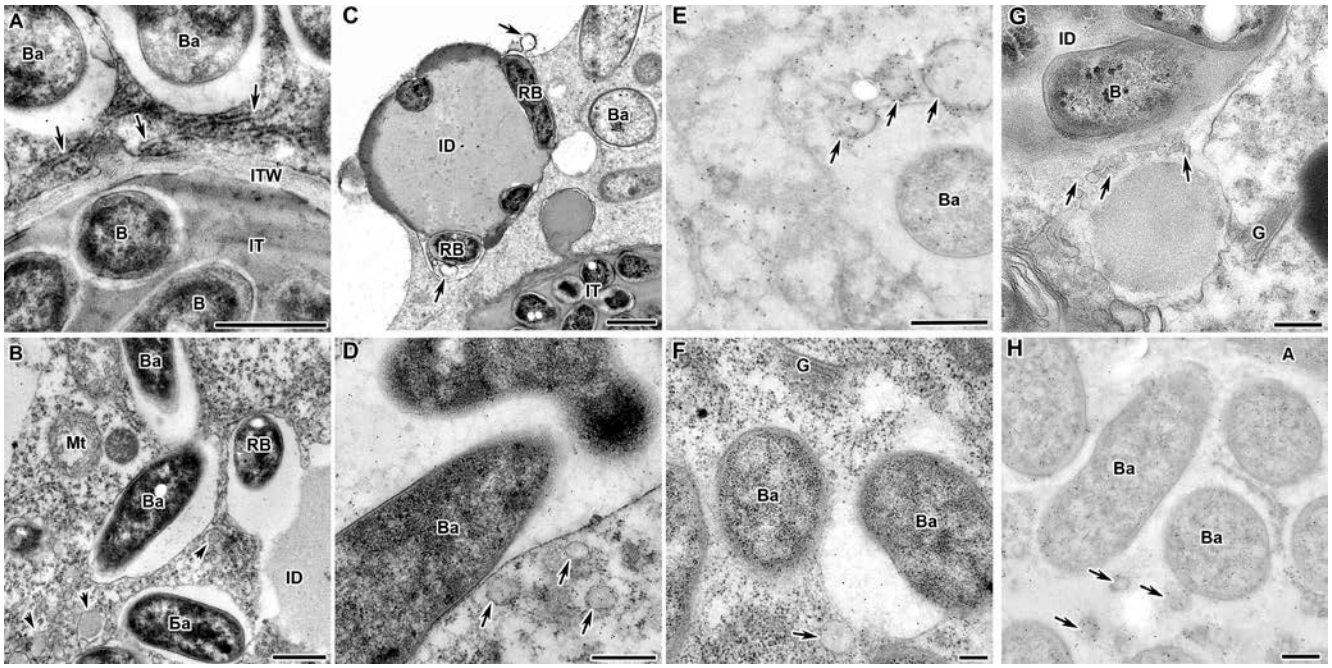

Transmission electron microscopy (A,B,C,G) and immunogold localization of cytokinin trans-zeatin riboside (D), gibberellic acid (E,H), and glutathione (F) in nodules of *Pisum sativum* wild-type SGE (A-F) and mutants SGEFix⁻-6 (*Pssym40-2*) (G) and SGEFix⁻-3 (*Pssym26*) (H). The secondary antibody used was the goat anti-rabbit IgG monoclonal antibodies conjugated to 10 nm diameter colloidal gold; (E,H) uncontrasted sections. (A) EPR tubules in close association with the infection thread wall. (B) Agranular EPR vesicles with matrix material of the infection droplet. (C,G) Vesicles attach to the plasma membrane when bacteria are released from infection droplets. (D) Vesicles carrying the trans-zeatin riboside label are located near the symbiosome membrane. (E,H) Vesicles carrying the gibberellic acid label attach to the symbiosome membrane. (F) A vesicle carrying a glutathione label attaches to the symbiosome membrane. G — Golgi apparatus, Mt — mitochondrion, A — amyloplast, IT — infection thread, ITW — infection thread wall, ID — infection droplet, B — bacterium, RB — released bacterium, Ba — bacteroid; arrows indicate EPR tubules and transport vesicles, arrowheads point to agranular EPR vesicles. Scale bar = 1 μm (C), = 500 nm (A,B,D,E), = 200 nm (F-H).

Figure A.29 — Endoplasmic reticulum and vesicular transport in nodules of wild type and mutants of *Pisum sativum*